
Global snowfall: A combined reanalysis and spaceborne remote sensing perspective

Marian E. MATELING

A thesis submitted in partial fulfillment of
the requirements for the degree of

Master of Science

(Atmospheric and Oceanic Sciences)

at the

UNIVERSITY OF WISCONSIN-MADISON

2016

Abstract

Global snowfall: A combined reanalysis and spaceborne remote sensing perspective

by Marian E. MATELING

An empirical *a priori* database using coincident CloudSat-derived surface precipitation rates and microwave radiometer observations was created to facilitate Day 1 Global Precipitation Measurement (GPM) Goddard Profiling Algorithm (GPROF) precipitation retrievals. This empirical database matches multi-frequency brightness temperature observations from the Advanced Microwave Scanning Radiometer-EOS (AMSR-E) and Microwave Humidity Sounder (MHS), thus containing a similar channel selection as the GPM Microwave Imager (GMI). The CloudSat/AMSR-E/MHS *a priori* database is currently used for precipitation retrievals over very cold surface types and provides critical information for Day 1 GPROF high latitude snowfall retrievals. This study presents results from an exhaustive analysis of higher latitude snowfall events contained in this dataset. Initially, an analysis of the ERA-Interim snowfall dataset is performed to set a precedent for global snowfall coverage. Next, the CloudSat snowfall dataset is independently compared to ERA-Interim snowfall accumulations for various surface types. The CloudSat surface snowfall rate dataset is then binned by two-meter temperature (T2m), total precipitable water amount (TPW), and surface emissivity type (SFC) in accordance with the GPROF retrieval scheme. This binning procedure allows us to determine snowfall event occurrence and snowfall rate intensity populating the respective

GPROF T2m/TPW bins. The *a priori* database is also partitioned by snowfall type (e.g., shallow cumuliform versus deep cloud structures) to show systematic trends within the GPROF bins classified by snowfall morphology to illustrate how global snowfall is distributed among these important environmental parameters. Further partitioning by general surface type (land versus ocean) and geography indicate varying snowfall populations that comprise a complete near-global snapshot of widely varying snowfall regimes. Lastly, the preliminary GPM database is binned by T2m and TPW to compare against the CloudSat database to illustrate possible systematic differences between the snowfall populations contained in each respective dataset.

“A careful study of this internal structure not only reveals new and far greater elegance of form than the simple outlines exhibit, but by means of these wonderfully delicate and exquisite figures much may be learned of the history of each crystal, and the changes through which it has passed in its journey through cloudland. Was ever life history written in more dainty hieroglyphics!”

Wilson “Snowflake” Bentley on the structure of snowflakes

Popular Scientific Monthly (1898)

Dedicated to my parents, John and Karen Mateling:

Dad, thank you for always treating me as if I was the second smartest person in the world (after you). It's because of you that I aspire to be a great scientist.

Mom, thank you for always being excited about my accomplishments and never failing to support me. Even when I almost decided to become an accountant.

Thank you both for showing me the world and raising me to believe that I can make a difference.

Acknowledgements

Mark Kulie: For invaluable guidance, editing my writing or code even late into the night, and helping me grow into a scientist.

Tristan L'Ecuyer: For always making time to critique my work to ensure highest accuracy and quality.

Samantha Tushaus, Norm Wood, Lisa Milani, and Dave Randel: for providing data and assistance understanding it.

Colleagues in the Department of Atmospheric and Oceanic Sciences and the Space Science and Engineering Center

Lastly, my incredibly supportive parents, brothers and sister, friends, and boyfriend Patrick.

Acknowledgement is also made to NASA for support under grants #NNX12AQ76G (NASA New Investigator Program), #NNX13AG47G (NASA Precipitation Measurement Missions), and #NNX14AB22G (CloudSat/CALIPSO).

Contents

Abstract	i
Dedication	iv
Acknowledgements	v
Contents	vi
List of Figures	viii
Abbreviations	xi
1 Introduction	1
2 Background	5
2.1 CloudSat	5
2.2 GPM	10
2.3 Shallow Snowfall	13
3 Data	17
4 Methodology	21
5 Results	25
5.1 ERA-Interim-only Analysis	25
5.2 CloudSat vs. ERA-Interim Analysis	33
5.3 CloudSat Snowfall Database Analysis	47
5.3.1 Global Analysis	51
5.3.2 Shallow Cumuliform vs. Nimbostratus Snowfall	53
5.3.3 Land vs. Ocean Snowfall	56
5.3.4 Hemispheric Analysis	61
5.4 GPM vs. CloudSat Analysis	65
6 Conclusions	79

7 Future Work

List of Figures

2.1	Relative frequency of occurrence of shallow snowfall, adapted from Kulie et al. (2016). This data is from the CloudSat 2C-SNOW-PROFILE product from June 2006 to December 2010.	14
5.1	ERA-Interim annual mean snowfall accumulations from January 1979 to December 2013 in meters per year.	26
5.2	Deviations of annual mean snowfall accumulations of ERA-Interim from the 35-year mean shown in Figure 5.1. The individual years (2007-2010) shown are the years that CloudSat was fully operational.	28
5.3	The percent deviation from the 35-year mean of ERA-Interim snowfall during CloudSat’s operational years (2007-2010) used in this study.	30
5.4	The ERA-Interim snowfall trend plotted as the total global accumulation per year from January 1979 to December 2013.	31
5.5	ERA-Interim normalized cumulative zonal total snowfall rate and weighted zonal total snowfall rate (weighted by latitude area) from 1979 – 2013. The orbital boundaries for CloudSat and GPM are both marked as well.	32
5.6	Spatial comparison of CloudSat and ERA-Interim annual mean snowfall accumulations during CloudSat’s operational years, 2007-2010.	34
5.7	The difference (in meters) between the ERA-Interim accumulation and the CloudSat global snowfall accumulation datasets for CloudSat’s operational years, 2007-2010.	36
5.8	Zonal mean snowfall accumulation from January 2007 to December 2010 for both CloudSat (solid lines) and ERA-Interim (dashed lines). The annual mean over this time period is plotted, as well as the zonal mean for each year.	38
5.9	Scatter plots of the ERA-Interim versus CloudSat snowfall rates. The first plot is the 4-year mean, and the remaining are the individual years that CloudSat was operational, 2007-2010. Each point represents a single latitude×longitude ($1^\circ \times 1^\circ$) grid box’s snowfall rate.	40
5.10	Same as Figure 5.9, but now only plotting for grid boxes that have (i) more than 60% of snowfall occurrences from cumulus or stratocumulus clouds and (ii) more than 60% of the snowfall rate due to these shallow cumuliform events. This makes use of CloudSat’s 2B-CLDCLASS product, which classifies cloud type.	43

5.11	Same as Figure 5.9, but now plots every grid box that was not plotted in Figure 5.10. These “non-shallow” grid boxes may have shallow snowfall events and rates from shallow cumuliform clouds, but does not meet the criteria specified to be a “shallow” grid box.	46
5.12	All occurrences of snowfall when the two-meter temperature (T2M) is less than or equal to 255 K, the criterion for using the CloudSat database in the Day 1 version of the GPROF algorithm for GPM.	49
5.13	CloudSat snowfall occurrences, fraction of occurrence, and mean snowfall rate binned by 2-meter temperature (T2m) and total precipitable water (TPW). Data spans from June 2006 to December 2010 and represents the <i>a priori</i> database used for the Day 1 version of the GPROF algorithm.	52
5.14	Same as Figure 5.13, but now showing shallow snowfall events (left column) and snowfall events occurring from nimbostratus clouds (right column).	54
5.15	Same as Figure 5.13, but now showing over-land snowfall events (left column) and over-ocean snowfall events (right column).	57
5.16	Same as Figure 5.13, but now showing over-land shallow snowfall events (left column) and over-ocean shallow snowfall events (right column).	59
5.17	Same as Figure 5.13, but now showing over-ocean Northern Hemisphere snowfall events (left column) and over-ocean Southern Hemisphere snowfall events (right column).	62
5.18	Same as Figure 5.13, but now showing over-ocean Northern Hemisphere shallow snowfall events (left column) and over-ocean Southern Hemisphere shallow snowfall events (right column).	64
5.19	Comparison of the frequency of occurrence of snowfall as observed by CloudSat, the GPM Mean Scan (MS), the GPM Normal Scan (NS) and the GPM Ku-band.	66
5.20	Comparison of the relative frequency of occurrence, or fraction, of snowfall as observed by CloudSat, the GPM Mean Scan (MS), the GPM Normal Scan (NS) and the GPM Ku-band.	67
5.21	Comparison of the mean snowfall rate as observed by CloudSat, the GPM Mean Scan (MS), the GPM Normal Scan (NS) and the GPM Ku-band.	68
5.22	Comparison of the frequency of occurrence of snowfall as observed by CloudSat, the GPM Mean Scan (MS), the GPM Normal Scan (NS) and the GPM Ku-band. CloudSat’s orbit is now limited to be within $ 65 ^\circ$ latitude.	70
5.23	Comparison of the relative frequency of occurrence, or fraction, of snowfall as observed by CloudSat, the GPM Mean Scan (MS), the GPM Normal Scan (NS) and the GPM Ku-band. CloudSat’s orbit is now limited to be within $ 65 ^\circ$ latitude.	71
5.24	Comparison of the mean snowfall rate as observed by CloudSat, the GPM Mean Scan (MS), the GPM Normal Scan (NS) and the GPM Ku-band. CloudSat’s orbit is now limited to be within $ 65 ^\circ$ latitude.	72

5.25	Comparison of the frequency of occurrence of snowfall as observed by CloudSat, the GPM Mean Scan (MS), the GPM Normal Scan (NS) and the GPM Ku-band. CloudSat's reflectivity is limited to an approximately equivalent minimum detectable reflectivity.	73
5.26	Comparison of the relative frequency of occurrence, or fraction, of snowfall as observed by CloudSat, the GPM Mean Scan (MS), the GPM Normal Scan (NS) and the GPM Ku-band. CloudSat's reflectivity is limited to an approximately equivalent minimum detectable reflectivity.	74
5.27	Comparison of the mean snowfall rate as observed by CloudSat, the GPM Mean Scan (MS), the GPM Normal Scan (NS) and the GPM Ku-band. CloudSat's reflectivity is limited to an approximately equivalent minimum detectable reflectivity.	75
5.28	Comparison of the frequency of occurrence of snowfall as observed by CloudSat, the GPM Mean Scan (MS), the GPM Normal Scan (NS) and the GPM Ku-band. CloudSat's reflectivity is limited to an approximately equivalent minimum detectable reflectivity and its orbit is limited to be within $ 65 ^\circ$ latitude.	76
5.29	Comparison of the relative frequency of occurrence, or fraction, of snowfall as observed by CloudSat, the GPM Mean Scan (MS), the GPM Normal Scan (NS) and the GPM Ku-band. CloudSat's reflectivity is limited to an approximately equivalent minimum detectable reflectivity and its orbit is limited to be within $ 65 ^\circ$ latitude.	77
5.30	Comparison of the mean snowfall rate as observed by CloudSat, the GPM Mean Scan (MS), the GPM Normal Scan (NS) and the GPM Ku-band. CloudSat's reflectivity is limited to an approximately equivalent minimum detectable reflectivity and its orbit is limited to be within $ 65 ^\circ$ latitude.	78

Abbreviations

AMSR-E	A dvanced M icrowave S canning R adiometer - E OS
CESM	C ommunity E arth S ystem M odel
CMIP5	5th Phase of the C oupled M odel I ntercomparison P roject
CPR	C loud P rofilng R adar (aboard CloudSat)
DPR	D ual-Frequency P recipitation R adar (aboard GPM)
ECMWF	E uropean C entre for M edium-Range W eather F orecasts
ERA-Interim	E CMWF R eanalysis
GMI	G PM M icrowave I mager
GPM	G lobal P recipitation M easurement M ission
GPROF	G oddard P rofilng A lgorithm
MERRA	M odern- E ra R etrospective A nalysis for R esearch and A pplications
MHS	M icrowave H umidity S ounder
MS	M ean S can
NCEP	N ational C enters for E nvironmental P rediction
NEXRAD	NEX t G eneration RAD ar
NMQ	N ational M ulti-Sensor M osaic Q PE
NS	N ormal S can
SSMIS	S pecial S ensor M icrowave I mager/ S ounder
T2m	T emperature at 2 M eters
TPW	T otal P recipitable W ater
TRMM	T ropical R ainfall M easuring M ission

V3 **V**ersion **3** (of DPR-derived precipitation rates)
WSR-88D **W**eather **S**urveillanc**e** **R**adar **1988** **D**oppler

Chapter 1

Introduction

Snowfall events are potentially high-impact weather events that have significant socio-economic impacts. Falling snow and its accompanying seasonal accumulated snowpack is also important from an Earth systems science standpoint, as it alters the Earth's radiative balance (Waliser et al., 2011) and plays a critical role in the hydrological cycle. While snowfall is mostly limited to high latitudes and mountainous regions, snowfall measurements are becoming increasingly important considering compelling evidence that high latitudes are extremely sensitive to a warming climate (Hinzman et al., 2005, Luckman et al., 2006, Stroeve et al., 2012). The scientific community has been undertaking global snowfall measurements for decades now, but sparse measurements in remote areas as well as the general difficulty of making accurate snowfall measurements devalue traditional ground-based observational means to properly quantify global snowfall. Turbulence in the surface boundary layer can alter snow depth and affect accumulation measurements;

microphysical properties of snow that vary and depend on environmental parameters can affect the amount of accumulation and complicate remote sensing signatures associated with falling snow. Snowfall also originates from different types of cloud structures that can dominate regional annual accumulations. For example, depending on the vertical extent of precipitating cloud structures and the physical process by which snow particles form, a snowfall event could be defined as either “deep” or “shallow convective.” Because these different modes of snowfall have varying impacts on the public and possibly unique remote sensing fingerprints, identifying specific types of snowfall could lead to better measurements of snowfall and improved forecasting by representing different snowfall modes more realistically within numerical weather models.

Snowfall measurements have greatly improved beyond use of precipitation gauges. The introduction of RADio Detection and Ranging (RADAR) and passive microwave retrievals has led to greater spatio-temporal coverage of measuring precipitation, both liquid and frozen. In a matter of decades, spaceborne radar retrievals have further improved spatio-temporal coverage of precipitation estimates, especially snowfall in the remote higher-latitudes. CloudSat’s Cloud Profiling Radar (CPR) is an example of spaceborne radar used for detecting and estimating amounts of snowfall. In order to reduce uncertainty with these estimates, microwave radiometer retrievals have been paired with radar retrievals synergistically in the radiometer-only Goddard Profiling (GPROF) algorithm. The microwave radiometer and radar making these observations were both placed onboard the Global Precipitation Measurement (GPM) Core Observatory, which launched in February 2014. Spaceborne estimates of snowfall have become invaluable to researchers, as

these datasets have become the best available measurements to quantify global snowfall through observational means. Improving snowfall retrievals from these instruments must be a top priority in order to continue ensuring spaceborne snowfall retrievals are as accurate as possible.

While the satellite snowfall retrievals are a major advancement in precipitation measurements, there is still room for improvement with satellite instruments. Different modes of snowfall have different microwave scattering and emission signatures and thus produce unique multi-frequency brightness temperatures measured by GPM's spaceborne radiometer. Because GPM uses a radiometer-only algorithm as both its primary precipitation retrieval tool and to provide consistent radiometer-only precipitation estimates from GPM affiliated constellation satellites with microwave radiometers, these unique vectors of brightness temperatures associated with diverse snowfall events help to populate a growing data record that holds promise to improve high latitude precipitation retrievals. However, physical limitations of the radar on GPM can cause the GPM radiometer algorithm to inaccurately assign lightly precipitating snowfall event as a non-precipitating event. For this reason, this research looks at the radiometer-only Goddard Profiling (GPROF) algorithm to assess the various databases used to assign precipitation retrievals in the early part of the operational GPM mission. A CloudSat snowfall database comprised of coincident microwave radiometer observations collected in the pre-GPM era will be therefore utilized to characterize global snowfall in meaningful ways to assess and improve GPM's snowfall retrieval capabilities. Independent evaluations of spaceborne snowfall estimates with global reanalysis datasets will also be undertaken to assess the

veracity of spaceborne snowfall datasets. All of these activities will address high priority steps to improve GPROF snowfall retrievals, identify potential high latitude precipitation retrieval deficiencies, and strive to make the GPROF as accurate as possible in order to maximize GPM's scientific value for snowfall measurements.

Chapter 2

Background

2.1 CloudSat

The first spaceborne W-band (94-GHz) radar is the nadir-pointing CPR onboard NASA's CloudSat satellite. Since CloudSat's launch in 2006, the CPR measurements have been used to make precipitation estimates (Ellis et al., 2009, Kulie and Bennartz, 2009, Liu, 2008). Thanks to CloudSat's high orbital extent of $|\pm 82|^\circ$ latitude, the global picture of snowfall is more complete with these precipitation estimates (Kulie et al., 2016). In addition to providing near-global spatial coverage, the CPR has a minimum detectable radar reflectivity of approximately -29 dBZ and is consequently sensitive to lighter precipitation events (Tanelli et al., 2008). This high sensitivity affords the CPR the ability to detect non-precipitating clouds (Stephens et al., 2002). CloudSat is a part of NASA's

afternoon constellation, or “A-Train”, and thus its observations can be paired with near-coincident observations from other satellites, including valuable passive microwave observations from the Advanced Microwave Scanning Radiometer-Earth Observing System (AMSR-E). CloudSat’s official snowfall rate product, the 2C-SNOW-PROFILE product (Wood et al., 2013), converts radar reflectivity (Z) to snowfall rate (S) and is used in this research.

CloudSat’s multi-year snowfall estimates have been compared against other observed and modeled snowfall datasets in the past. Hiley et al. (2011) tested the accuracy of CloudSat’s snowfall retrievals against ground-based snow gauge measurements in Canada. The CloudSat snowfall estimates were more accurate in higher-latitudes due to greater temporal sampling and greater likelihood of precipitation being frozen versus potentially mixed precipitation associated with warmer temperatures (Hiley et al., 2011). The authors noted the difficulty in comparing CloudSat observations to ground-based observations due to spatial limitations as well as the fact that there is not a universally applicable Z - S relationship, which is a mathematical relationship between radar reflectivity and snowfall rate. Despite the inherent Z - S uncertainties related to single-frequency radar snowfall retrievals, there have been several analyses performed comparing ground-based observations of snowfall to CloudSat’s snowfall estimates.

CloudSat's 2C-SNOW-PROFILE product was first compared against the National Multi-Sensor Mosaic QPE System (NMQ) in Cao et al. (2014). NMQ heavily utilizes the Next-Generation Radar (NEXRAD) scanning radar network that operates at longer wavelengths than CloudSat. CloudSat is found to detect light snowfall events approximately 90% of the time, though it is less accurate at assigning snowfall rates as the rates increase. However, the authors state that NMQ does not detect light snowfall as well as CloudSat and, consequently, CloudSat may be even better at detecting light snowfall than their results suggest. According to Cao et al. (2014), CloudSat's accuracy begins to degrade at snowfall rates above 1 mm h^{-1} ; above 5 mm h^{-1} , it degrades heavily. One cause for CloudSat versus NMQ discrepancies at higher snowfall rates is W-band attenuation (shorter wavelength radars are more susceptible to gaseous and hydrometeor attenuation). Additionally, non-Rayleigh scattering effects can cause reflectivity to be underestimated. This attenuation most likely causes CloudSat to underestimate these heavier-precipitating snowfall events.

A 4-year comparison study by Smalley et al. (2014) between CloudSat and the National Centers for Environmental Prediction (NCEP) Stage IV observed dataset, which is a merged dataset of Weather Surveillance Radar-1988 Doppler (WSR-88D) radar and rain gauge measurements. The results showed that CloudSat more frequently observes precipitation, especially when it is light or frozen. The best agreement between datasets was in the southeast United States where precipitation events were relatively heavier and observational ground coverage was less sparse. Lastly, they conclude that CloudSat performs better than the NCEP Stage IV dataset when near-surface temperatures are below freezing (Smalley et al., 2014).

Norin et al. (2015) compared CloudSat’s 2C-SNOW-PROFILE product to a ground-based network of radars in Sweden. The results showed more agreeable snowfall rates in the range of $0.1 - 1.0 \text{ mm h}^{-1}$ as well as when CloudSat’s observations were made closer to a ground-based radar. Above 1 mm h^{-1} , CloudSat has difficulty assigning precipitation rates, the same snowfall rate identified in Cao et al. (2014). Both observation platforms are prone to missing shallower snowfall events: ground-based scanning radars overshoot these structures when they are too far from the radar site, and CloudSat could miss shallow snowfall due to ground clutter (Maahn et al., 2014).

Based on these studies, further comparative analyses between CloudSat’s snowfall estimates and independent datasets are warranted to gauge how differently an observational and modeled dataset can be. In order to perform a global analysis of snowfall, the European Centre for Medium-Range Weather Forecasts (ECMWF) global atmospheric reanalysis (ERA-Interim) model output is used. Since 2011, ERA-Interim output is available from January 1979 to the present (Berrisford et al., 2011) and is a well-vetted reanalysis product, though there remains uncertainty with its precipitation output (Simmons et al., 2010). Despite this, the ERA-Interim product has an updated and improved hydrological cycle since the preceding ECMWF reanalysis product, ERA-40 (Dee et al., 2011, Lorenz and Kuntzmann, 2012). Comparing the CloudSat snowfall dataset to a trusted reanalysis dataset aids in identifying any biases between the two independent datasets.

ERA-Interim, like CloudSat, can provide information about snowfall in remote regions, such as higher latitudes. Screen and Simmonds (2012) analyzed snowfall in the Arctic

using ERA-Interim output and station observations in Canada. While they state that ERA-Interim's snowfall output may not be as accurate as its temperature output, they conclude that there are declining snowfall occurrences in the Arctic, while precipitation amounts haven't changed (i.e. more rain than snow). This result, they state, has likely contributed to the amplification of the warming Arctic (Screen and Simmonds, 2012) and further motivates more studies of snowfall at high latitudes.

Palerme et al. (2014) performed a comparison study of CloudSat snowfall rates and ERA-Interim accumulations in Antarctica from August 2006 to April 2011, similar to the comparison done in this study. CloudSat's annual snowfall estimates generally exceeded the ERA-Interim accumulations, though the opposite was true in regions with less precipitation. CloudSat may have missed very shallow precipitation and was less accurate in the interior regions of Antarctica, but overall the snowfall estimates were determined to be very similar to ERA-Interim.

The analysis by Palerme et al. (2014), while encouraging in its finding that CloudSat and ERA-Interim snowfall estimates are not too different, is limited to just the Antarctic region. This study will expand upon the Palerme et al. (2014) CloudSat and ERA-Interim comparison by performing a similar analysis of snowfall on a global-scale to identify any consistent regional biases in the two snowfall datasets. Different regions will have varying environmental and atmospheric characteristics that may change snowfall mode. A global analysis of snowfall is useful because CloudSat's entire snowfall dataset is used

(at very cold near-surface temperatures) for estimating precipitation in the radiometer-only GPROF precipitation retrieval algorithm, and independent CloudSat-only retrievals have not, to date, been evaluated with ERA-Interim results globally.

2.2 GPM

The Global Precipitation Measurement (GPM) Core Observatory launched in February 2014 with a scanning Dual-Frequency Precipitation Radar (DPR) and GPM Microwave Imager (GMI) onboard. GPM flies in the GPM Mission constellation, which is comprised of several other research and operational satellites and with the goal of improving spaceborne precipitation measurements. The DPR operates at 13-GHz (Ku-band) and 35-GHz and is the first spaceborne dual-frequency radar, and the GMI is a conical-scanning radiometer whose 13 channels range from 10 to 183 GHz (Hou et al., 2014). GPM orbits up to $|65|^\circ$ latitude, affording it latitudinal coverage up to the Arctic and Antarctic circles. The minimum detectable reflectivity of the Ka-band (Ku-band) DPR is approximately 13 (18) dBZ, making it less prone to attenuation than the CPR, but also less sensitive to very light precipitation (Hou et al., 2014).

GPM uses the Goddard Profiling (GPROF) precipitation retrieval algorithm, which utilizes an empirical *a priori* database of coincident brightness temperatures and radar reflectivities to observe a precipitation rate and its associated vertical structure (Kummerow et al., 2015, 2011). The radar component of these databases was used only to (1) assess whether a given multi-frequency radiometer observation was associated with

possible precipitation and (2) if so, assign a quantitative precipitation estimate using a Z-R (radar reflectivity – rain rate) or Z-S relationship.

The Tropical Rainfall Measuring Mission (TRMM), GPM’s predecessor, also used a version of the GPROF algorithm, though its orbital extent of $|35|^\circ$ latitude prevented it from frequently observing snowfall. The newest version of the GPROF to be created using a GMI/DPR database will be fully parametric (Kummerow et al., 2015). This Bayesian inversion methodology employed minimizes the error by also searching the database for empirical, near-matching physical and environmental parameters. For “Day 1” of GPM’s retrievals, the GPROF algorithm used databases comprised of *a priori* coincident measurements from CloudSat/AMSR-E/MHS (for very cold surfaces), NEXRAD/SSMIS (over land), and TRMM (everywhere else) as well as surface emissivity and ERA-Interim 2-meter temperature (T2m) and total precipitable water (TPW). This database is limited to very cold ($T2m \leq 255$ K) surfaces because CloudSat is subject to erroneous measurements (such as attenuation or multiple scattering effects) when precipitation is heavy (Cao et al., 2014, GPROF ATBD, cited 2016, Norin et al., 2015). However, light precipitation does occur at warmer temperatures and heavy precipitation does occur at cold temperatures. After approximately one year of GPM measurements were collected, the DPR and GMI measurements replaced these databases with its own self-consistent *a priori* database. Additionally, the Day 1 GPROF algorithm will eventually be replaced by the fully parametric Version 1 of the GPROF 2016 to be used by other satellite radiometers in the GPM constellation (Kummerow et al., 2015).

For very cold surfaces, i.e. an ad hoc T2m threshold less than or equal to 255 K, the GPROF searched a database of AMSR-E/MHS brightness temperature vectors to match to the observed (GMI) brightness temperature vector (GPROF ATBD, cited 2016). AMSR-E brightness temperatures approximately match the lower frequency GMI channels, and the MHS brightness temperatures approximately match the higher frequency GMI channels. To optimize retrievals, the database also searched for similar T2m and TPW provided by CloudSat's ECMWF-AUX product as well as surface emissivity type. After finding the best match, the GPROF algorithm assigned a CloudSat-derived precipitation rate if and only if there was an associated precipitation event. The CPR radar reflectivities would not match exactly those measured by the DPR, as the two instruments operate at different frequencies. Similarly, the AMSR-E and MHS channels are not exact replicas of the GMI channels, but are close enough to simulate the GMI in the GPROF during Day 1 (Hou et al., 2014). Since the GPROF is a radiometer-only algorithm, the large discrepancy between the DPR and CPR operating frequencies will only affect the rate of precipitation, not the identification of it (differences in minimum detectable reflectivities between the two radar notwithstanding). In other words, the GMI is well simulated by the AMSR-E and MHS channels, and thus the brightness temperature vector used to search the databases would not be so different. Because CloudSat and AMSR-E are in the A-Train constellation together, the measurements from each are approximately coincident.

2.3 Shallow Snowfall

CloudSat has not only provided useful global snowfall estimates, but its product suite has been exploited to partition global snowfall events between different snowfall modes, such as shallow convective versus deeper snowfall associated with mid-latitude synoptic weather systems. Kulie et al. (2016) separates CloudSat snowfall events by using cloud types from the CloudSat 2B-CLDCLASS product to present a global snowfall census of shallow cumuliform snowfall. Shallow cumuliform snowfall is identified as snowfall from cumulus or stratocumulus clouds, as those have been shown more likely to have relatively lower cloud-top heights in the CloudSat dataset (when compared to nimbostratus clouds, for example; Kulie et al. (2016)). Additionally, shallow snowfall events have relatively lower reflectivities with potentially different microphysical composition and radiometric signatures compared to deeper snowfall events (Kulie et al., 2016). While the GPM GMI may observe distinct radiometric responses associated with shallow convective snow events, the DPR's relatively high minimum detectable reflectivity may cost it the ability to observe these systematically lighter snowfall events. However, CloudSat's CPR has proven its ability to detect these events (Cao et al., 2014, Kulie et al., 2016). Shallow precipitating structures occur in mid- and high-latitudes and can be in the form of lake-effect snow, orographic snow, or snow from shallow Arctic mixed-phase clouds. Note that not all shallow snowfall events are lightly precipitating, and not all deep snowfall events are heavily precipitating.

Figure 2.1, adapted from Kulie et al. (2016), displays the high relative frequency of

occurrence of shallow snowfall over ocean, especially in the mid-latitudes. The fact that CloudSat identifies some regions are dominated by shallow snowfall demonstrates the importance of accurately detecting and measuring these types of events. Due to the shallow structure of some precipitating events, ground-based scanning radar networks can overshoot and underestimate the intensity or spatial extent of a shallow precipitating cloud. For this reason, spaceborne instruments have been used in the past to more accurately capture the spatial as well as vertical extent of shallow precipitating structures. A shallow rainfall estimate census study similar to the Kulie et al. (2016) census was done previously using the Tropical Rainfall Measuring Mission (TRMM) Precipitation Radar (Liu and Zipser, 2009, Schumacher and Houze, 2003, Short and Nakamura, 2000) as well as with CloudSat (Lebsock and L'Ecuyer, 2011, Lebsock et al., 2011, Rapp et al., 2013). This

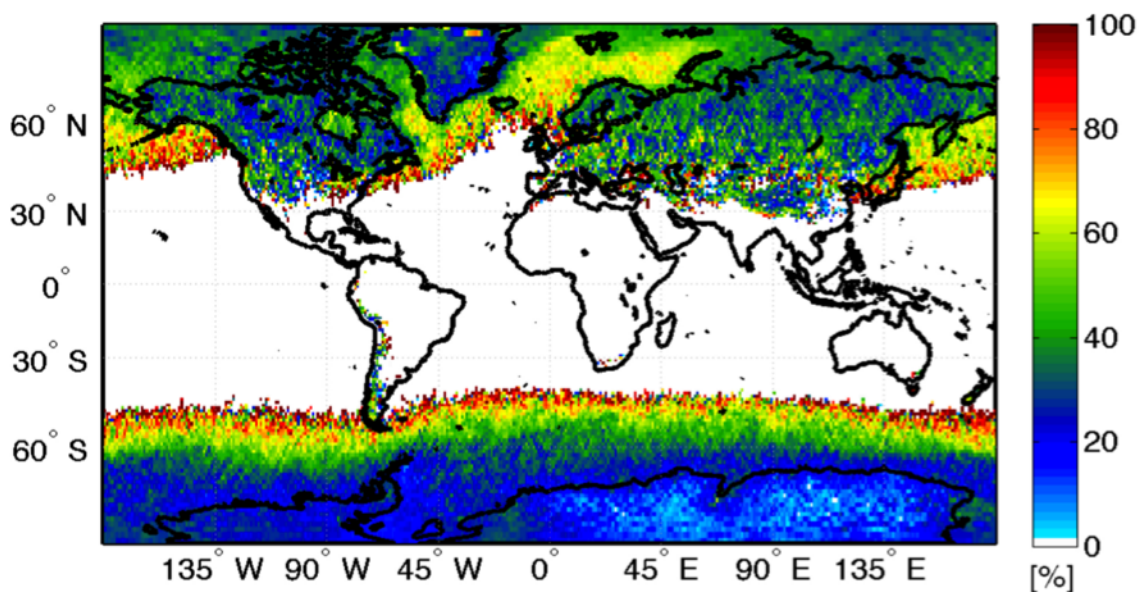


FIGURE 2.1: Relative frequency of occurrence of shallow snowfall, adapted from Kulie et al. (2016). This data is from the CloudSat 2C-SNOW-PROFILE product from June 2006 to December 2010.

study aims to compare the Day 1 GPROF and its associated CloudSat/AMSR-E/MHS database against the succeeding version of the GPROF and its associated GMI/DPR database in their ability to detect specific snowfall modes, especially shallow cumuliform snowfall cases.

During the Day 1 GPROF era, when GPM observations are associated with $T2m \leq 255$ K, the vector of brightness temperatures measured by the GMI will be best-matched to a vector of brightness temperatures within the *a priori* database (i.e. from AMSR-E and MHS). The cold surface temperature limit was chosen due to CloudSat attenuation that occurs with heavily precipitating events (Cao et al., 2014, GPROF ATBD, cited 2016). This procedure works to minimize the error between each frequency's database brightness temperature and measured brightness temperature. After optimizing by also matching T2m, TPW, and surface type, the GPROF will assign an associated (CPR-derived) snowfall rate if these search criteria had previously been matched to a snowfall rate. This vector of brightness temperatures thus plays a very important role in the assignment of precipitation rates. After Day 1, when the database of DPR/GMI retrievals is being used by GPROF, a shallow snowfall event (or any snowfall event) that has radar reflectivity below 12 dBZ may not be assigned a precipitation rate because the DPR will not have detected it. Therefore, a final comparison of the two different databases will be performed to identify any systematic differences in the way snowfall rates would be assigned.

This work is motivated by several factors. Shallow snowfall, while sometimes too light

for detection, is an important component of Earth's hydrologic cycle. Additionally, the GPROF retrieval algorithm for GPM's first year uses several empirical, *a priori* databases to assign precipitation rates, including a CloudSat/AMSR-E/MHS database for very cold surfaces. While GPM's dual-frequency radar and scanning instruments are great improvements on spaceborne instruments, CloudSat's larger orbital extent and more sensitive radar can provide important global snowfall context to assess and improve GPM snowfall retrievals.

The primary goals of this study are:

1. Analyze extended ERA-Interim datasets to highlight model-derived global snowfall estimates and establish a baseline climatological perspective of the CloudSat snowfall database time period.
2. Independently evaluate the CloudSat 2C-SNOW-PROFILE product against the ERA-Interim snowfall dataset.
3. Analyze the CloudSat 2C-SNOW-PROFILE dataset through the lens of the GPROF retrieval scheme (i.e. using the environmental parameters that the GPROF uses for retrieval optimization).
4. Compare the preliminary GPM snowfall database to the CloudSat snowfall database to assess any systematic differences in the respective global snowfall datasets.

Chapter 3

Data

This study employs the following three primary data sources: ERA-Interim reanalysis data, CloudSat data products (e.g., 2C-SNOW-PROFILE, 2B-CLDCLASS, and ECMWF-AUX), and GPM data products. This section provides a brief overview of each respective data product, while the following section describes methodological steps taken to synthesize and analyze merged datasets.

Global snowfall accumulations from the ERA-Interim reanalysis dataset is analyzed both independently, as well as against CloudSat-derived annual snowfall accumulations. The reanalysis is a run of the ECMWF model that uses multiple observational streams to nudge model output in the right direction. The data downloaded are 3-hourly snowfall accumulations and meteorological conditions that are used to optimize the GPROF retrievals (T2m and TPW). For the ERA-Interim-only analysis (section 1 of the results),

a grid size of $0.75^\circ \times 0.75^\circ$ is used; for the comparison against CloudSat (section 2 of the results), ERA-Interim’s higher resolution gridded dataset is interpolated to a $1.0^\circ \times 1.0^\circ$ resolution to accommodate direct comparisons with CloudSat gridded data fields. The data are downloaded at 12-hour time steps at 00Z and 12Z analysis times. For reproduction, the data used in this study are downloaded from the ECMWF data portal (<http://apps.ecmwf.int/datasets/data/interim-full-daily/levtype=sfc/>).

A separate CloudSat database is used for sections 2 and 3 of this research. In section 2, which compares ERA-Interim and CloudSat snowfall on an annual timescale, a $1.0^\circ \times 1.0^\circ$ CloudSat snowfall dataset is used (Kulie et al., 2016). This dataset contains annual mean accumulations of snowfall per latitude/longitude grid box derived from CloudSat 2C-SNOW-PROFILE instantaneous snowfall rates from orbital swath data (Wood et al., 2013). Section 3 uses this orbital swath data, but just uses the instantaneous snowfall rates from 2C-SNOW-PROFILE. This orbital swath data extends to $|82|^\circ$ latitude, as that is CloudSat’s boundary, and is made up of ~ 46 million possible snowfall entries. This product uses CPR reflectivities to estimate vertical profiles of snowfall rate (240 m vertical data bin spacing and ~ 1.5 km spatial footprint) as well as near-surface snowfall. To avoid errors caused by ground clutter (Kulie and Bennartz, 2009, Maahn et al., 2014), the surface snow is calculated using estimated snow properties from a near-surface data bin defined as the third CPR bin above ground level (AGL) over ocean and the fifth bin AGL over land surfaces. These snow properties are derived using *a priori* cloud microphysical information obtained from field campaign observations to better constrain snowfall rates retrieved in an optimal estimation algorithm. The 2C-SNOW-PROFILE

algorithm uses particle size distribution to choose a Z-S relationship, which converts CPR reflectivities to snowfall rates (Wood et al. 2014, Wood et al. 2015). This product is the first spaceborne radar snowfall retrieval scheme, thus making it very valuable to global snowfall research.

The CloudSat 2B-CLDCLASS product is used to identify cloud types and thus for separating out different snowfall modes. This product uses a combination of CPR-measured reflectivity features, a precipitation flag, ECMWF-derived meteorological conditions, surface topography, and rules governing hydrometeors to identify cloud type (Sassen and Wang, 2008). This product is used for identifying cumulus, stratocumulus, nimbostratus, and other types of clouds. Cumulus and stratocumulus, or “cumuliform”, clouds are both systematically shallower and lighter-snowing than nimbostratus clouds (Kulie et al., 2016), and thus can be filtered out to determine conditions in which CloudSat sees this unique snowfall mode.

CloudSat’s ECMWF-AUX product provides T2m and TPW data coincident with the 2C-SNOW-PROFILE and 2B-CLDCLASS data. These parameters, as well as surface emissivity, are matched in order to optimize the GPROF retrievals. CloudSat’s 2C-SNOW-PROFILE snowfall rates and the coincident ECMWF-AUX T2m and TPW are used in the CloudSat database for the Day 1 version of the GPROF algorithm, which is accessed when $T2m \leq 255$ K. All three of these CloudSat products are orbital swath data and can be downloaded from the CloudSat Data Processing Center (<http://cloudsat.atmos.colostate.edu/data>).

A GPM-affiliated Colorado State University group provided the GPM measurements and products used in this study. The data used are the Version 3 (V3) DPR-derived snowfall rates, which covers April 2014 to March 2015. The products are the Ku-band retrieval, the mean scan (MS) Ku- and Ka-band Combined Product, and the normal scan (NS) Ku Combined Product. The MS is 25 pixels wide and the NS is 49 pixels wide. The precipitation used is the frozen precipitation variable. Each pixel is assigned a precipitation rate and is then averaged over a GMI footprint, and thus the frozen precipitation may include mixed precipitation as well.

Chapter 4

Methodology

This research aims to evaluate the CloudSat snowfall dataset and compare the separate CloudSat and GPM databases used for the GPROF precipitation retrieval algorithm over very cold surfaces. First, the ERA-Interim global snowfall dataset is independently evaluated to establish a climatology of snowfall since 1979. Next, the CloudSat 2C-SNOW-PROFILE dataset is introduced and compared to ERA-Interim's snowfall output. Then, the CloudSat database (i.e. what is used for GPM GPROF Day 1 retrievals) is analyzed based on meteorological conditions and from a regional perspective. Lastly, the new GPM snowfall database is compared against CloudSat to identify any systematic differences between the datasets.

Section one will focus only on ERA-Interim's snowfall dataset. ERA-Interim is a well-vetted reanalysis product that has snowfall data available since 1979. Initially, a climatological analysis of the ERA-Interim snowfall dataset from January 1979 to December 2013 is performed. Preparing for a comparison to CloudSat's snowfall dataset and to provide climatological context to better interpret the multi-year CloudSat snowfall products, the annual mean accumulations for 2007-2010 are found, as well as the deviation from the 1979-2013 mean. While ERA-Interim provides global snowfall data, it is still subject to errors and thus cannot be considered perfect. For the purposes of this study, however, it is used as a comparative tool for the CloudSat snowfall dataset.

The second section is a near-global evaluation of CloudSat's snowfall dataset. Both qualitative and quantitative comparisons of CloudSat and ERA-Interim annual accumulation are performed during full years of CloudSat's operation, 2007-2010. This is done statistically (i.e. finding a bias and other statistical measures between annual snowfall accumulations) as well as regionally per latitude/longitude grid box. Using CloudSat's 2B-CLDCLASS product, each latitude/longitude grid box is identified as either predominantly shallow (based on if the cloud type is cumulus or stratocumulus) or non-shallow snowfall for both CloudSat and ERA-Interim. Because neither dataset is perfect, this comparison is meant to simply gauge how CloudSat's snowfall dataset compares to other datasets available.

The next section of this research focuses specifically on how CloudSat's snowfall would be assigned through the GPROF algorithm. Snowfall occurrences are binned by T2m and

TPW in order to analyze the entire population of CloudSat-identified snowfall events during the 4.5-year dataset (June 2006 – December 2010). Again making use of CloudSat’s 2B-CLDCLASS product, this binning can also be done for different snowfall modes (shallow cumuliform versus nimbostratus events). This process is repeated for over-ocean only, over-land only, northern hemisphere ocean, and southern hemisphere ocean (all events as well as shallow events). Snowfall from nimbostratus clouds, which are systematically deeper in vertical height than cumulus or stratocumulus clouds (Kulie et al., 2016), is also binned by T2m and TPW. Lastly, this same binning procedure is performed to show (instead of occurrences) mean snowfall rate. This analysis of CloudSat shows how regional or meteorological differences can change how CloudSat identifies a snowfall event and assigns it a precipitation rate. This exhaustive analysis of CloudSat snowfall through the perspective of environmental parameters demonstrates the wide range of environments where CloudSat has identified snowfall. It is this analysis that leads into a comparison with GPM’s DPR-derived snowfall.

The fourth and final section of the thesis is to compare a preliminary GPM database against the CloudSat database analyzed in the previous section. This comparison will help identify biases in either dataset by determining under what environmental conditions each instrument observes snowfall. In other words, this section aims to see how the GPROF algorithm would assign snowfall rates during the Day 1 GPROF era (using CPR-derived snowfall rates) and after Day 1 (using DPR-derived snowfall rates). GPM does not have a product that allows for separation of snowfall modes, and therefore CloudSat’s database can only be compared for all types of snowfall. After a comparison of all snowfall,

the CloudSat database is limited to see only what is captured by CloudSat within a $|\pm 65|^\circ$ latitude orbit. Next, the CloudSat database is limited to have an approximately equivalent minimum detectable reflectivity. This CPR-DPR reflectivity equivalent is approximate because the CPR is a W-band radar and the DPR has Ku- and Ka-band radars. A proxy of 5 dBZ is chosen to be an approximately equivalent minimum detectable signal for limiting CloudSat's database. Lastly, CloudSat's database is limited by both orbit and minimum detectable reflectivity to make the comparison as direct as possible. These results will show any differences in how the DPR and CPR assign snowfall rates based on meteorological conditions, which are the parameters for the GPROF algorithm.

Chapter 5

Results

5.1 ERA-Interim-only Analysis

The ERA-Interim snowfall dataset from January 1, 1979 to December 31, 2013 is first analyzed to understand how snowfall looks from a global climatological perspective and to provide critical context for the shorter duration CloudSat snowfall dataset that spans from 2006-2010. In Figure 5.1, the annual mean ERA-Interim liquid water equivalent snowfall accumulation is shown on a global map. Snowfall accumulation occurs mostly at higher latitudes due to colder atmospheric temperatures allowing snow formation. Mountainous regions, such as the Rockies in North America, the Himalayas in Asia, and the Andes in South America, have relatively higher annual snowfall accumulations between ~ 0.25 - 0.5 m yr^{-1} likely due to orographic (or topographically-forced) snowfall. The southeast coast of Greenland and coastal Antarctica also show higher mean accumulations exceeding

ERA-Interim Annual Mean Snow Accumulation (1979 – 2013)

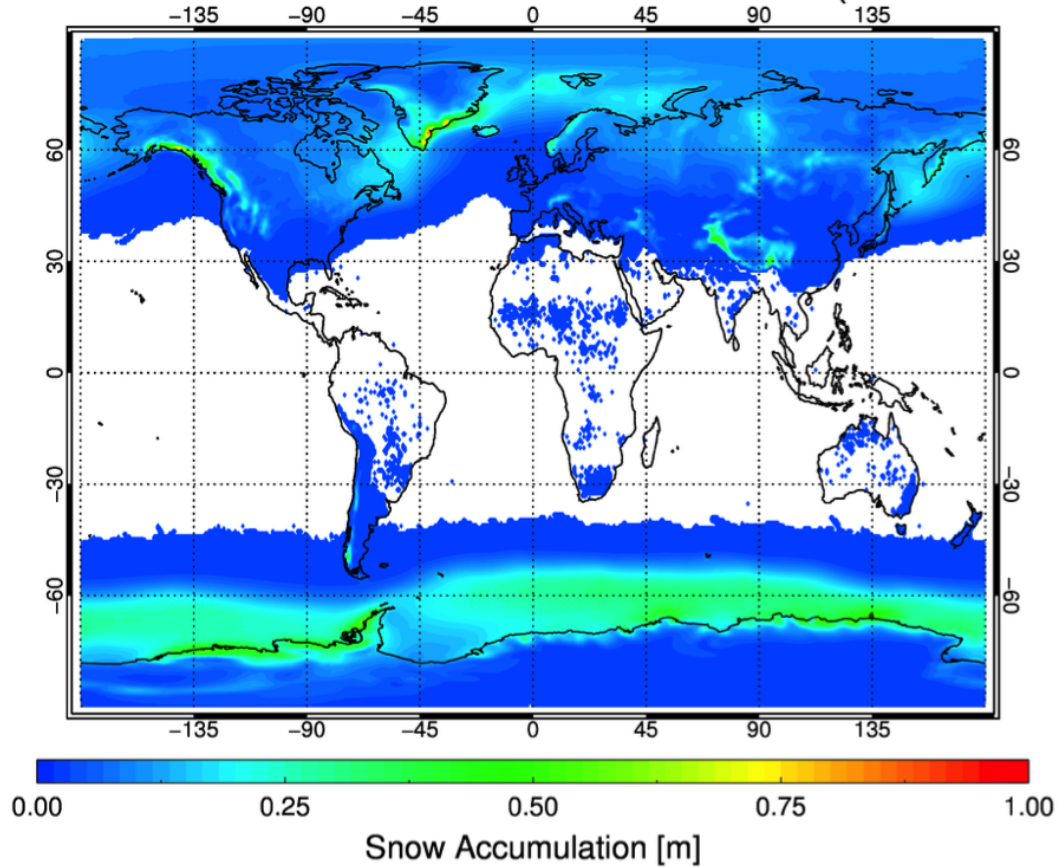


FIGURE 5.1: ERA-Interim annual mean snowfall accumulations from January 1979 to December 2013 in meters per year.

0.25 m yr⁻¹. Interestingly, inland East Antarctica has very little annual accumulation and is the only large-scale cold region exhibiting negligible snowfall accumulation over the entire globe. Over this 35-year period, the global maximum of mean accumulation is 0.873 m yr⁻¹ and occurs in Southeast Greenland. This region systematically has the highest global snowfall accumulation per year, with 1995 having the lowest maximum global accumulation value (0.88 m yr⁻¹) and 2003 having the highest (1.84 m yr⁻¹).

The separate hemispheres also show different characteristics due to the difference in land

coverage: the Southern hemisphere has much more ocean, which is a source of water vapor for snow formation. The northern hemisphere shows a lower latitudinal boundary for snowfall accumulations that looks similar to the typical mid-latitude storm track that is strongly influenced by land masses and ocean currents. The Southern hemisphere has a zonal upper latitude limit for snowfall accumulation (except for the Andes and New Zealand), just as the ocean currents have zonal flow through the Antarctic Circumpolar Current. According to the 35-year global mean ERA-Interim weighted accumulation, $\sim 45.7\%$ of snowfall occurs in the Northern Hemisphere, while the Southern Hemisphere receives the remaining $\sim 54.3\%$. The non-weighted (by latitude area) amount of snowfall that falls in the Northern and Southern hemispheres are $\sim 46.5\%$ and $\sim 53.5\%$, respectively. These regional characteristics allow for easy qualitative comparison to the CloudSat 2C-SNOW-PROFILE dataset in the next section.

The CloudSat data used in this study is available from June 2006 to December 2010, so quantitative annual comparisons against the ERA-Interim dataset are performed between January 2007 and December 2010 (see Section 5.2 of the Results). Data is still available through 2016, as CloudSat is still operational, but the 2006 – 2010 dataset was chosen for two reasons: (i) near-coincident AMSR-E observations were available during this time, which allowed the coincident radar/radiometer dataset to be constructed for GPM GPROF purposes and (ii) CloudSat experienced battery anomalies in 2011 that led to long data outages and an eventual transition to daylight-only operations. Figure 5.2 shows each individual year’s ERA-Interim snowfall accumulation deviation from the 35-year mean (shown in Figure 5.1). For all years except 2007 (which was a sea-ice minimum

ERA-Interim: Snowfall deviation from 1979-2013 Annual Mean

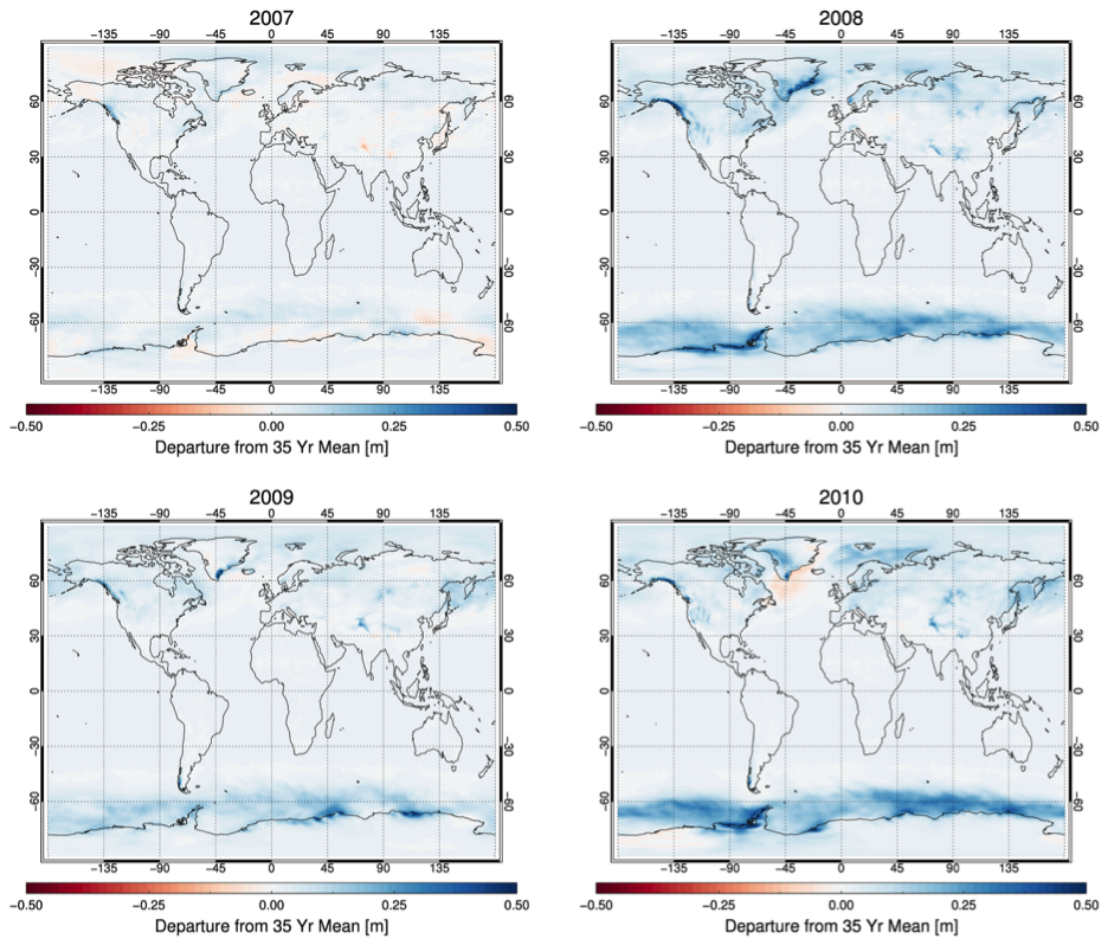


FIGURE 5.2: Deviations of annual mean snowfall accumulations of ERA-Interim from the 35-year mean shown in Figure 5.1. The individual years (2007-2010) shown are the years that CloudSat was fully operational.

year; Comiso et al. 2008), the regions that have higher annual mean accumulation show that snowfall accumulation is actually greater than the climatological mean. The Rocky Mountains, coastal Antarctica and Greenland, and the Southern Ocean have especially higher deviations of ~ 0.5 m from the mean. Seemingly, the only pronounced negative deviation from the mean occurs in the Atlantic Ocean southeast of Greenland in 2010, Other regions display distinct negative snowfall accumulation anomalies of lesser magnitudes in

2007: Alaska and Arctic Ocean north of Alaska, Atlantic Ocean north of Scandinavia, Himalaya Mountains, and some Southern Ocean regions near Antarctica. In fact, 2007 was the year with the highest global negative deviation from the mean (0.169 m below average) during the CloudSat observational period considered in this study. The highest positive global deviation from the mean occurred in 2008 (0.771 m above average). These images show that regions that generally have higher snowfall accumulations (based on the 35-year mean) experienced anomalously higher snowfall accumulations during CloudSat's early operations.

To analyze the difference between the mean and individual years' snowfall accumulation in more depth, the percent deviation from the mean is shown in Figure 5.3. The largest negative value achievable is -100%, which means that there is a mean snowfall value in the grid box but there was no accumulation for the given year. Across the years, there are very large percent deviations from the mean in isolated regions that typically receive small amounts of snowfall, with the lowest maximum deviation in 2007 (at 3708%) and the largest maximum deviation occurring in 2010 (at 5718%). The lower latitudes tend to have the higher percent deviation from the mean, which is apparent each year over the Southern Ocean. There are many interesting regional features that can be pointed out for each year, but in 2010 there are two that stand out: Western Europe received larger than average snowfall, and the North Atlantic (southeast of Greenland) received less than average snow accumulation.

ERA-Interim: Snowfall % deviation from 1979-2013 Annual Mean

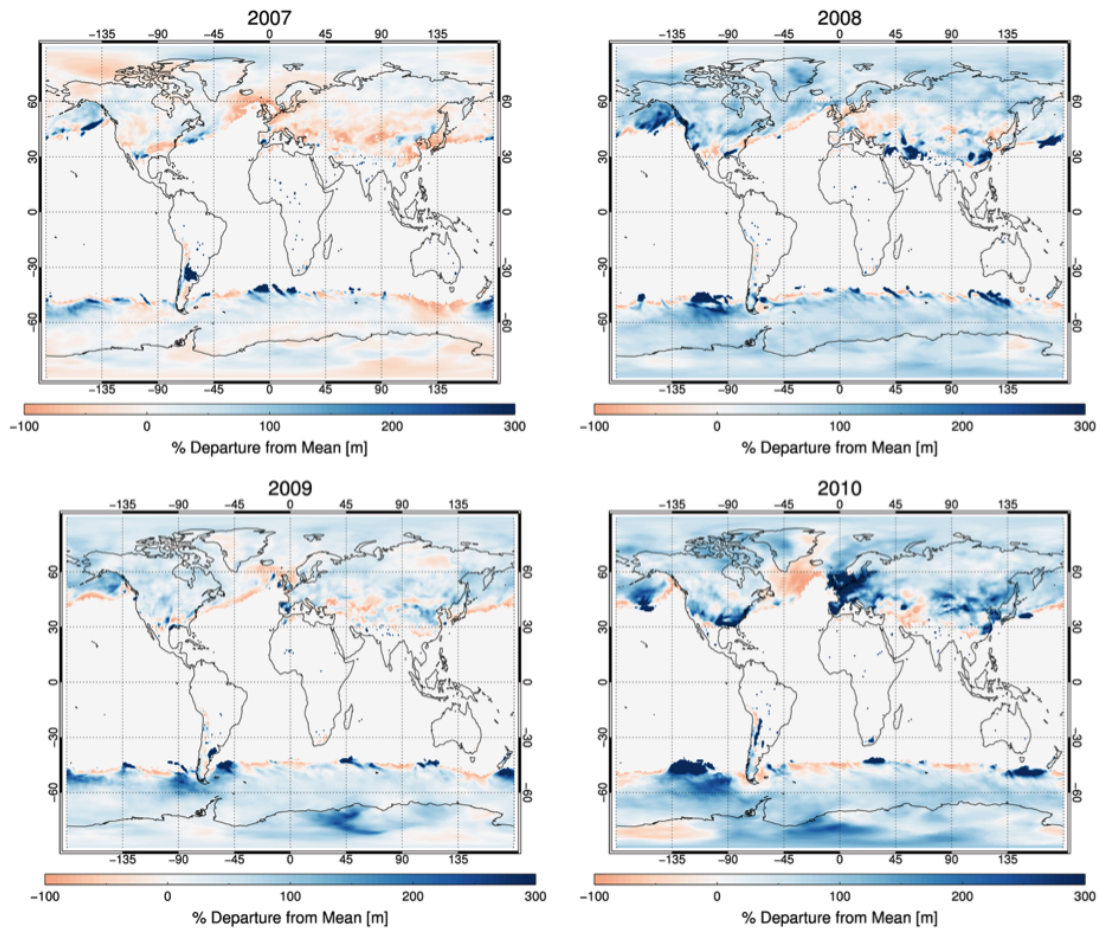
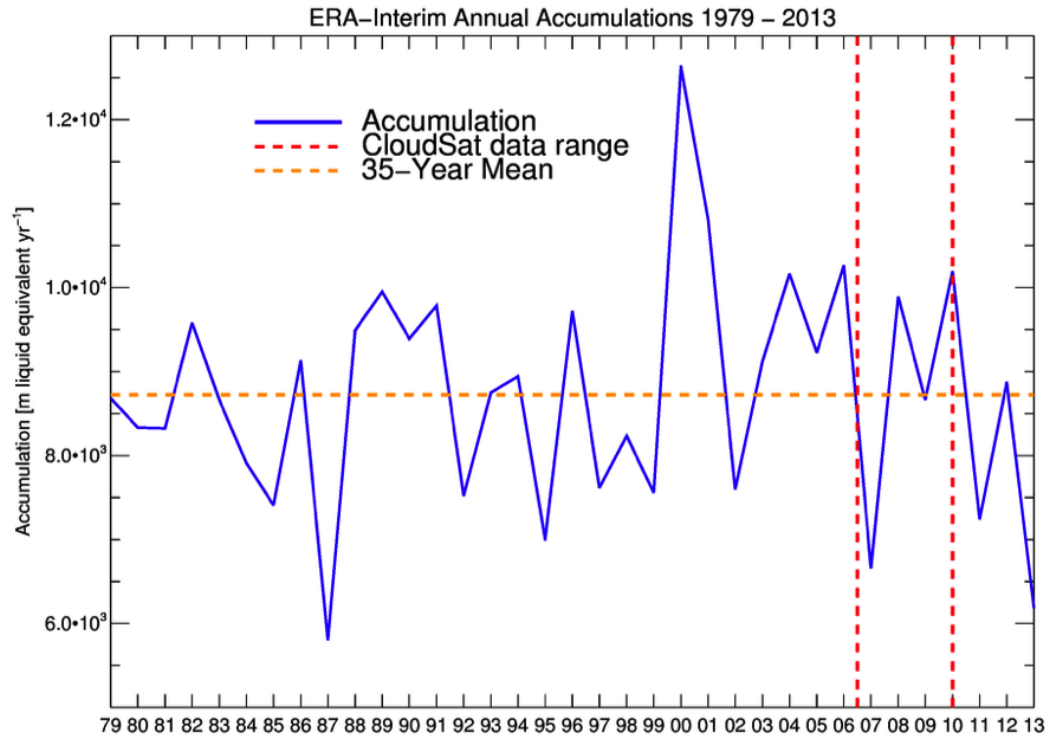


FIGURE 5.3: The percent deviation from the 35-year mean of ERA-Interim snowfall during CloudSat's operational years (2007-2010) used in this study.

Figure 5.4 shows the trend of ERA-Interim global snowfall accumulations and the 35-year mean. The average of the total global annual accumulation is 8723.6 m yr^{-1} , and is plotted as the orange line. The largest positive deviation from the 35-year mean is in 2000 with 3921.2 m yr^{-1} more snowfall accumulation (globally) and the largest negative deviation is in 1987 with 2922.2 m yr^{-1} less snowfall accumulation (globally) than the mean. The range of years marked by vertical lines represents the CloudSat data range



..

FIGURE 5.4: The ERA-Interim snowfall trend plotted as the total global accumulation per year from January 1979 to December 2013.

used in this study. In 2008 and 2010, the annual global snowfall accumulation was higher than average, while 2007 was much lower than average and 2009 is close to the mean. While 2009 is considered a climatologically average year from a global snowfall perspective, note that significant regional snowfall anomalies occurred (Figure 5.3).

Lastly, the ERA-Interim snowfall dataset was analyzed zonally as cumulative zonal totals starting at the equator and ending at each pole as well as latitude weighted zonal totals. The annual average of total snowfall rate is plotted in Figure 5.5. The Northern hemisphere experiences increasing snowfall accumulations toward the North Pole, but the

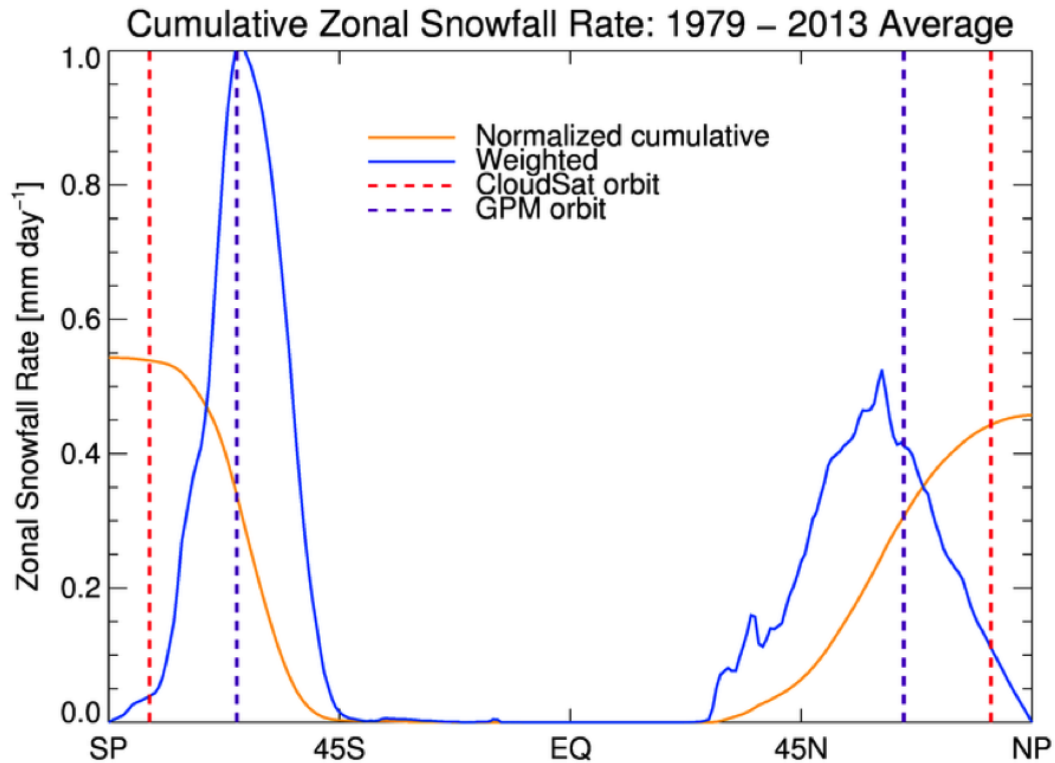


FIGURE 5.5: ERA-Interim normalized cumulative zonal total snowfall rate and weighted zonal total snowfall rate (weighted by latitude area) from 1979 – 2013. The orbital boundaries for CloudSat and GPM are both marked as well.

Southern Hemisphere’s cumulative snowfall appears to plateau somewhere between the southern orbital extent of GPM (65° S) and CloudSat (82° S). This indicates that there is a smaller percentage of global snowfall occurring at these very high southern latitudes compared to snowfall between approximately 45° S and 75° S. The Southern Hemisphere, despite snowfall accumulation falling off toward the pole, still accumulates on average 410.79 m (liquid equivalent) yr^{-1} more snowfall than the Northern Hemisphere. When considering the orbital extent of snowfall remote sensing satellites, it is useful for a science team to know where most of the desired snowfall is occurring. Using the 35-year mean,

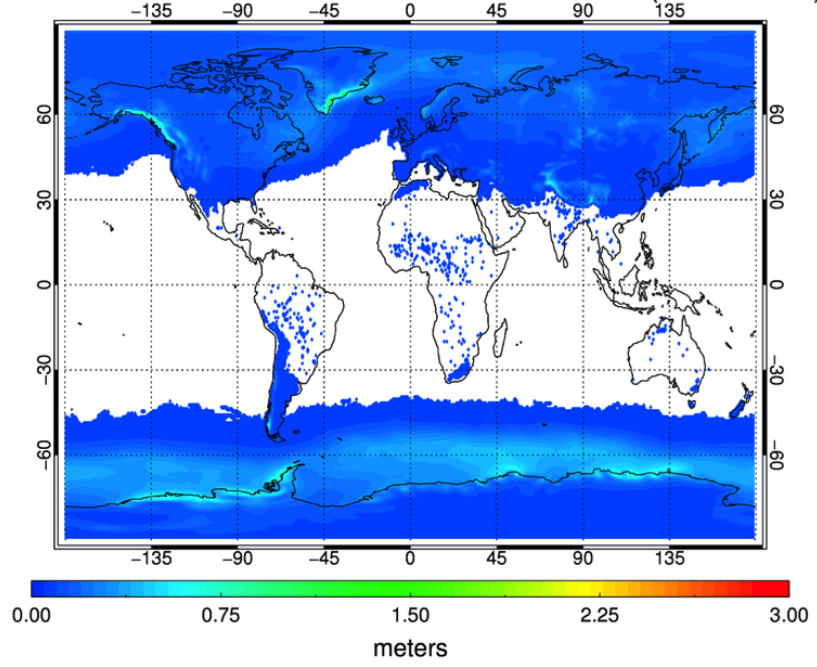
the percentage of snowfall missed by both CloudSat ($|82|^\circ$ orbital extent) and GPM ($|65|^\circ$ orbital extent) is computed (based on what ERA-Interim models to accumulate above the orbital boundaries for each instrument). CloudSat, on average, misses an estimated 9.3% of ERA-Interim’s global snowfall and GPM, on average, misses 46.0% of ERA-Interim’s global snowfall.

5.2 CloudSat vs. ERA-Interim Analysis

After analyzing the ERA-Interim dataset for a climatological and spatial perspective on global snowfall, the independent CloudSat observational dataset is now compared against it. The snowfall datasets in this section start in January 2007 in order to simplify the annual mean snowfall accumulation computation. CloudSat’s latitudinal boundaries are approximately $|82|^\circ$ and thus data is not available above these latitudes. The native ERA-Interim dataset is produced in approximately $0.7^\circ \times 0.7^\circ$ grid boxes and is interpolated to $1.0^\circ \times 1.0^\circ$ and latitudinally constrained to match the CloudSat grid. Additionally, the CloudSat dataset’s mean annual unconditional snowfall rate [mm h^{-1}] for each grid box was converted to units of accumulation per year (m y^{-1}).

Figure 5.6 shows a spatial comparison of the CloudSat 2C-SNOW-PROFILE product and ERA-Interim snowfall dataset as an annual mean snowfall accumulation from January 2007 to December 2010. The two datasets agree especially well in the Northern hemisphere: the Rocky Mountains, the Himalayan Mountains, and the southeast coast of Greenland have relatively higher annual mean accumulation, and a lower boundary

ERA-Interim Annual Mean Snow Accumulation (2007–2010)



CloudSat Annual Mean Snow Accumulation (2007–2010)

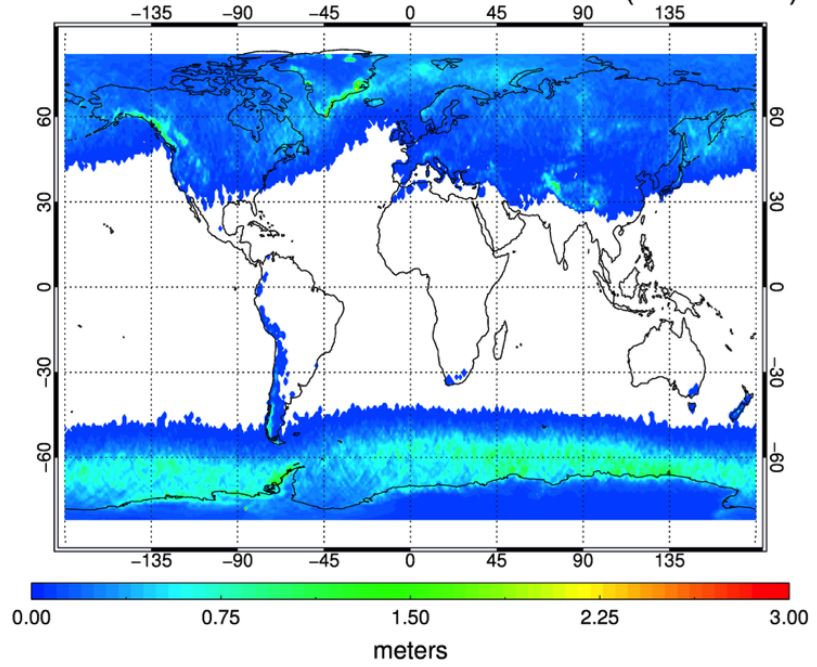


FIGURE 5.6: Spatial comparison of CloudSat and ERA-Interim annual mean snowfall accumulations during CloudSat’s operational years, 2007-2010.

of snowfall accumulation resembles that of a storm track. CloudSat appears to show higher snowfall accumulations than ERA-Interim in the North Atlantic and North Pacific (closer to 0.75 m), both regions where shallow convective snow is prevalent (Figure 2.1). The CloudSat dataset also displays a larger area of accumulation in Eastern Europe and central interior Russia.

The Southern hemisphere in Figure 5.6 is less consistent among the datasets. There is spatial agreement on the accumulation in the Andes Mountain and Southern ocean/Antarctic coast, as well as the less sinusoidal shape of the upper boundary compared to the Northern Hemisphere. However, CloudSat consistently samples higher snowfall rates over land (e.g. New Zealand and the southern Andes Mountains) and the ocean. Only along the Antarctic Peninsula and the coast of East Antarctica do the ERA-Interim snowfall accumulations appear relatively higher.

Spatial grid box differences between the CloudSat and ERA-Interim snowfall datasets are plotted in Figure 5.7. The CloudSat snowfall is subtracted from ERA-Interim, and thus positive (negative) values indicate higher accumulations in the ERA-Interim (CloudSat) dataset. Above 82° , no data is plotted. The annual mean as well as the individual years show many regions where CloudSat systematically estimates higher snowfall rates and thus has higher accumulations annually. The Southern Ocean stands out prominently in all plots, and is especially larger in individual years. The annual mean shows lighter shades of red, indicating that each year has different areas that ERA-Interim and CloudSat disagree on (though these areas are small). On average, mountainous regions

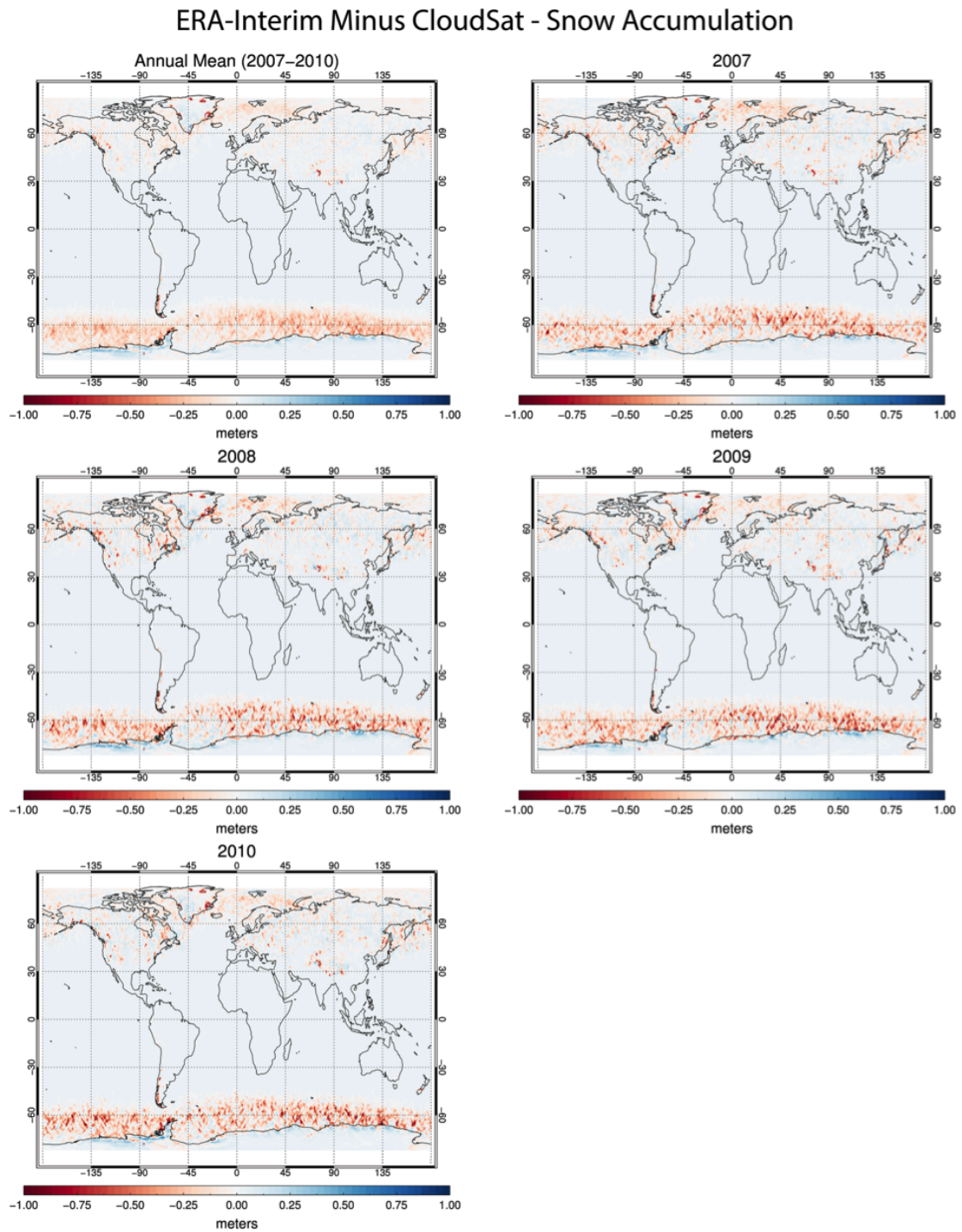


FIGURE 5.7: The difference (in meters) between the ERA-Interim accumulation and the CloudSat global snowfall accumulation datasets for CloudSat's operational years, 2007-2010.

show relatively higher differences, with CloudSat's snowfall accumulation higher than ERA-Interim. Greenland also shows large inconsistencies among the datasets, specifically along the southeast coast. Differences in isolated grid boxes on the periphery of Greenland are caused by radar ground clutter, as CloudSat erroneously overestimates the snowfall rate due to high radar reflectivities associated with complex terrain Kulie and Bennartz (2009), Kulie et al. (2016). The most noticeable positive anomaly, where ERA-Interim's accumulation exceeds CloudSat's, is on the Antarctic Peninsula and the east coast of Antarctica. There is a shift from negative anomalies over the Southern Ocean to positive anomalies over Antarctica, indicating that there may be systematic differences dependent upon surface type between the model-derived and the observed snowfall datasets. There are consistently large positive ERA-Interim anomalies over the extreme southern Greenland coastline. ERA-Interim also produces consistently more snowfall over many parts of interior Greenland, although the anomalies are not as pronounced compared to the southern Greenland coastline. Globally, during these years, CloudSat systematically produces a higher snowfall accumulation than ERA-Interim. Possible causes for these differences are discussed in Chapter 6.

Zonal mean snowfall rates are plotted in Figure 5.8 for each individual year, as well as the average of those years. The CloudSat data only extends up to 82° , but the ERA-Interim reaches both poles. The Southern hemisphere (between 45° S and the South Pole), according to both datasets, has higher zonal mean snowfall rates per grid box than the Northern hemisphere, and was computed earlier to make up (on average) approximately 54% of global snowfall. The peak for the CloudSat zonal mean snowfall

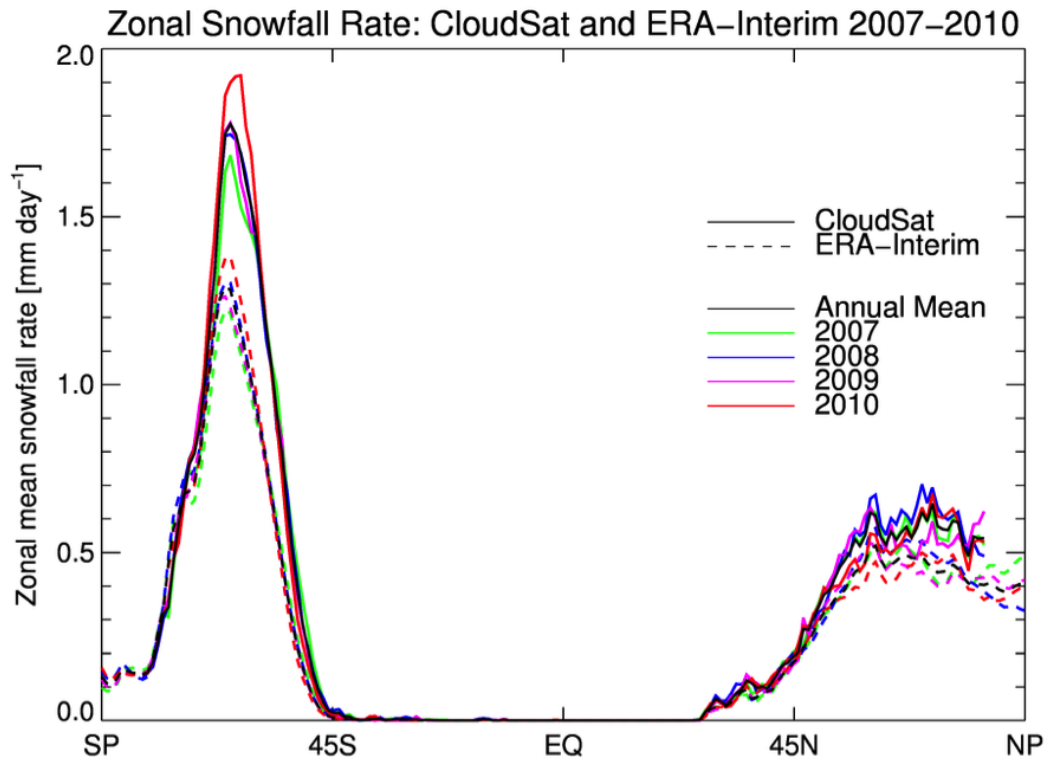


FIGURE 5.8: Zonal mean snowfall accumulation from January 2007 to December 2010 for both CloudSat (solid lines) and ERA-Interim (dashed lines). The annual mean over this time period is plotted, as well as the zonal mean for each year.

rates, 1.92 mm day^{-1} , was in 2010 at 63°S latitude. The peak for the annually averaged CloudSat zonal mean accumulations, 1.78 mm day^{-1} , is at 65°S latitude. The ERA-Interim zonal mean peaked in 2010 as well, at 1.38 mm day^{-1} , but at a slightly higher latitude than the CloudSat zonal mean accumulation in 2010, 65°S . The averaged zonal mean accumulation for the ERA-Interim snowfall dataset peaks at 1.29 mm day^{-1} at 66°S latitude, also a slightly higher latitude than the analogous CloudSat zonal mean snowfall rate. The maximum zonal mean snowfall rate for the ERA-Interim dataset is consistently at slightly higher latitudes than the CloudSat dataset when each individual

year is checked.

The snowfall accumulation in the Northern Hemisphere, according to Figure 5.8, stretches down to lower latitudes than the Southern Hemisphere. There is also no obvious peak of snowfall at a specific latitude, though snowfall accumulation is higher northward of 45°N. There is less of a spread between datasets of the zonal averages of the snowfall in the Northern hemisphere than in the Southern Hemisphere. The area under each curve represents the total of the zonal means for each year and each dataset. ERA-Interim's peak year for modeled snowfall accumulation occurred in 2008 in both the Southern hemisphere (24.2 mm day⁻¹) and in the Northern hemisphere (20.3 mm day⁻¹). CloudSat's peak year for snowfall observations in the Southern hemisphere occurred in 2010 (30.7 mm day⁻¹) and in the Northern hemisphere, occurred in 2008 (21.3 mm day⁻¹). Overall, in agreement with the spatial plots shown in Figure 5.7, CloudSat's zonal mean accumulation is generally higher than ERA-Interim's.

A quantitative comparison between ERA-Interim and CloudSat snowfall accumulations is shown in Figure 5.9. Each point represents a single (1.0°×1.0°) grid box's snowfall rate as the 4-year mean snowfall rate (in the first panel) or each individual year's snowfall rate (other panels). CloudSat's mean global snowfall rate (the 4 year average) is approximately 0.03 m yr⁻¹ (21.6%) higher than ERA-Interim's, and this pattern is seen throughout the individual years as well. Both datasets agree that 2008 had the highest global snowfall rate, with CloudSat observing 0.1138 m yr⁻¹ and ERA-Interim modeling 0.0903 yr⁻¹.

ERA-Interim vs. CloudSat Snowfall Rates

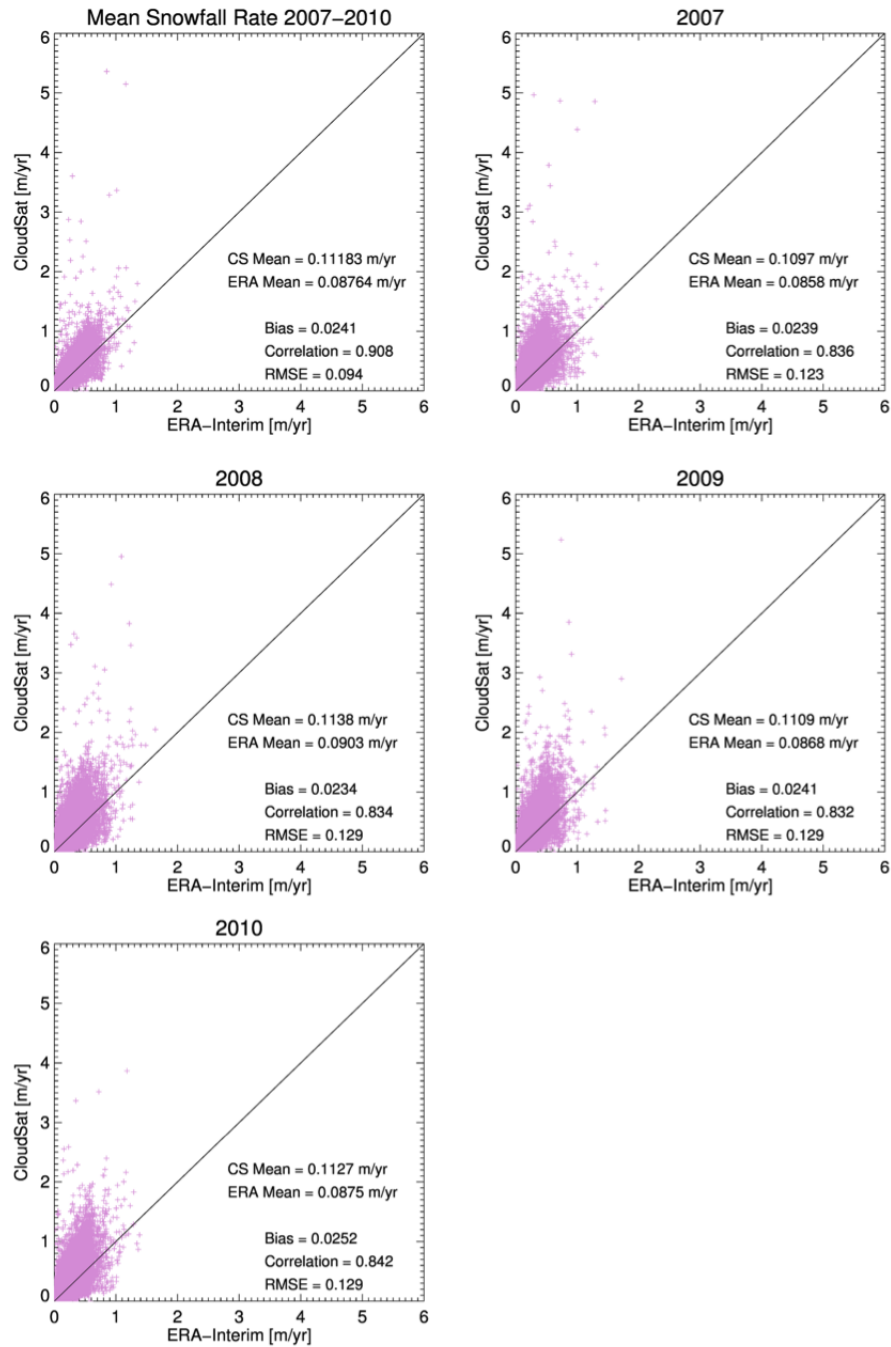


FIGURE 5.9: Scatter plots of the ERA-Interim versus CloudSat snowfall rates. The first plot is the 4-year mean, and the remaining are the individual years that CloudSat was operational, 2007-2010. Each point represents a single latitude \times longitude ($1^\circ\times 1^\circ$) grid box's snowfall rate.

Even though 2008 experienced the highest global mean snowfall rate in both datasets, the largest difference between datasets occurred in 2010 (CloudSat's mean exceeds ERA-Interim's by 0.0252 m yr^{-1}). The remainder of the years shows CloudSat observing, on average, between $0.1097 - 0.1138 \text{ m yr}^{-1}$, and ERA-Interim modeling, on average, $0.0858 - 0.0903 \text{ m yr}^{-1}$ of snowfall. The minimum mean snowfall rate for both datasets occurs in 2007, which was a sea-ice minimum year (Comiso et al., 2008). The datasets are well correlated, with a correlation of approximately 0.91 for the 4-year average dataset. Each individual year's correlations are slightly lower (0.832-0.842) than the averaged dataset. The bias for the averaged dataset is 0.0241, and the individual years' biases are between 0.0234 - 0.0252. All of these biases are positive, and indicating that CloudSat is biased high compared to ERA-Interim. This is consistent with the zonal mean snowfall rates in Figure 5.8 as well as the spatial difference plots in Figure 5.7. The root mean square error (RMSE) is approximately 0.094 m yr^{-1} for the 4-year average, and is between $0.123-0.129 \text{ m yr}^{-1}$ for the individual years. The bias and correlation are highest in 2010 and the RMSE is lowest in 2007. It is apparent by the shape of the scatter plots that there are several grid boxes where CloudSat snowfall greatly exceeds that of ERA-Interim, likely due to clutter specks (Maahn et al., 2014). There are also a few grid boxes where ERA-Interim greatly exceeds CloudSat snowfall, which could be due to CloudSat sampling issues at equatorward latitudes.

In preparation for Section 5.3 of the Results, where the CloudSat snowfall dataset is examined by partitioning the dataset by snowfall mode and through the lens of the GPROF algorithm by examining the environmental conditions associated with CloudSat

snowfall events, Figure 5.9 is recreated twice with various filters. In Figure 5.10, only grid boxes with (i) $\geq 60\%$ of snowfall events due to cumulus or stratocumulus clouds and (ii) $\geq 60\%$ of the snowfall rate due to cumulus or stratocumulus clouds are plotted. Figure 5.10 aims to isolate grid boxes dominated by shallow snow by using the ad hoc thresholds described to investigate whether systematic differences in the two respective datasets might be caused by the unique shallow snowfall mode. Recall that Kulie et al. (2016) found cumulus and stratocumulus to be shallower and generally produce more light snowfall than nimbostratus clouds (with the exception of sometimes intense over-water convective snow), and thus Figure 5.10 snowfall cases are identified for convenience as “shallow.” Figure 5.11 is simply the complement of Figure 5.10’s categorization; every grid box that is not plotted on the “shallow” plots of Figure 5.10 is plotted as “non-shallow” snowfall in Figure 5.11. Note that the ad hoc definition of non-shallow dominated grid boxes may still contain significant shallow snowfall contributions approaching 60%, so the Figure 5.11 comparisons have shallow snowfall contributions inherently included in the published statistical measures.

The shallow mean snowfall rate in Figure 5.10 is much lower than the global total snowfall rate, as there is no non-shallow snowfall (as seen in Figure 5.11) taken into account. Note that an individual year may have a grid box that meets the criteria of shallow, but the remainder of the years may not meet that criteria. Therefore, what was a “shallow” grid box in one year may not be for the average of the 4 years. The 4-year and global mean snowfall rate for shallow snowfall in Figure 5.10 is 0.0526 m yr^{-1} (according to CloudSat) or 0.0385 m yr^{-1} (according to ERA-Interim), with CloudSat’s observational mean

ERA-Interim vs. CloudSat Shallow Snowfall Rates

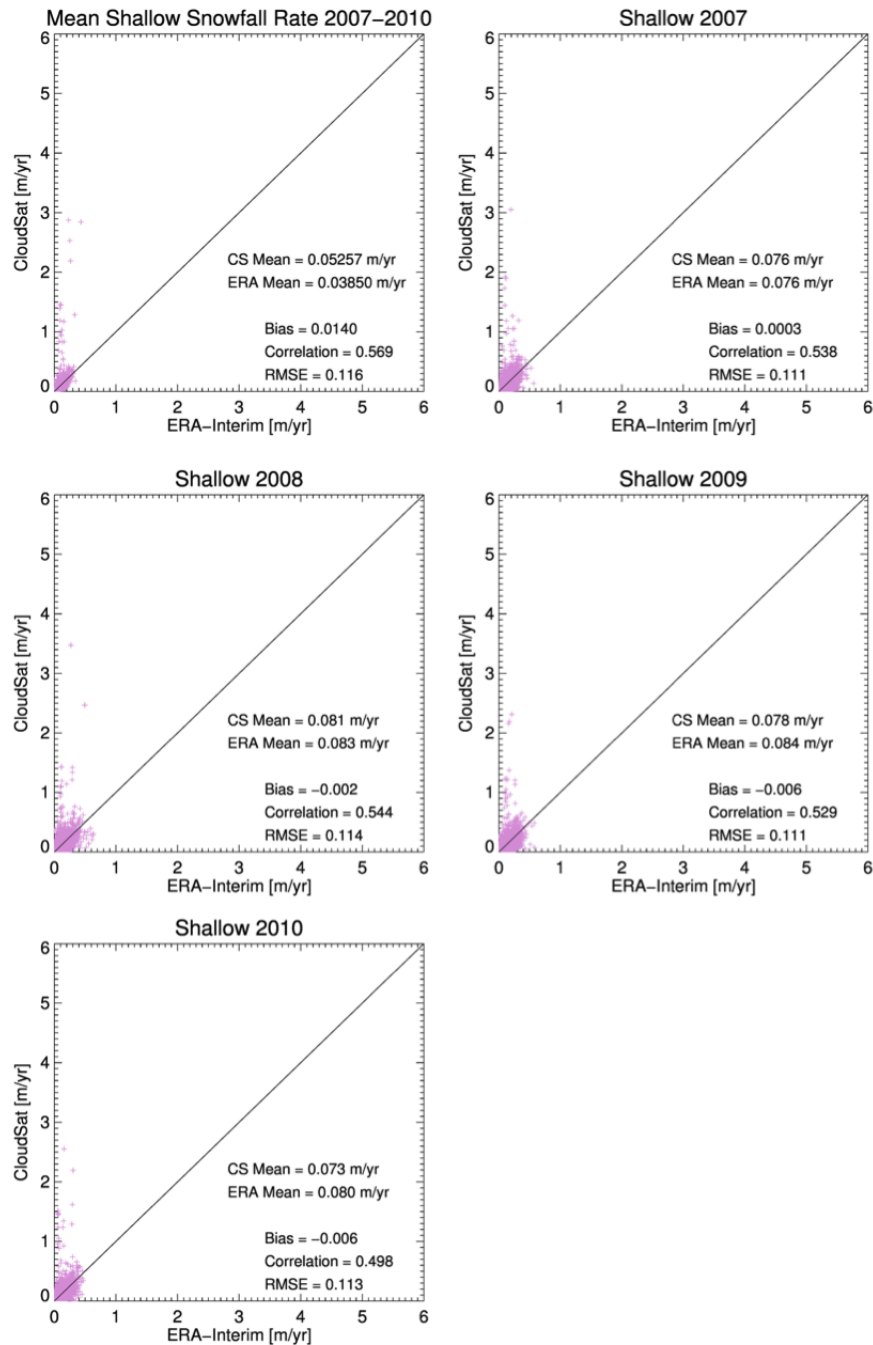


FIGURE 5.10: Same as Figure 5.9, but now only plotting for grid boxes that have (i) more than 60% of snowfall occurrences from cumulus or stratocumulus clouds and (ii) more than 60% of the snowfall rate due to these shallow cumuliform events. This makes use of CloudSat’s 2B-CLDCLASS product, which classifies cloud type.

exceeding that of ERA-Interim's modeled mean by approximately 0.0141 m yr^{-1} . The largest difference in mean snowfall rate occurs in 2010 (ERA-Interim accumulation is 0.007 m yr^{-1} higher). In 2007, a year that had a lower mean snowfall rate (as seen in Figure 5.9) and was a sea-ice minimum (Comiso et al., 2008), has a very small difference between the datasets' global mean snowfall rates and consequently, the lowest bias. The bias between both datasets for the 4-year averaged shallow snowfall is 0.014, and the correlation is only 0.569. Just as was the case in Figure 5.9, there are several grid boxes where CloudSat snowfall greatly exceeds ERA-Interim, which is likely due to ground clutter (Maahn et al., 2014), especially because the 2B-CLDCLASS product identified these clouds as cumulus or stratocumulus, which are likely to be shallow (Kulie et al., 2016). The bias between shallow snowfall datasets during 2008-2010 is negative, while the bias in 2007 is positive; all years individually have extremely small biases between datasets, less than 0.01. The absolute value of the bias is largest in 2010 (when taking into account more significant figures than is shown on the plot), the correlation is highest in 2008, and the RMSE is lowest in 2009 (again, when looking at more significant figures). The highest mean snowfall rate is in 2008 for CloudSat (0.081 m yr^{-1}) and in 2009 for ERA-Interim (0.084 m yr^{-1}). The negative bias during each year except 2007 indicates that the ERA-Interim snowfall output is higher than the CloudSat snowfall when filtered through this lens. However, because ERA-Interim grid boxes were vetted using CloudSat's cloud identification data (from 2B-CLDCLASS), ERA-Interim is including snowfall events that are not "shallow" (i.e. from cumulus or stratocumulus clouds within the model) and could be accumulations from deeper snowfall, which typically is associated with higher

snowfall rates (Kulie et al., 2016).

Lastly, the scatter plot of non-shallow snowfall cases in ERA-Interim output and CloudSat observations is shown in Figure 5.11. These events complement the shallow snowfall cases and thus make up the large difference between “all” snowfall events and shallow. The CloudSat non-shallow mean global snowfall rate exceed that of ERA-Interim by 0.0541 m yr^{-1} for the 4-year average. Just as was the case for “all” and shallow events, 2010 has the largest difference between datasets’ snowfall rates, with CloudSat’s mean 0.0665 m yr^{-1} higher. The 4-year averaged bias is approximately 0.0541 , which more than twice the bias of “all” snowfall events and almost four times the bias for shallow snowfall events for the 4-year average. Additionally, the 4-year average RMSE is lowest for “all” snowfall events and highest for the non-shallow (0.137 m yr^{-1}). This means that when shallow snowfall dominated grid boxes are filtered out in this manner, the datasets start to disagree more on snowfall accumulations, and could be an indicator of different snowfall modes occurring between the datasets. For individual years, the correlation and bias are highest in 2010 and the RMSE is lowest in 2007, just as was the case for “all” events (shallow events in 2010 also had the largest bias of all years, though it was negative). The highest global mean snowfall rate is in 2008 for both CloudSat (0.2763 m yr^{-1}) and ERA-Interim (0.2148 m yr^{-1}).

The comparison of these two snowfall datasets reveals a few differences between the modeled ERA-Interim snowfall and the observed CloudSat snowfall. First, global distributions of snowfall portray CloudSat observations as having higher snowfall rates than

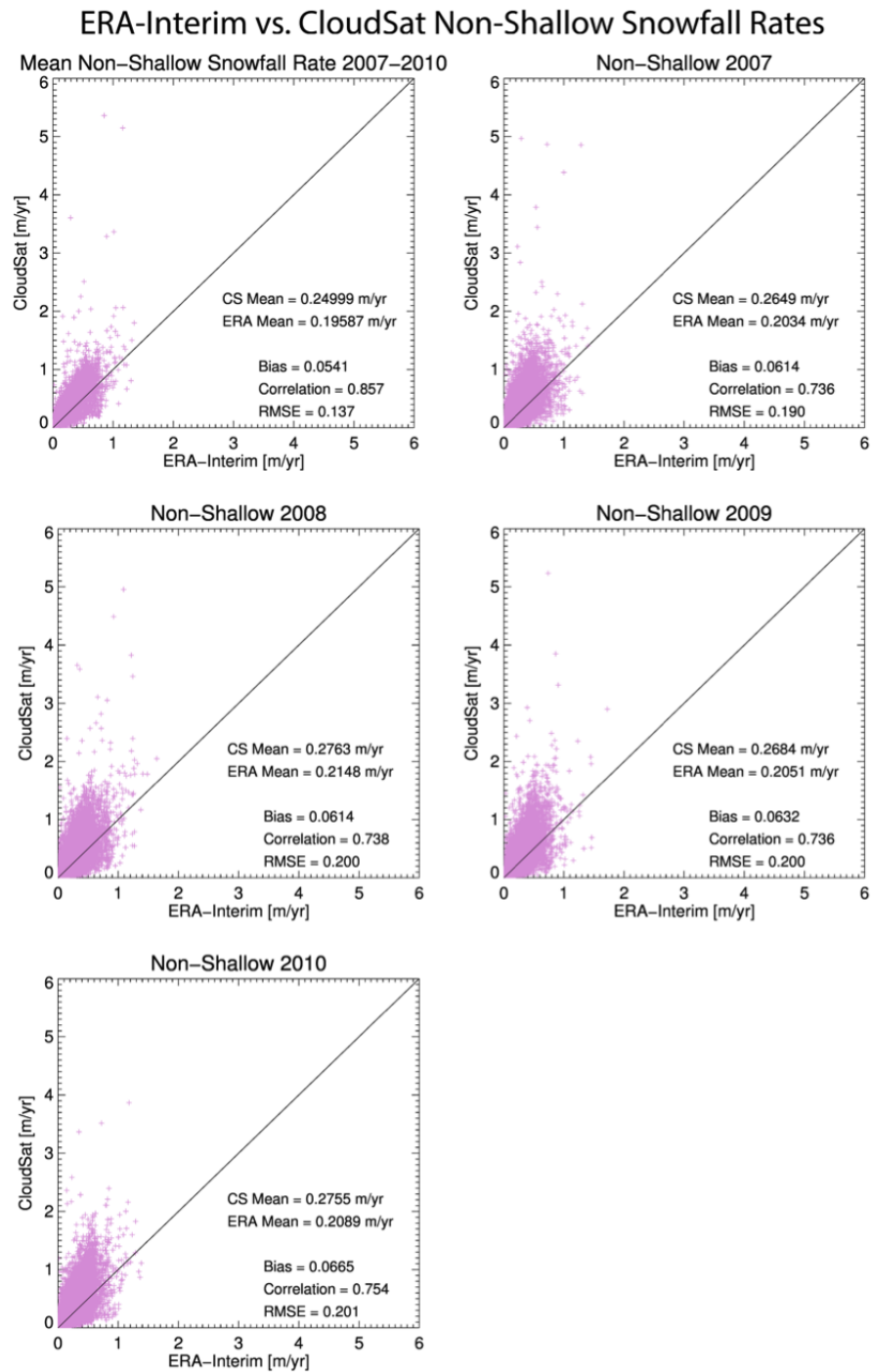


FIGURE 5.11: Same as Figure 5.9, but now plots every grid box that was not plotted in Figure 5.10. These “non-shallow” grid boxes may have shallow snowfall events and rates from shallow cumuliform clouds, but does not meet the criteria specified to be a “shallow” grid box.

ERA-Interim, especially in southeast Greenland and the Southern Ocean. The zonal mean of snowfall rates agrees with this finding and is especially apparent in the Southern hemisphere. Also in the Southern hemisphere, the zonal mean snowfall rate peaks in 2010 for CloudSat and 2008 for ERA-Interim, whereas the Northern hemisphere experienced its highest accumulation in 2008, according to both datasets. Lastly, comparing rates and splitting up snowfall events by mode (using CloudSat’s 2B-CLDCLASS product) shows that CloudSat’s higher bias of snowfall rate can be attributed to cases identified as “non-shallow.” This is because ERA-Interim has higher rates of snowfall in the grid boxes that CloudSat identifies as dominated by shallow events (according to the definition used earlier), but when considering all snowfall events, ERA-Interim has lower snowfall rates. As a result, one of three scenarios is true: (i) ERA-Interim is modeling too little snowfall, (ii) CloudSat is observing or estimating too much snowfall (some of which could be ground clutter), (iii) or both datasets are incorrect.

5.3 CloudSat Snowfall Database Analysis

For the Day 1 version of the GPM GPROF radiometer precipitation algorithm, CloudSat’s 2C-SNOW-PROFILE and ECMWF-AUX products from June 2006 to December 2010, combined with coincident AMSR-E brightness temperatures, were chosen to construct an *a priori* database for very cold surface temperatures ($T_{2m} \leq 255$ K). The Day 1 GMI observed multi-frequency brightness temperature vectors would be matched, along with surface emissivity type and ECMWF-derived T_{2m} and TPW, to a CloudSat/AMSR-E/MHS *a priori* database entry that possessed a minimized brightness temperature

difference with the GMI observation. If the matched CloudSat database entry had a precipitation rate associated with it, the CPR-derived (2C-SNOW-PROFILE) snowfall rate would be assigned to this GMI observation. While the CloudSat/AMSR-E/MHS database temporarily played an important role in the GPROF retrieval scheme during the early phases of the GPM mission, the CloudSat/AMSR-E/MHS database contains a wealth of information regarding global snowfall that has yet to be sufficiently exploited. This section investigates the CloudSat snowfall dataset in a unique fashion by providing a global snowfall perspective using ambient environmental fields such as T2m and TPW. As previously mentioned, these environmental parameters are used by GPROF to search *a priori* database entries with similar T2m/TPW magnitudes to economize the GMI observation-*a priori* database matching procedure (the *a priori* database is populated by millions of profiles, so considering database entries with similar T2m and TPW values as the GMI observation under consideration greatly reduces computation time). The CloudSat database provides an unprecedented opportunity to characterize global snowfall by these key environmental parameters and other cloud macrophysical parameters and geographical constraints, thus serving as an important post Day 1 GPROF snowfall retrieval calibration and evaluation tool.

To understand where CloudSat's observed snowfall at these very cold surface temperatures ($T2m \leq 255 \text{ K}$) is typically located, Figure 5.12 displays spatial distributions of snowfall occurrences for both the 2006-2010 period as well as each individual year. Note the changed color bar for the 4.5-year plot, as well as the fact that the 2006 data is half the length (temporally) of the rest of the years. CloudSat samples more data at higher

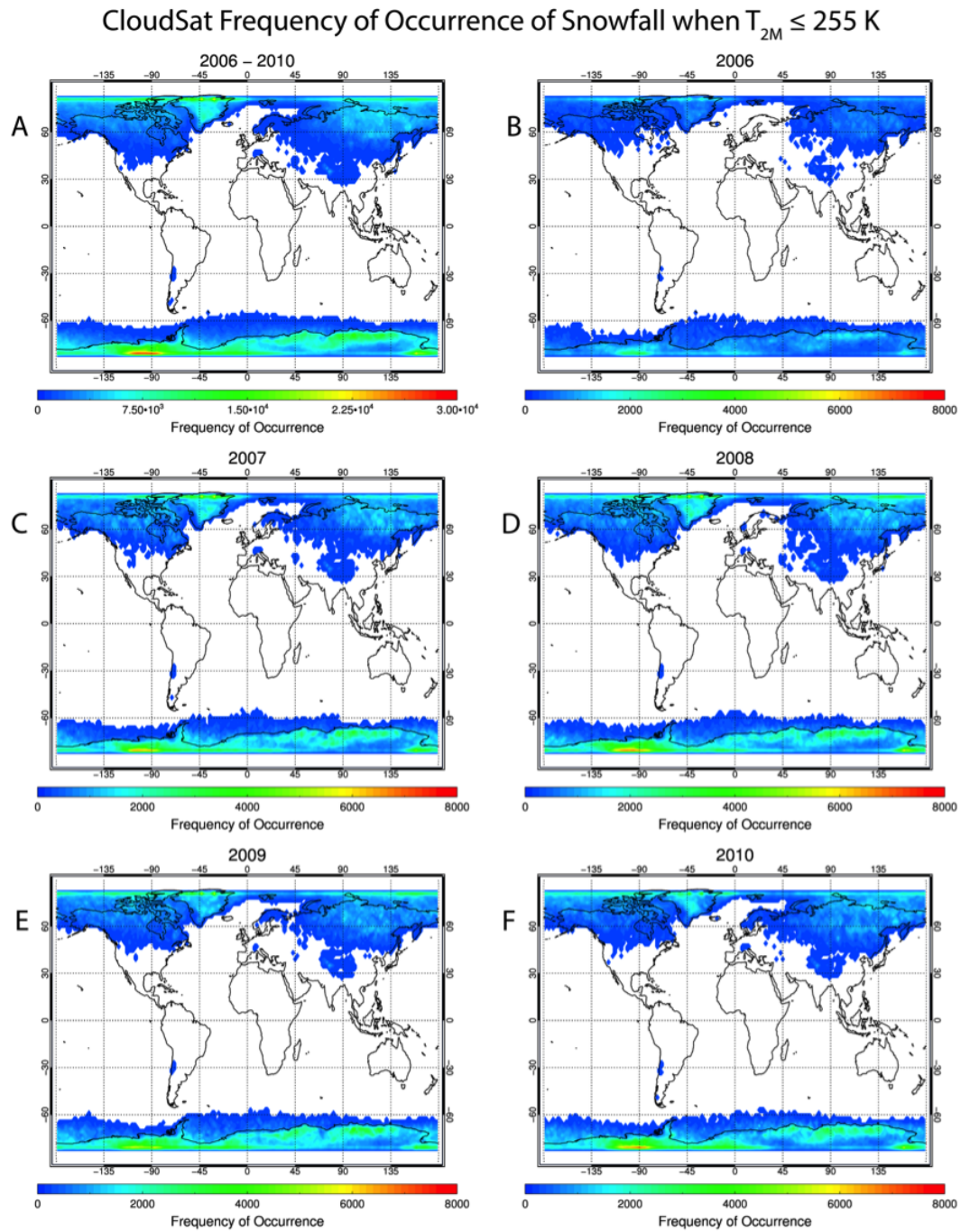


FIGURE 5.12: All occurrences of snowfall when the two-meter temperature (T_{2M}) is less than or equal to 255 K, the criterion for using the CloudSat database in the Day 1 version of the GPROF algorithm for GPM.

latitudes, which causes a seemingly linear band of increased snowfall occurrences near the upper bounds of CloudSat's orbit (this is especially apparently in the Northern hemisphere pan-Artic region). In the Northern Hemisphere, $T2m \leq 255$ K snowfall occurrences reach to latitudes as far south as 30°N , especially over land. Snowfall occurrences in the Northern Hemisphere when $T2m \leq 255$ K are over land 56.9% of the time, and over ocean 42.7% of the time (the remaining $\sim 0.5\%$ of occurrences are over coasts). In the Southern hemisphere, $T2m \leq 255$ K snowfall is much more restricted, with most occurrences south of 60°S with the exception of the Andean Mountain range. Snowfall occurrences in the Southern Hemisphere when $T2m \leq 255$ K are over land 71.2% of the time, and over ocean 28.6% of the time (the remaining $\sim 0.2\%$ of occurrences are over coasts). Approximately 91.4% of snowfall occurrences where $T2m \leq 255$ K are above $|65|^\circ$ latitude, the upper limit on GPM's latitudinal extent. Recall from Figure 2.1, from Kulie et al. (2016), that CloudSat snowfall events identified as "shallow" occur relatively frequently and contribute substantially to regional snowfall accumulations (compared to deeper snowfall events) in the Southern ocean, as well as the North Atlantic and Pacific Oceans. These results imply that the CloudSat database, used for Day 1 retrievals when $T2m \leq 255$ K, is underutilized in regions with higher frequency of occurrence of shallow cumuliform snowfall events. The following discussion related to Figures 5.13 - 5.18 highlight this potential underutilization issue further.

5.3.1 Global Analysis

The CloudSat database that contains over 46 million possible snowfall entries can be visualized as a function of environmental parameters by binning snowfall occurrences and mean snowfall rates by T2m and TPW, as is done in Figure 5.13. Figure 5.13a is frequency of occurrence, Figure 5.13b is relative frequency of occurrence (or fraction, where 1 is the normalized total number of occurrences across all T2m and all TPW bins), and Figure 5.13c is the mean snowfall rate per T2m/TPW bin. Only snowfall events with rates below 5 mm h^{-1} are considered in the mean snowfall rate figures, as the quality of CloudSat’s snowfall rates degrades above $\sim 1 \text{ mm h}^{-1}$ and displays progressively increasing negative biases compared to independent ground-based datasets above $\sim 5 \text{ mm h}^{-1}$ (Cao et al., 2014). Extremely high snowfall rates could also be caused by imperfections of the 2C-SNOW-PROFILE clutter flag. Of these occurrences between 0.0 and 5.0 mm h^{-1} , only 22.5% of CloudSat’s snowfall occurs when $T2m \leq 255 \text{ K}$. The mean snowfall rate plots also consider only T2m/TPW bins with at least 100 occurrences of snowfall to avoid including bins that contain a limited number of snow events over the 4.5 year period. This constraint is apparent in the snowfall rate figures, as the mean snowfall rate joint histograms do not extend as wide or as tall as the frequency of occurrence or fraction plots.

The bounding shape of the joint histogram shown in Figure 5.13 can be partially explained by the Clausius-Clapeyron equation, which relates increasing TPW to increasing

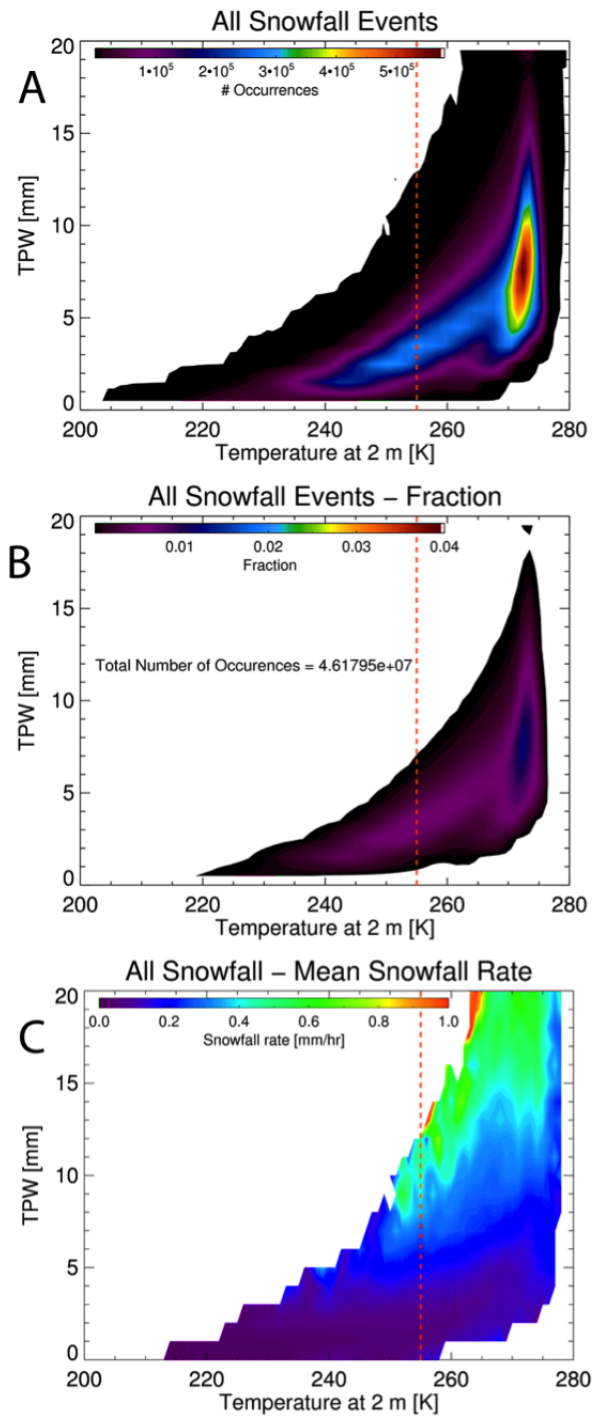


FIGURE 5.13: CloudSat snowfall occurrences, fraction of occurrence, and mean snowfall rate binned by 2-meter temperature (T2m) and total precipitable water (TPW). Data spans from June 2006 to December 2010 and represents the *a priori* database used for the Day 1 version of the GPROF algorithm.

temperature (Petty, 2008). A dotted line on all graphs shows where $T2m = 255$ K so as to visually illustrate what portion of the entire CloudSat dataset is potentially used by the Day 1 GPM GPROF retrieval. Including all snowfall events shows a large maximum near 273 K and between approximately 5 and 10 mm TPW in Figure 5.13a. This T2m/TPW range is where the most occurrences of snowfall are located, which is confirmed by fraction of events in Figure 5.13b. About 13.5% of all snowfall events are located between T2m and TPW ranges of 270-273 K and 5-10 mm, respectively. There is an obvious tail-like feature that extends below 255 K at low (< 10 mm) TPW, indicating that CloudSat does observe a large number of snowfall events at very cold near-surface temperatures. Figure 5.13c, the mean snowfall rate histogram for all snowfall events, shows increased snowfall rates for increased TPW and T2m values. Note that some of the higher bin-averaged snowfall rates are associated with T2m/TPW bins populated by relatively few snowfall occurrences, but the general trend of higher bin-averaged snowfall rates with warmer temperatures and larger TPW values exists for bins populated by larger snowfall event frequencies. Only about 22.5% of all snowfall events occur at or below 255 K, though, so a large portion of the CloudSat database was not considered in the Day 1 GPROF algorithm.

5.3.2 Shallow Cumuliform vs. Nimbostratus Snowfall

In order to illustrate systematic differences between snowfall mode and environmental parameters, Figure 5.14 shows the same analysis as Figure 5.13, but the CloudSat snowfall dataset is partitioned into shallow cumuliform (left column) versus nimbostratus (right

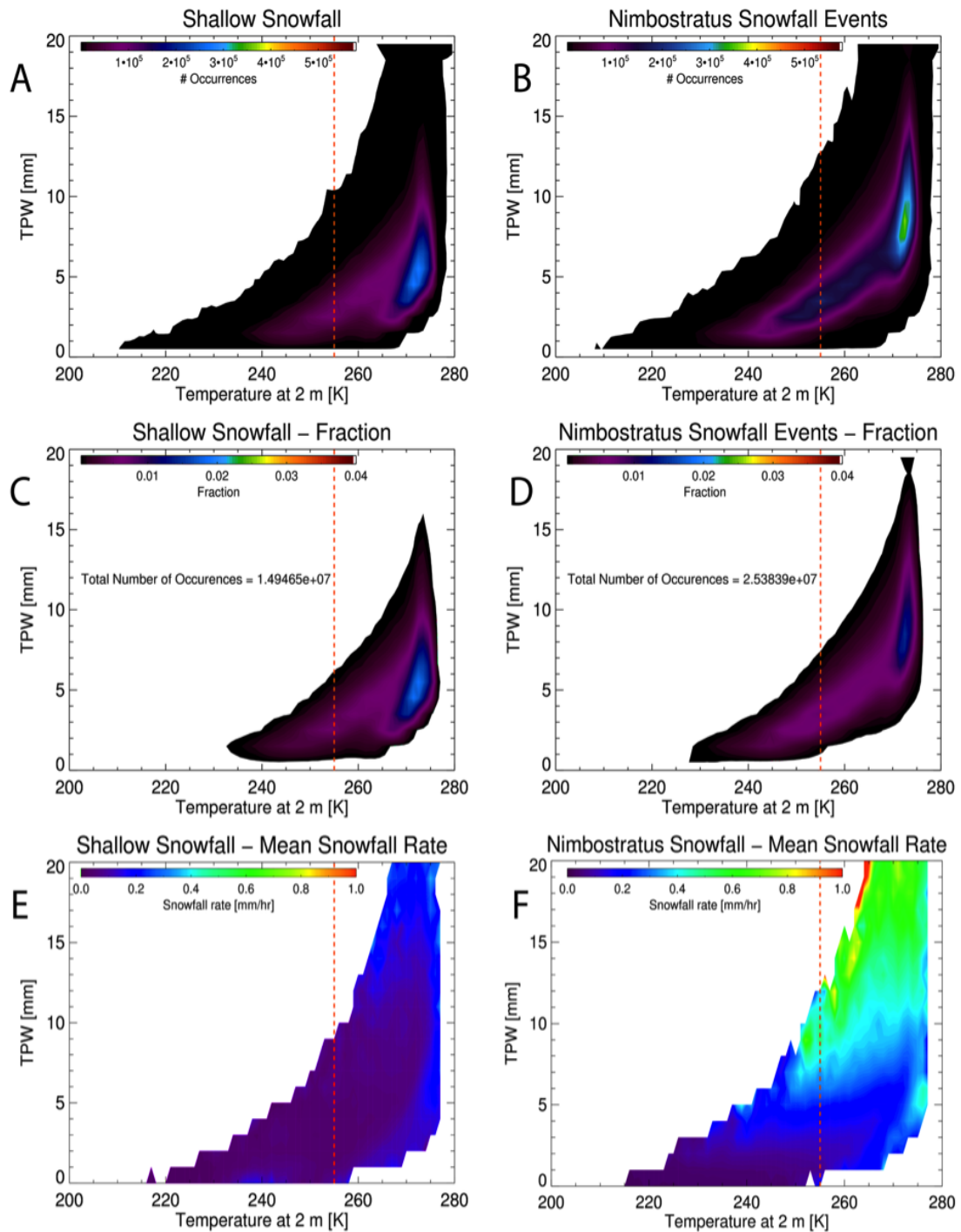


FIGURE 5.14: Same as Figure 5.13, but now showing shallow snowfall events (left column) and snowfall events occurring from nimbostratus clouds (right column).

column) snowfall events using the CloudSat 2B-CLDCLASS cloud identification product and methodology outlined in Kulie et al. (2016). According to CloudSat observations, Kulie et al. (2016) found the nimbostratus snowfall events to be systematically both deeper and heavier-snowing, although an intense shallow snowfall signature was evident and attributed to vigorous over-water convective snow events that comprised a small percentage of the CloudSat dataset. Shallow snowfall events make up far fewer events ($\sim 37\%$ of the CloudSat snowfall database) compared to the nimbostratus category ($\sim 63\%$). Similar to Figure 5.13a, there is also a frequency of occurrence peak near 273K when only shallow events are considered, but it is at an obviously lower TPW value (centered near 5 mm) than the nimbostratus snowfall category (centered near $\sim 8-9$ mm) in Figure 5.14a-b. About 19.6% of all shallow snowfall events (between 0.0 and 5.0 mm h⁻¹) occur between T2m and TPW ranges of 270-273K and 3-8 mm (Figure 5.14c). The nimbostratus category contains about 14.6% between T2m and TPW ranges of 270-273K and 6-11 mm (Figure 5.14d). The nimbostratus category is the primary cause of frequency of occurrence maxima tail extending to lower T2m/TPW values (Figure 5.14b,d) that was discussed in Figure 5.13a. This same feature also exists in the shallow snowfall category (Figure 5.14a,c), but is much less pronounced. The tail end of snowfall occurrences from nimbostratus snowfall events below 255 K is definitely larger than for shallow snowfall. Figures 5.13 and 5.14 reveal that CloudSat observes snowfall below 255 K, including shallow snowfall, and these snowfall occurrences are included in the CloudSat database for the Day 1 GPROF algorithm. Note, however, that 13.7% of shallow cumuliform and 22.6% of nimbostratus snowfall events occur at or below the 255 K T2m threshold.

From a bin-averaged snowfall rate perspective (Figure 5.14e-f), the nimbostratus category (Figure 5.14f) largely mimics the all snowfall event snowfall rate plot shown in Figure 5.13c. Higher snowfall rates exceeding 0.6 mm h^{-1} are generally associated with higher TPW values, with the only exception being an isolated snowfall rate maximum of $\sim 0.4 \text{ mm h}^{-1}$ evident at very warm temperatures (near 274-275K) and TPW values near 5 mm. This feature, however, coincides with T2m/TPW bins containing very few nimbostratus events. Very low nimbostratus bin-averaged snowfall rates (near 0.1 mm h^{-1}) are associated with low T2m and TPW values. For shallow snowfall events (Figure 5.14e), this trend is similar – generally higher T2m/TPW bin-averaged snowfall rates are evident at warmer temperatures with more columnar water vapor. The magnitudes of bin-averaged snowfall rates are universally much less than the nimbostratus category (not exceeding $\sim 0.4 \text{ mm h}^{-1}$ even in high TPW and T2m environments).

5.3.3 Land vs. Ocean Snowfall

Because the CloudSat/AMSRE/MHS database is only used for very cold near-surface temperatures that occur primarily over land in the GPROF Day 1 algorithm (NEXRAD/SSMIS is used over land for $255\text{K} < \text{T2m} < \sim 275\text{K}$, while a modified TRMM database is used over oceans for potentially snowing observations associated with possible snowing events), Figure 5.15 splits all snowfall events into over-land (left column) and over-ocean (right column) categories. Land versus ocean designations for each CloudSat observation are obtained from CloudSat products and based on a digital elevation map. Over-ice observations are included in the land category. An immediate distinction between the

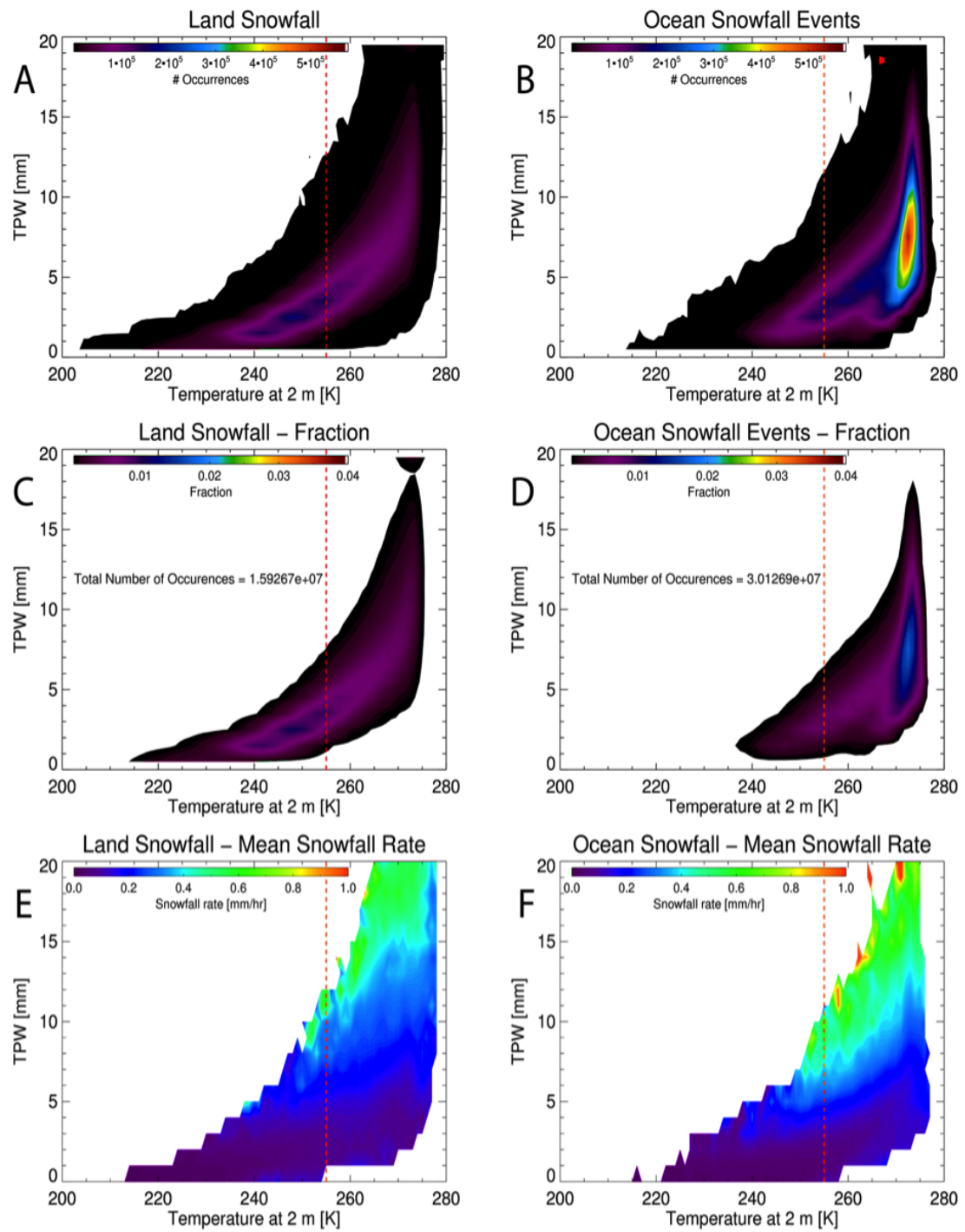


FIGURE 5.15: Same as Figure 5.13, but now showing over-land snowfall events (left column) and over-ocean snowfall events (right column).

two joint histograms (Figure 5.15a-b) is the much higher occurrence of snowfall over ocean than over land. Over-ocean snowfall clearly makes up the larger portion of all snowfall events (65.2%), though over-land snowfall appears to make up a larger portion of the tail end of snowfall occurrences that happen below 255 K (65.2% of occurrences where $T2m \leq 255K$). The frequency of occurrence joint histogram for oceanic snowfall does closely resemble that of all snowfall (Figure 5.13a), especially the bifurcated maxima that occurs between $T2m$ ranges of 265-275K and TPW values below ~ 5 mm. This bifurcation is not evident in the land snowfall frequency of occurrence figures, thus isolating the strong oceanic influence on global snowfall that is presumably linked to convective processes (see also Figure 5.13). The over-land mean snowfall rate histogram (Figure 5.15e) more closely resembles that for all snowfall, although both land and ocean generally display decreasing bin-averaged snowfall rates with decreasing $T2m/TPW$ values. An odd feature that appears in the over-ocean frequency of occurrence of snowfall plot is a very high number of occurrences around 265 K and 19 mm TPW. This unexplained feature is likely a dataset anomaly that needs to be explored further. Overall, both over-land and over-ocean snowfall events are present in the database used for the Day 1 version of the GPROF, although 42.6% of land and 11.9% of ocean occur at $T2m$ values at or below 255 K.

To establish how much shallow snowfall occurs over ocean versus over land, Figure 5.16 shows the $T2m/TPW$ joint histograms for each category. Over land, the number of shallow snowfall occurrences is significantly less than over ocean (23.6% of shallow occurrences are over land). Over-ocean shallow snowfall makes up the largest fraction of

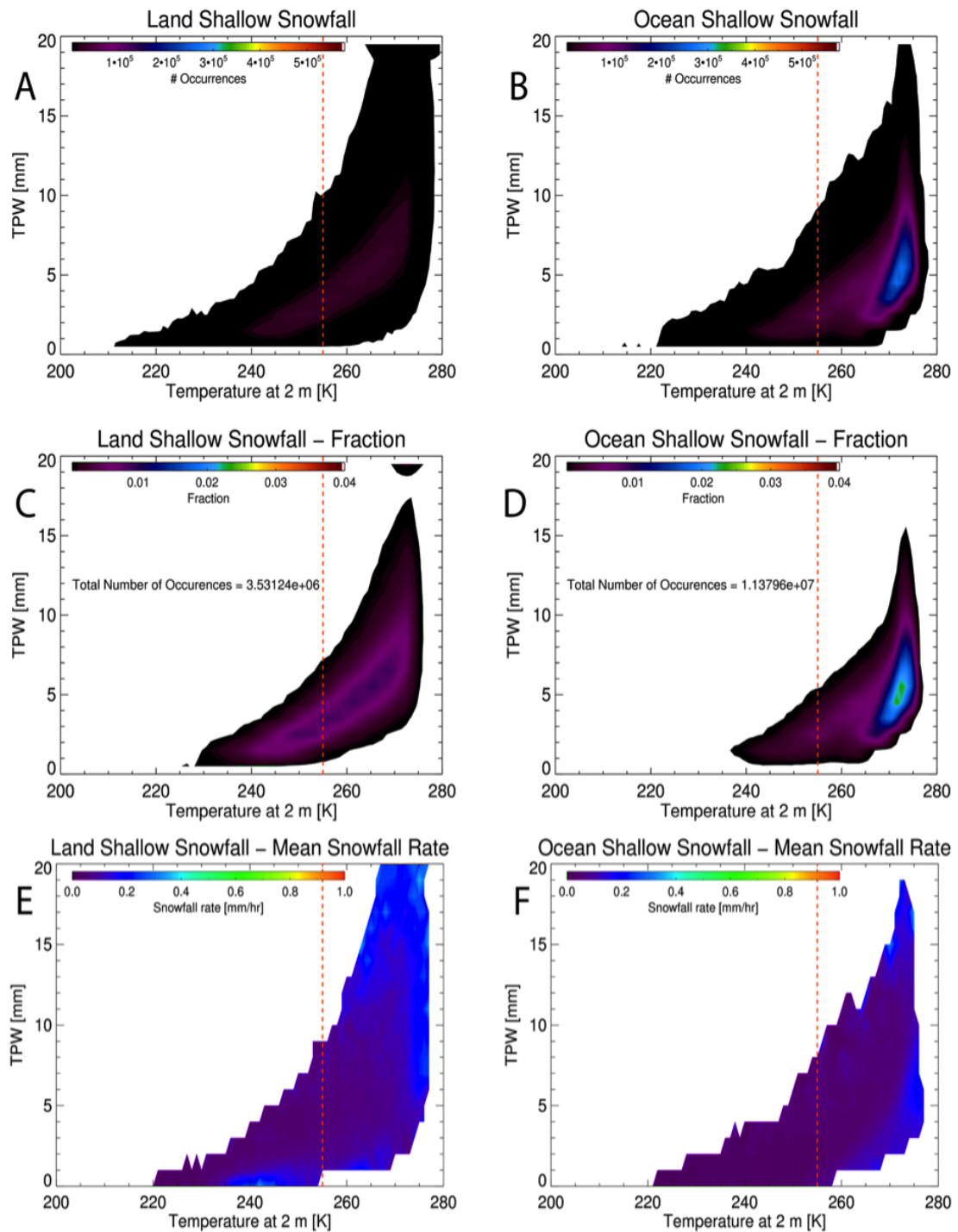


FIGURE 5.16: Same as Figure 5.13, but now showing over-land shallow snowfall events (left column) and over-ocean shallow snowfall events (right column).

shallow snow (76.1%), and still maintains the peak and tail end that is seen in the shallow snow joint histogram (Figure 5.14a,c). The fraction of over-land shallow snowfall does not appear to be biased toward higher or lower temperatures, whereas for over-ocean shallow snowfall, the likelihood for snowfall to occur near freezing is much higher. Figure 5.16b shows the same maximum frequency of occurrence of snowfall events that is seen as a bifurcation at low TPW in Figure 5.15b, implying that over-ocean convective snowfall largely causes this feature. The mean snowfall rate plots (Figure 5.16e-f) look somewhat similar to those in Figure 5.15e-f, though with relatively lower snowfall rates. Mean snowfall rates in bins populated by large snowfall rate counts are generally lower (less than $\sim 0.2 \text{ mm h}^{-1}$) and therefore indicate a large fraction of shallow snowfall rates with very light snowfall – a feature also discussed in Kulie et al. (2016). Over land, the mean snowfall rate increases to $\sim 0.2 \text{ mm h}^{-1}$ at high T2m and high TPW, but there are very few occurrences of snowfall that populate these bins (Figure 5.16a). Additionally, there is a large area of increased snowfall rates (less than 0.2 mm h^{-1} higher than surrounding bins) between 235-255 K and at very low TPW that could plausibly be associated with convective snow associated with cold air outbreaks in very low TPW environments; however, this cluster of elevated bin-averaged snowfall rates could also be caused by ground clutter contamination (Kulie and Bennartz, 2009, Maahn et al., 2014). Over ocean, this feature is nonexistent. While the over-land feature may be ground clutter, it is still included in the CloudSat/AMSR-E/MHS database. A significant population of shallow CloudSat-indicated shallow snowfall events over ocean associated with warmer temperatures (91.0%), however, would not be considered in the Day 1 GPROF retrieval

scheme. Land shallow snowfall occurrences at warmer temperatures than 255K are a lower percentage (71.5%) than the over-ocean shallow snowfall category.

5.3.4 Hemispheric Analysis

Additional partitioning of the CloudSat snowfall data into over-ocean in the Northern and Southern hemispheres is shown in Figure 5.17 to illustrate any inherent differences in snowfall as a function of T2m and TPW. Based on Figures 5.15 and 5.16 displaying higher occurrence of snowfall over ocean than land, and the fact that the surface area of the ocean is greater in Southern Hemisphere than the Northern, the data is split to Northern and Southern Hemispheric snowfall over-ocean. The Southern hemisphere's ocean, as suspected due to the greater surface area, has more occurrences of snowfall than the Northern hemisphere. About 53.4% of all global snowfall cases occur in the Southern Hemisphere (Figure 5.17a-d). The Northern hemisphere's over-ocean snowfall is apparently responsible for the anomalous feature seen in the over-ocean snowfall histogram of Figure 5.15 at high TPW near 265 K. The fraction of snowfall events in the Northern hemisphere below 255 K is 41.4% versus 58.6% in Southern hemisphere, though the Southern hemisphere's snowfall is much more likely to occur near freezing than the Northern hemisphere's snowfall. The mean snowfall rate histograms (Figure 5.17e-f) are not drastically different, though in the Southern hemisphere, snowfall rates are approximately 0.2 mm h^{-1} higher at TPW between 5-15 mm compared to the Northern hemisphere. Both the Southern and Northern hemisphere's oceans experience snowfall below 255 K that would be included in the CloudSat database.

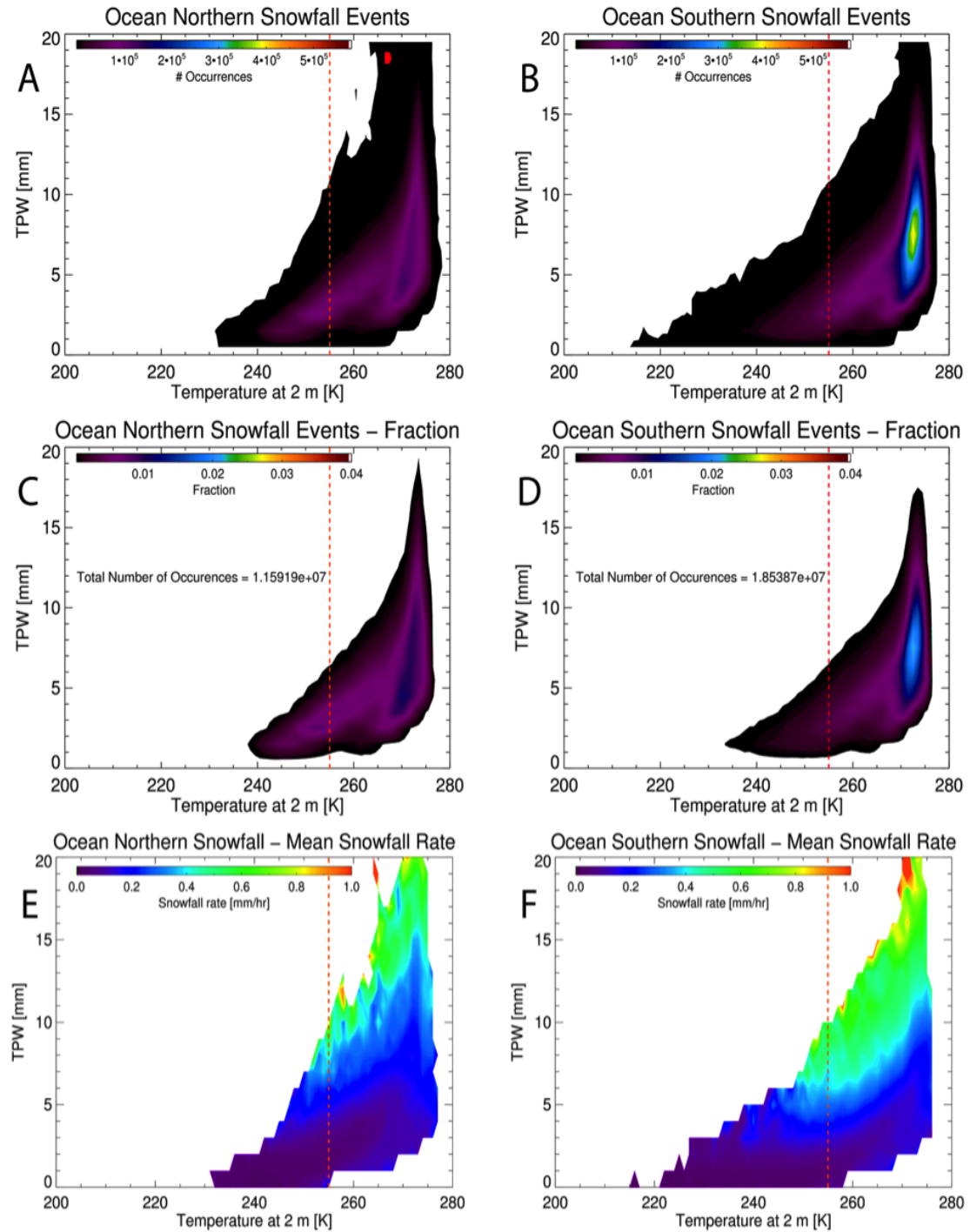


FIGURE 5.17: Same as Figure 5.13, but now showing over-ocean Northern Hemisphere snowfall events (left column) and over-ocean Southern Hemisphere snowfall events (right column).

The final partition of this dataset is done by recreating the previous plot, but for shallow snowfall events only (see Figure 5.18). As was the case for all over-ocean snowfall events, the number of occurrences of shallow snowfall in the Southern hemisphere (56.6% of all over-ocean shallow snowfall cases) exceeds that of the Northern hemisphere (43.4%). The fraction of shallow snowfall in the Northern hemisphere (Figure 5.18c) is now higher near freezing, unlike the slightly more uniform fraction of occurrence of all snowfall in the Northern hemisphere, Figure 5.17c. The Southern hemisphere's fraction of shallow snowfall, Figure 5.18d, has increased near freezing, making shallow snowfall events much more likely (than it was for all snowfall events) to occur near freezing. The fraction in the Southern hemisphere is also higher at higher TPW than the Northern hemisphere, reflecting the colder and drier environments in which shallow snowfall occurs in the Northern hemisphere. Interestingly, when analyzing the mean snowfall rate histograms (Figure 5.18e-f), there isn't too much of a difference between the hemispheres, though the Southern hemisphere shows snowfall rates occurring at colder temperatures, the Northern hemisphere plot may not be showing any snowfall rates due to the constraint of at least 100 occurrences of snowfall in the bin.

Figures 5.13-5.18 indicate how different snowfall populations are when partitioned by snowfall mode (e.g. shallow versus nimbostratus), land versus ocean, and/or Northern versus Southern hemispheres. The CloudSat snowfall dataset, no matter how it was partitioned in this section, always had observations of snowfall events occurring at or below 255 K. These snowfall rates, paired with T2m and TPW, are used for the Day 1

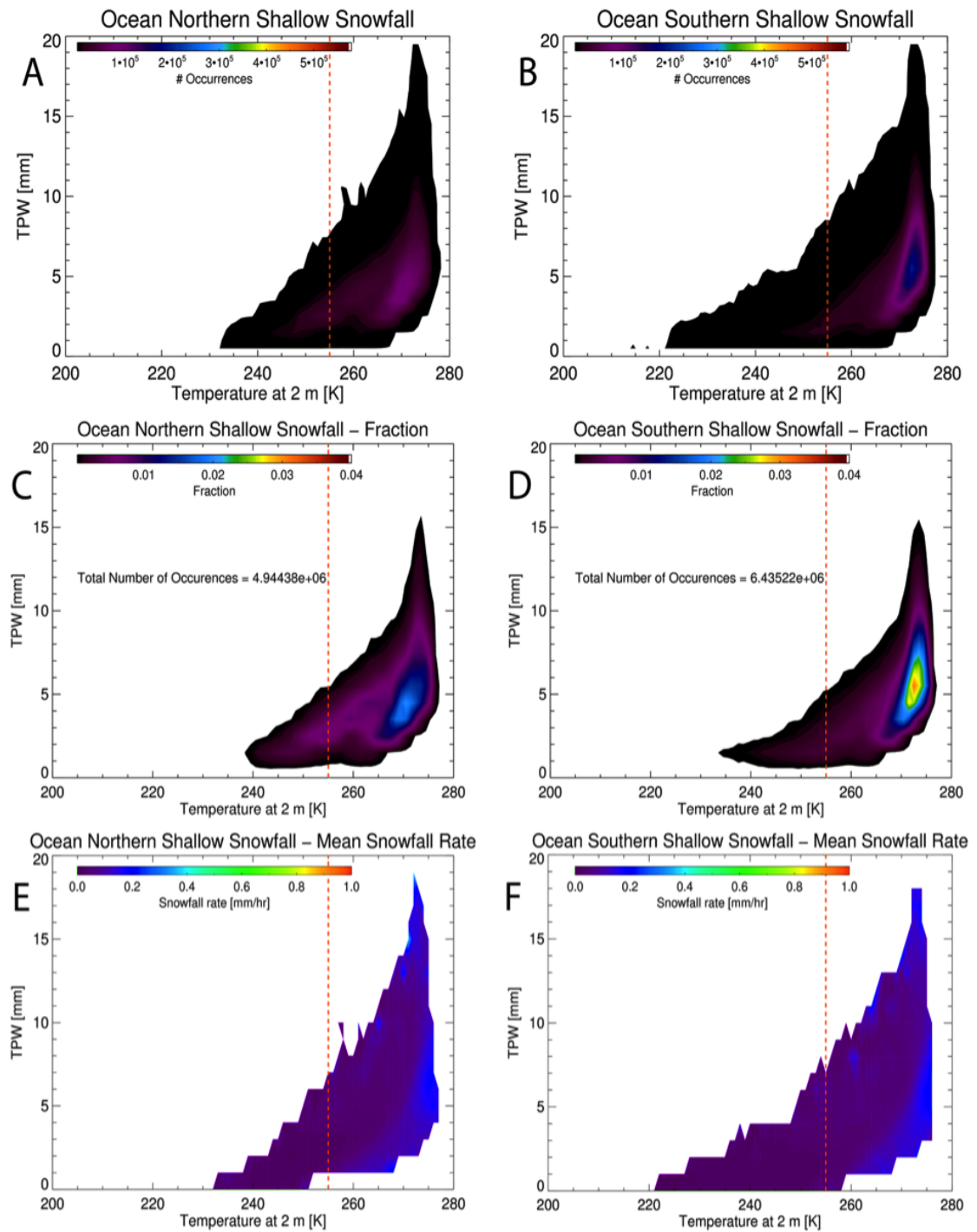


FIGURE 5.18: Same as Figure 5.13, but now showing over-ocean Northern Hemisphere shallow snowfall events (left column) and over-ocean Southern Hemisphere shallow snowfall events (right column).

version of the GPROF precipitation retrieval algorithm. After Day 1, a completely new dataset of GPM DPR-derived precipitation rates and matching GMI brightness temperatures will replace the CloudSat/AMSR-E/MHS database for the GPROF 2016 Version 1 (Kummerow et al., 2015). The next section will compare the GPM-only database (consisting of the DPR-derived precipitation rates) to the CloudSat database just analyzed. Ideally, both *a priori* datasets would realistically reflect the natural variability of global snowfall; a comparison will, therefore, identify systematic shortcomings in either dataset.

5.4 GPM vs. CloudSat Analysis

Each of the GPM Version 3 frozen precipitation products (Ku-band, NS Combined Ku-band, and MS Combined Ku- and Ka-bands) is compared against CloudSat’s snowfall product to analyze under what meteorological conditions each satellite observes snowfall. Figure 5.19 displays the frequency of occurrence of snowfall, Figure 5.20 displays the normalized relative frequency of occurrence (or fraction) of snowfall, and Figure 5.21 displays the mean snowfall rate for each respective T2m/TPW bin for all four datasets. For each figure, panel A is CloudSat, panel B is the GPM Mean Scan (MS), panel C is the GPM Normal Scan (NS), and panel D is the GPM Ku-band snowfall. The GPM data is a year-long dataset measured with a scanning radar, and the CloudSat data is more than 4 years of data measured with a non-scanning, near-nadir pointing radar. The total number of CloudSat snowfall cases is $\sim 4.62 \times 10^7$ occurrences, GPM MS cases is 1.91×10^7 occurrences, GPM NS cases is 1.91×10^7 occurrences (535 fewer occurrences than GPM

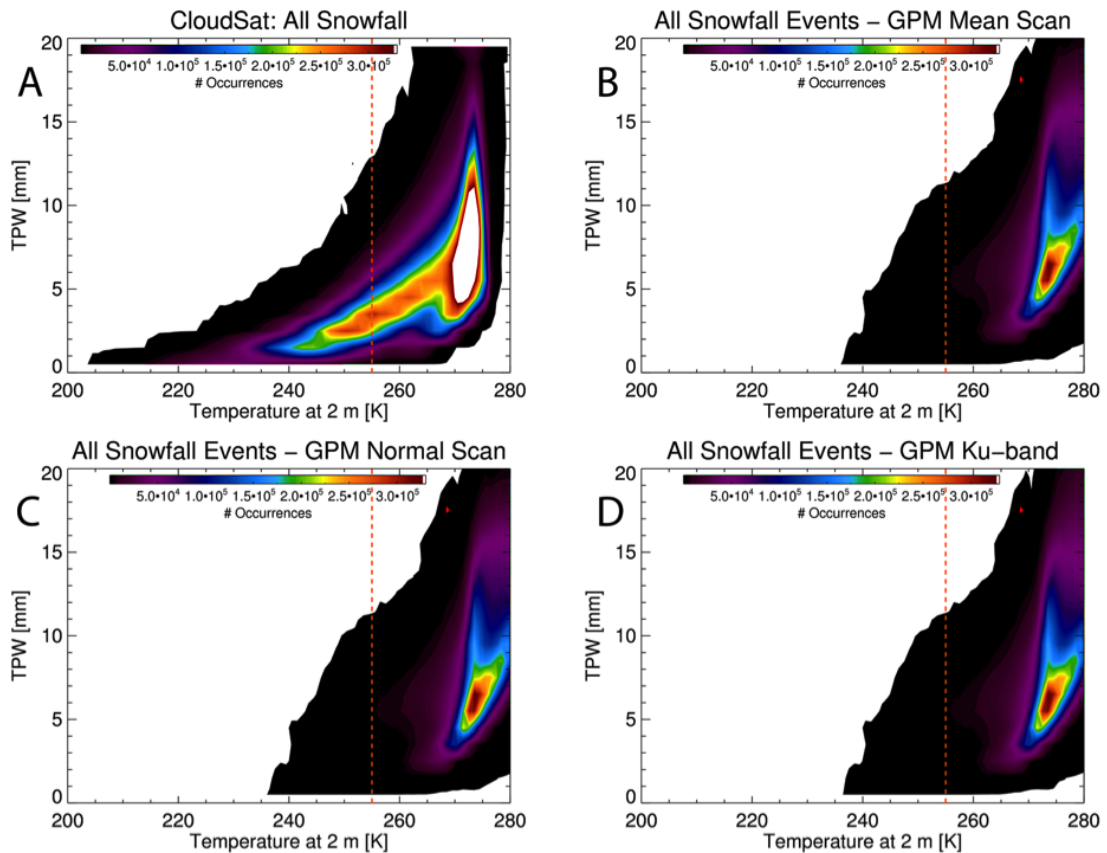


FIGURE 5.19: Comparison of the frequency of occurrence of snowfall as observed by CloudSat, the GPM Mean Scan (MS), the GPM Normal Scan (NS) and the GPM Ku-band.

MS), and GPM Ku-band cases is $\sim 2.50 \times 10^7$ occurrences. This means that CloudSat only has approximately twice as many snowfall occurrences than each of the GPM scans/bands. The lower limit for GPM data to plot is at least 50 occurrences of frozen precipitation (half of CloudSat's 100 occurrence minimum, though CloudSat has more data). Note that the CloudSat histogram looks different when compared to the previous section, as the color bar was changed to match the GPM plots (and the GPM dataset contains less snowfall, as it is only one year of data). Each of the GPM datasets looks entirely different from the CloudSat dataset, in that there appears to be more snowfall occurring

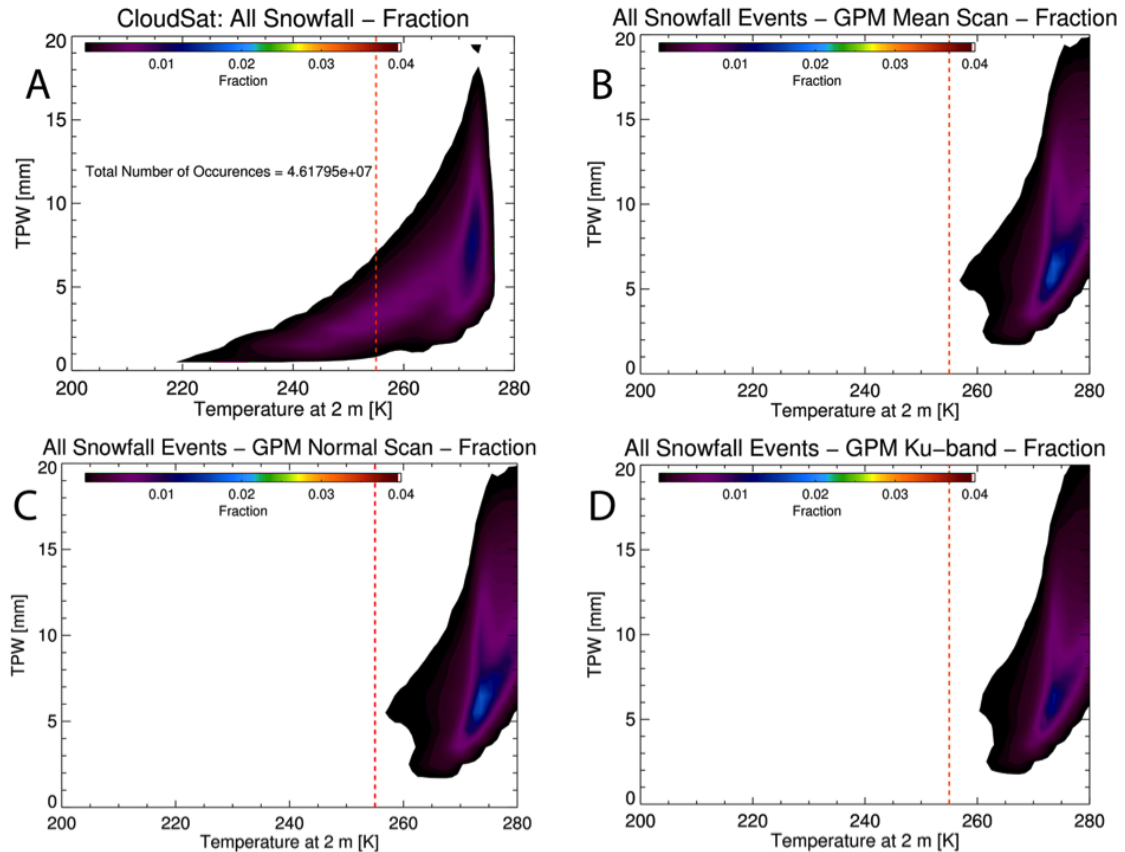


FIGURE 5.20: Comparison of the relative frequency of occurrence, or fraction, of snowfall as observed by CloudSat, the GPM Mean Scan (MS), the GPM Normal Scan (NS) and the GPM Ku-band.

at warmer temperatures and less snowfall occurring at colder temperatures in the GPM datasets. The three GPM products appear to mostly agree on frequency of occurrence, and there doesn't appear to be very many snowfall occurrences measured below 255 K (especially when compared with CloudSat; only 0.94% of MS cases, 0.94% of NS cases, and 0.7% of cases occur at $T_{2m} \leq 255$ K compared to CloudSat's 22.5%). An interesting feature shared among the GPM datasets that isn't present in the CloudSat dataset is a bifurcation at warmer temperatures and higher TPW and no obvious bifurcation in the lower T_{2m}/TPW regime as indicated in the CloudSat dataset. This new feature in

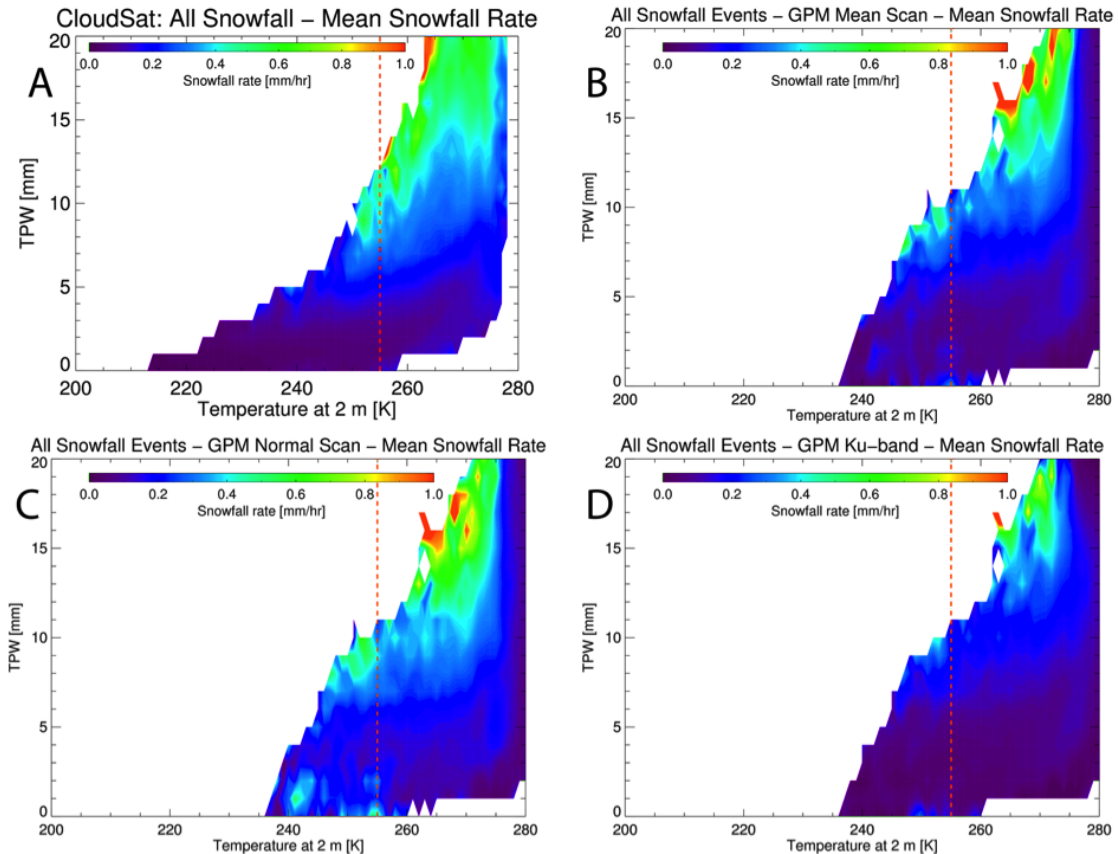


FIGURE 5.21: Comparison of the mean snowfall rate as observed by CloudSat, the GPM Mean Scan (MS), the GPM Normal Scan (NS) and the GPM Ku-band.

the GPM plots could be the result of mixed precipitation being included in the frozen precipitation products.

The fraction of occurrence plots for the three GPM datasets are also very similar, though the Ku-band (non-combined) product, Figure 5.20d, shows a relatively lower fraction of occurrence of snowfall near freezing, similar to what CloudSat shows near freezing in Figure 5.20a. The lack of a tail below 255 K is even more apparent in the fraction plots, Figure 5.20, as the fraction is so low that it does not show up at all below 255 K. The mean snowfall rate plots, Figure 5.21, do show snowfall being detected at colder

temperatures, though the CloudSat plot is still masking out bins that have fewer than 100 occurrences of snowfall measured. The NS (Figure 5.21c) shows relatively higher snowfall rates occurring at colder temperatures and low TPW, while the Ku-band and MS snowfall rates (Figure 5.21b,d) more closely resemble CloudSat snowfall (though the MS and Ku products do appear to have slightly higher snowfall rates than CloudSat shows). Fewer snowfall occurrences below 255 K and higher snowfall rates could be a result of GPM's orbit being so limited, while CloudSat has more than 20° latitude more coverage than GPM. CloudSat's higher radar sensitivity may also play a role in detecting additional light snowfall events that cannot be effectively detected by GPM's radar (see discussion associated with following figures).

In order to more fairly assess these two datasets, the CloudSat dataset is limited to include only observations made within the same latitudinal boundaries as the GPM observations, $|\leq 65|^\circ$ latitude. The frequency of occurrence of snowfall is plotted in Figure 5.22, the relative frequency of occurrence in Figure 5.23, and the mean snowfall rate in Figure 5.24. The GPM plots remain the same, and are now just being compared to the limited CloudSat dataset. The amount of snowfall observations has universally decreased in Figure 5.22a, as higher latitudes that would be more likely to snow (than the mid-latitudes or, obviously, the tropics) are no longer included in the dataset. The tail of observations that extended below 255 K has receded remarkably, though there are still more occurrences of snowfall than the GPM dataset. The fraction of occurrence for CloudSat (Figure 5.23a) has increased near freezing due to fewer meteorological conditions under which snowfall is being observed. However, there is still a larger fraction of snowfall occurrences below 255

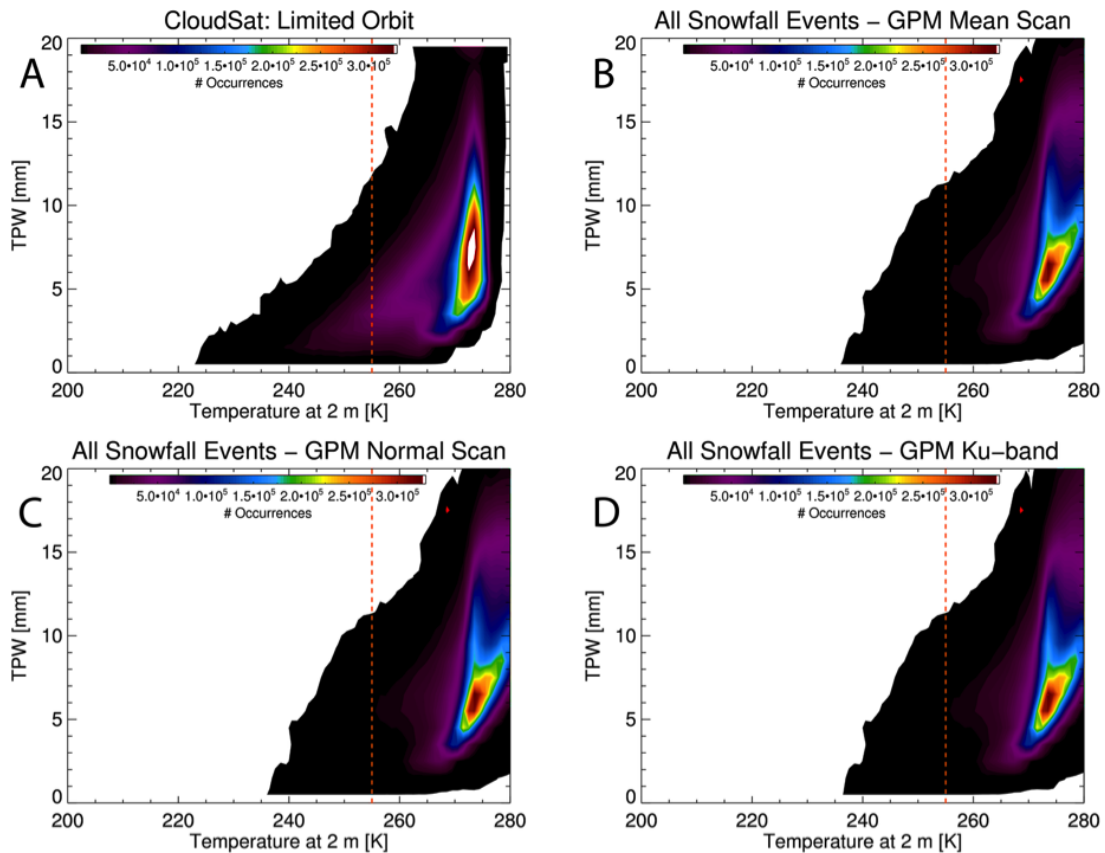


FIGURE 5.22: Comparison of the frequency of occurrence of snowfall as observed by CloudSat, the GPM Mean Scan (MS), the GPM Normal Scan (NS) and the GPM Ku-band. CloudSat's orbit is now limited to be within 65° latitude.

K than the GPM datasets show. The mean snowfall rate plot (Figure 5.24a) shows more bins with higher snowfall rates due to fewer events with low snowfall rates being included. Knowing that GPM's less sensitive radar bands are biased to observe higher reflectivities (which corresponds to higher snowfall rates), these plots (Figure 5.24b-d) could imply that GPM is less likely to overpass snowfall events with such low reflectivities that the DPR would not be able to detect it. In order to investigate this complicating factor, the following plots are made.

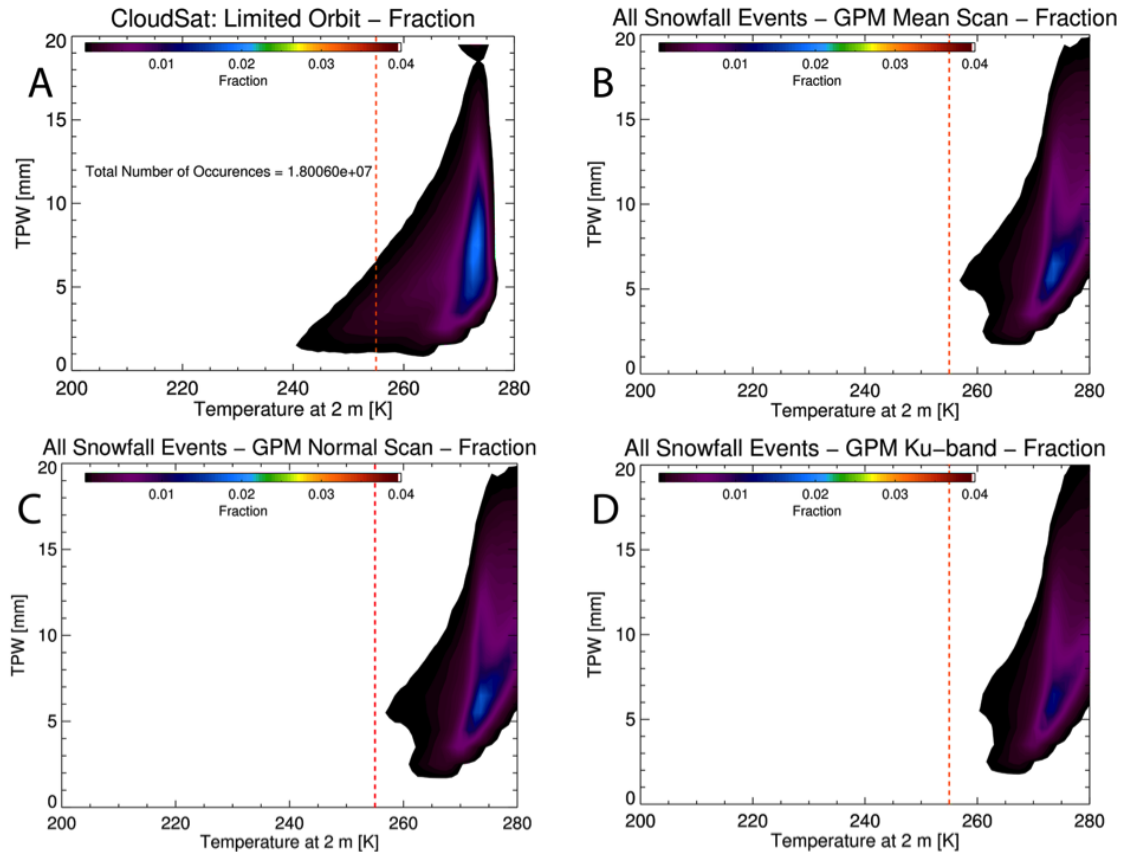
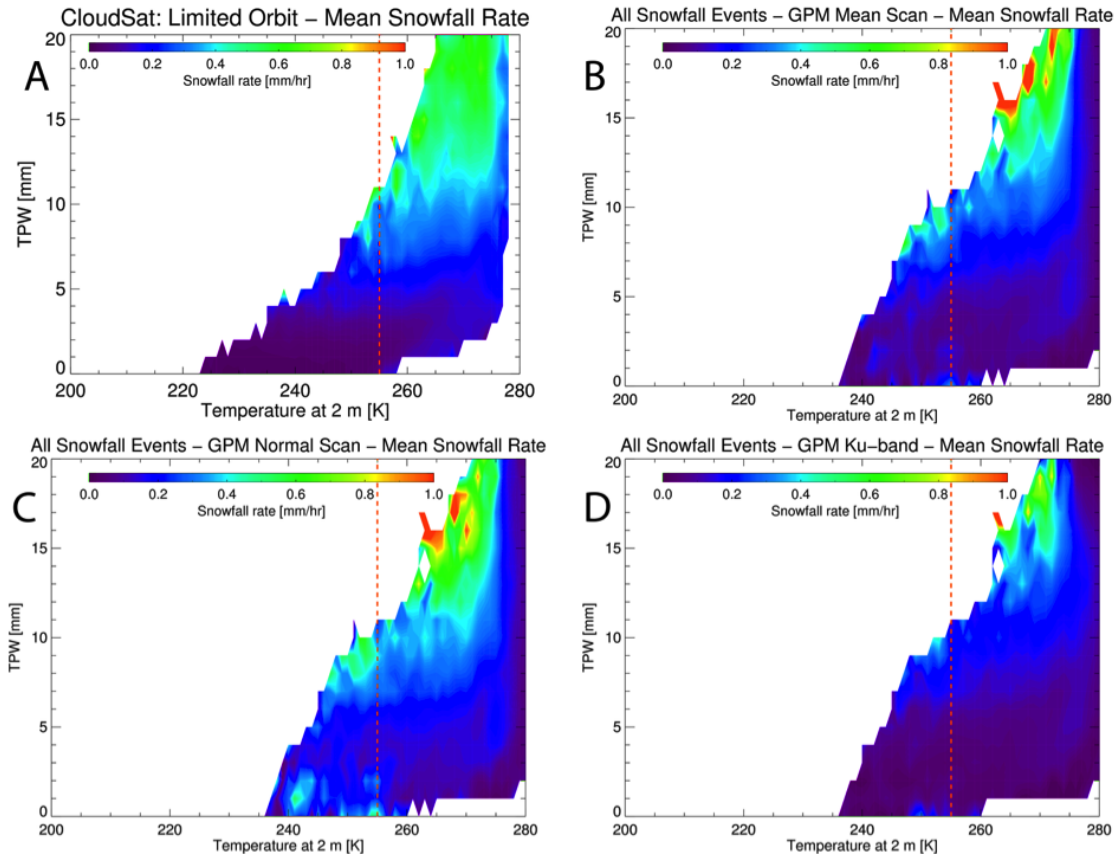


FIGURE 5.23: Comparison of the relative frequency of occurrence, or fraction, of snowfall as observed by CloudSat, the GPM Mean Scan (MS), the GPM Normal Scan (NS) and the GPM Ku-band. CloudSat’s orbit is now limited to be within $|\leq 65^\circ|$ latitude.

The DPR operates at two frequencies (Ka- and Ku-band, or 35 and 13 GHz respectively) that are not the same as CloudSat (W-band, or 94 GHz). The Ka-band radar is the more sensitive of the two radars, with a minimum detectable reflectivity of approximately 12 dBZ (Hou et al., 2014). CloudSat, however, has a minimum detectable reflectivity of approximately -29 dBZ (Tanelli et al., 2008), and thus the two datasets cannot be compared fairly without limiting CloudSat’s minimum detectable reflectivity. Thus, an approximately equivalent minimum detectable reflectivity of 5 dBZ is used to limit the CloudSat dataset. The 5-dBZ equivalent reflectivity value is admittedly a conservative



..

FIGURE 5.24: Comparison of the mean snowfall rate as observed by CloudSat, the GPM Mean Scan (MS), the GPM Normal Scan (NS) and the GPM Ku-band. CloudSat's orbit is now limited to be within $|\pm 65|^\circ$ latitude.

ad hoc choice. Additional theoretical reflectivity calculations using ice models should be undertaken to choose a more appropriate – and maybe higher – equivalent W/Ka reflectivity value. Figure 5.25 shows the frequency of occurrence, Figure 5.26 shows the relative frequency of occurrence, and Figure 5.27 shows the mean snowfall rate. Limiting the reflectivity has lessened the number of occurrences that CloudSat observes much more than limiting the orbit did. However, the fraction of occurrence (Figure 5.26a) still looks similar, indicating that limiting either orbit or reflectivity range causes relatively more occurrences to be observed near freezing. The mean snowfall rate (Figure 5.27a) has also

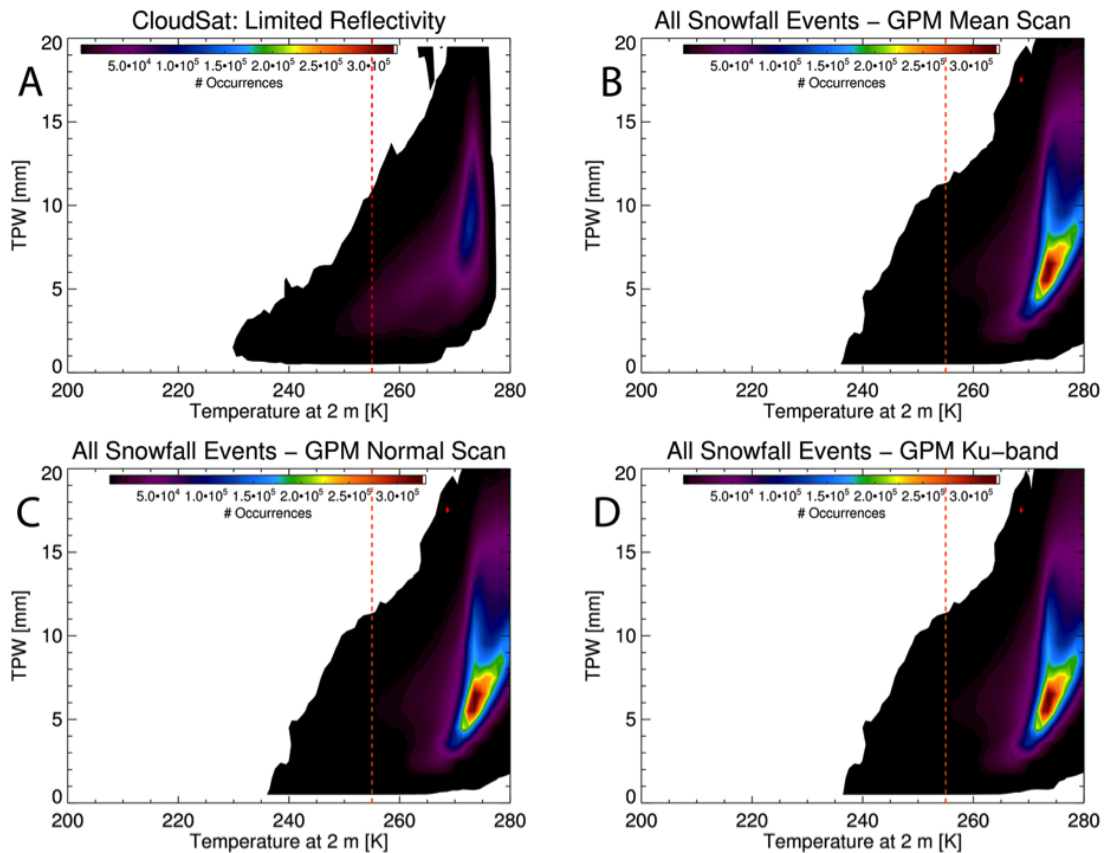
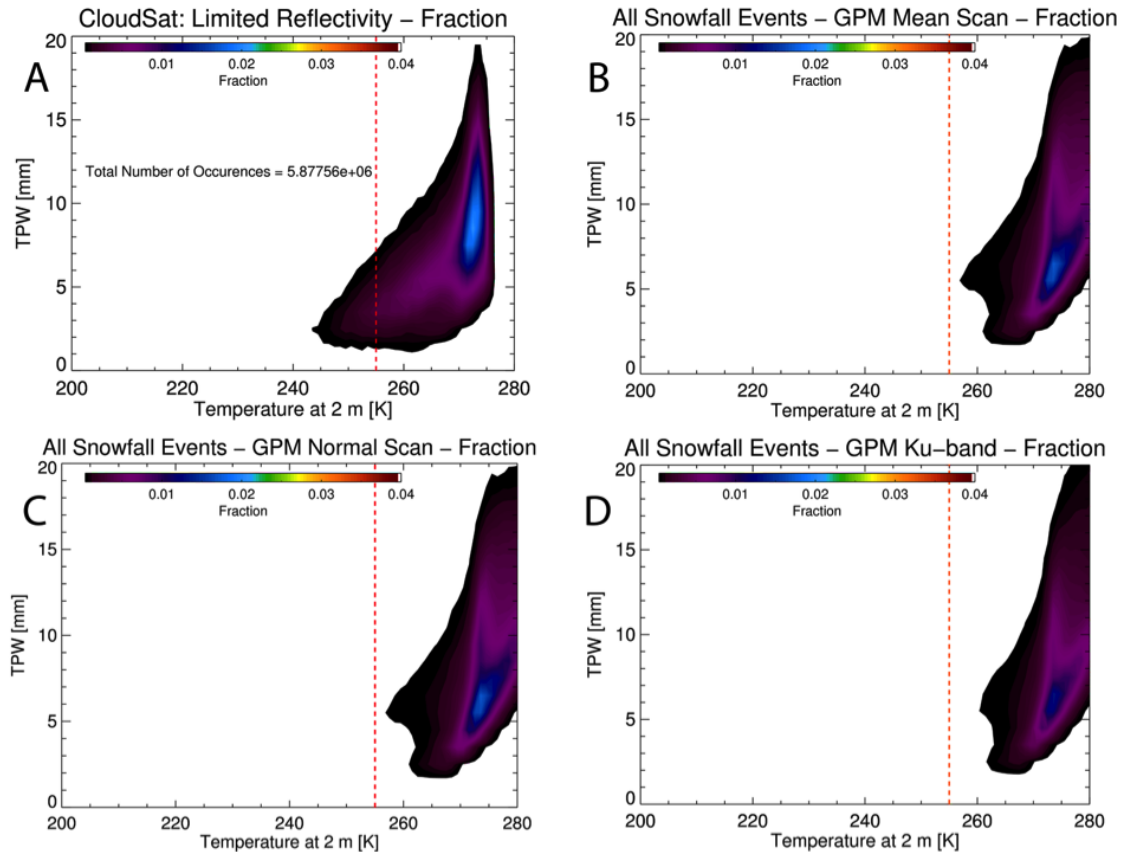


FIGURE 5.25: Comparison of the frequency of occurrence of snowfall as observed by CloudSat, the GPM Mean Scan (MS), the GPM Normal Scan (NS) and the GPM Ku-band. CloudSat’s reflectivity is limited to an approximately equivalent minimum detectable reflectivity.

seemingly increased across all bins, indicating fewer light snowfall events being observed.

Compared to GPM’s observations, limiting the reflectivity causes CloudSat to see far fewer occurrences of snowfall and biases CloudSat to see higher snowfall rates. Despite these limitations, CloudSat still observes snowfall below 255 K, whereas GPM does not.

Finally, the CloudSat data is limited by both orbit and the reflectivity in Figures 5.28-5.30. The CloudSat snowfall dataset is significantly reduced (by 93.8%), with very few snowfall occurrences showing up below 255 K ($0.2\% \leq 255 \text{ K}$ compared to $22.5\% \leq$



..

FIGURE 5.26: Comparison of the relative frequency of occurrence, or fraction, of snowfall as observed by CloudSat, the GPM Mean Scan (MS), the GPM Normal Scan (NS) and the GPM Ku-band. CloudSat's reflectivity is limited to an approximately equivalent minimum detectable reflectivity.

255K for entire CloudSat dataset). The frequency of occurrence of snowfall by GPM (Figure 5.28b-d) shows how much more frozen precipitation GPM is seeing, even with the tighter orbital constraints and the less sensitive DPR. The fraction of occurrence of snowfall in the CloudSat dataset (Figure 5.29a) has spiked near freezing, while GPM (Figure 5.29b-d) is slightly less biased (though still biased nonetheless) to observe snowfall/frozen precipitation near freezing. It is apparent from these plots that CloudSat is

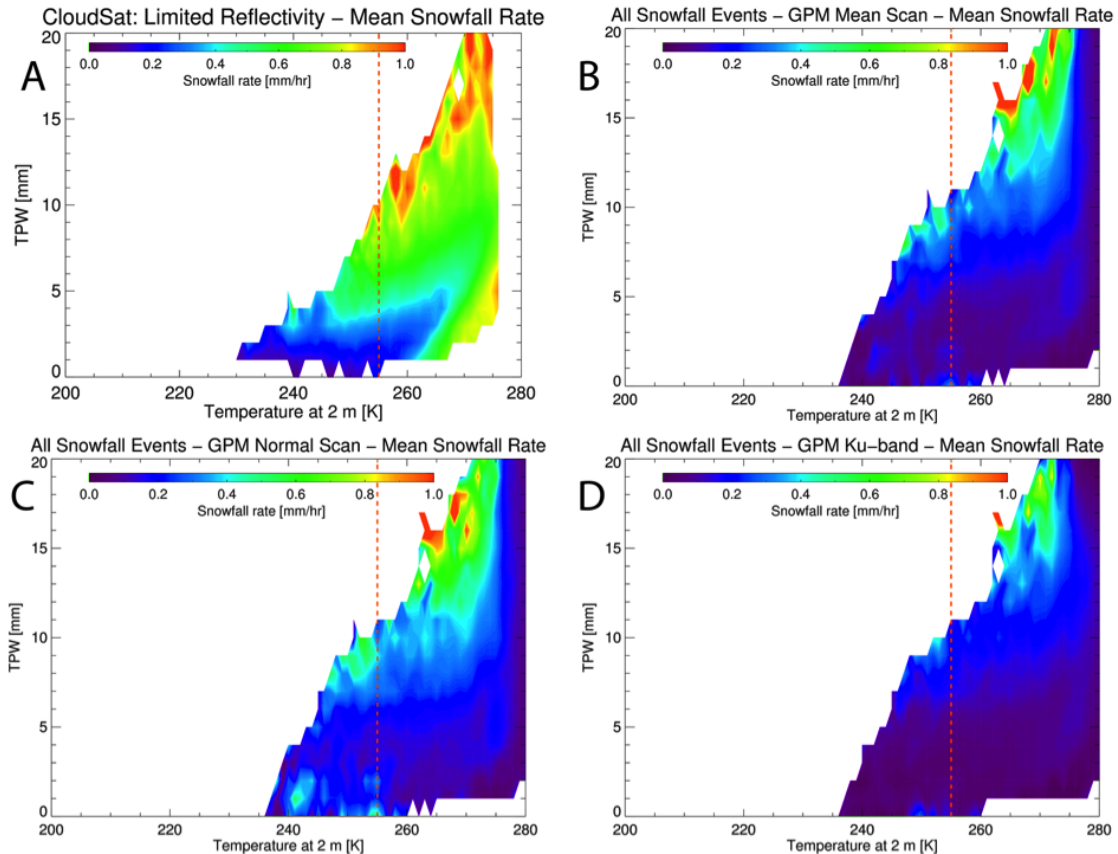


FIGURE 5.27: Comparison of the mean snowfall rate as observed by CloudSat, the GPM Mean Scan (MS), the GPM Normal Scan (NS) and the GPM Ku-band. CloudSat’s reflectivity is limited to an approximately equivalent minimum detectable reflectivity.

observing a very different snowfall dataset compared to GPM from a T2m/TPW perspective, as the peak fraction of occurrence for CloudSat exists at higher TPW than for GPM. Finally, the mean snowfall rate of CloudSat (Figure 5.30a) has increased in all bins, indicating that CloudSat is more biased to find heavier snowfall than GPM (Figure 5.30b-d) when limited in the same way GPM is. The higher latitudinal coverage and more sensitive radar on CloudSat made the existence of a CloudSat database at $T2m \leq 255K$ possible, and is something to be considered for future satellite missions that aim to measure global snowfall. These comparisons afford the following result from the GPM

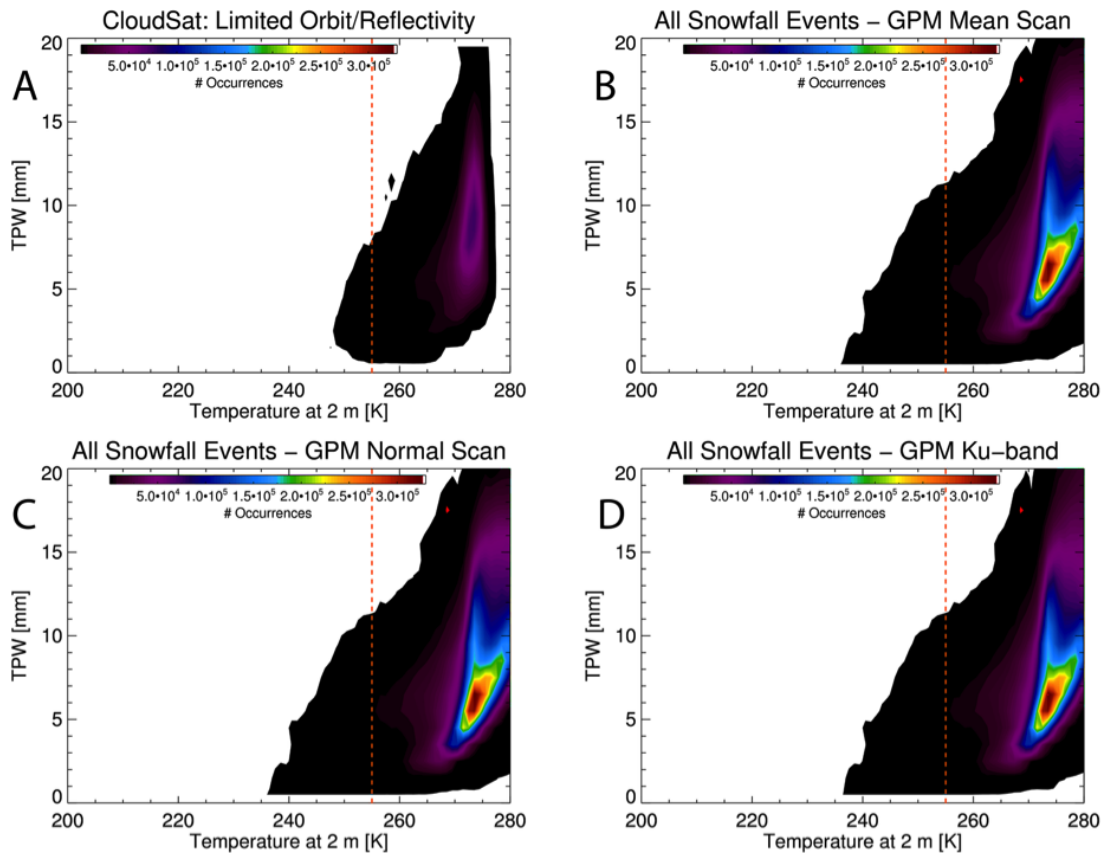


FIGURE 5.28: Comparison of the frequency of occurrence of snowfall as observed by CloudSat, the GPM Mean Scan (MS), the GPM Normal Scan (NS) and the GPM Ku-band. CloudSat’s reflectivity is limited to an approximately equivalent minimum detectable reflectivity and its orbit is limited to be within 65° latitude.

and CloudSat databases.

During Day 1 GPROF era, for which GPM used the CloudSat database to assign snowfall rates, there were far more snowfall events available to populate a database of coincident snowfall, T2m, and TPW. If CloudSat’s orbit and minimum detectable reflectivity were limited in such a way that matches GPM as closely as possible, CloudSat’s snowfall database is significantly reduced in number as well as biased to find higher snowfall rates, even compared to the less sensitive DPR. The 255 K boundary for using the CloudSat

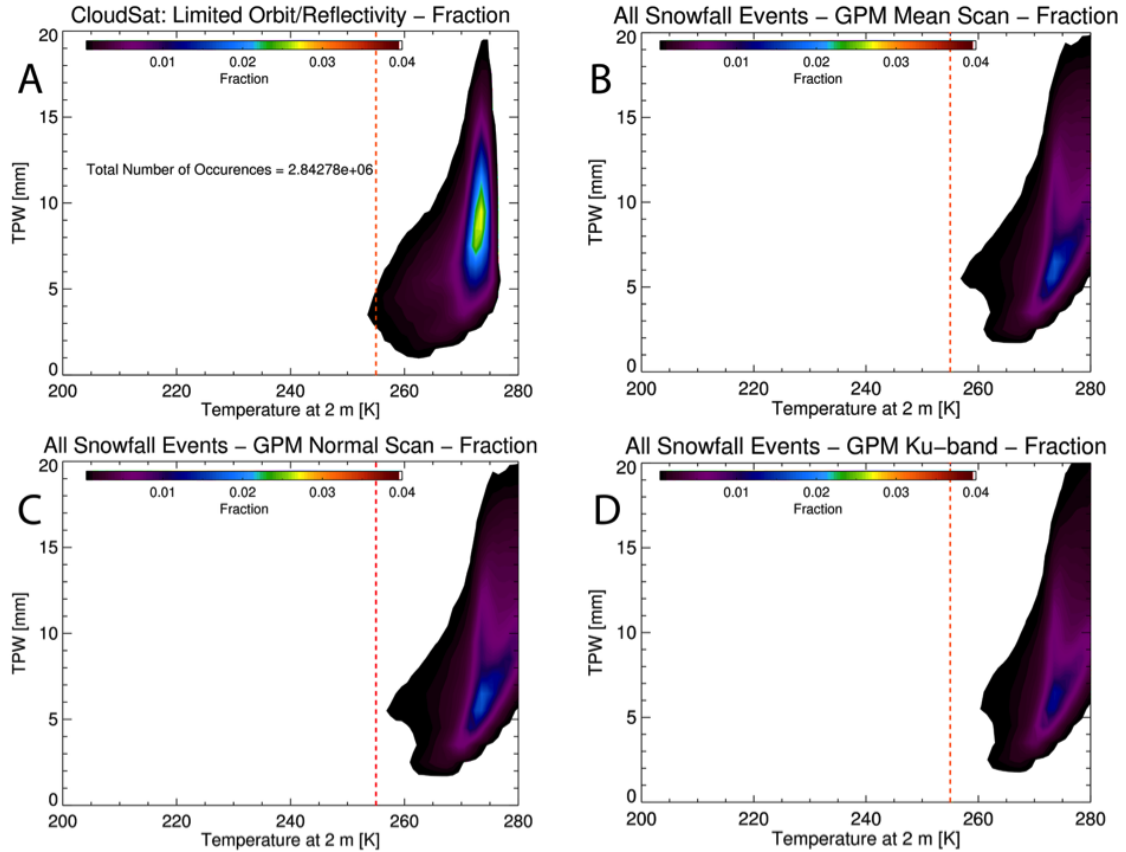
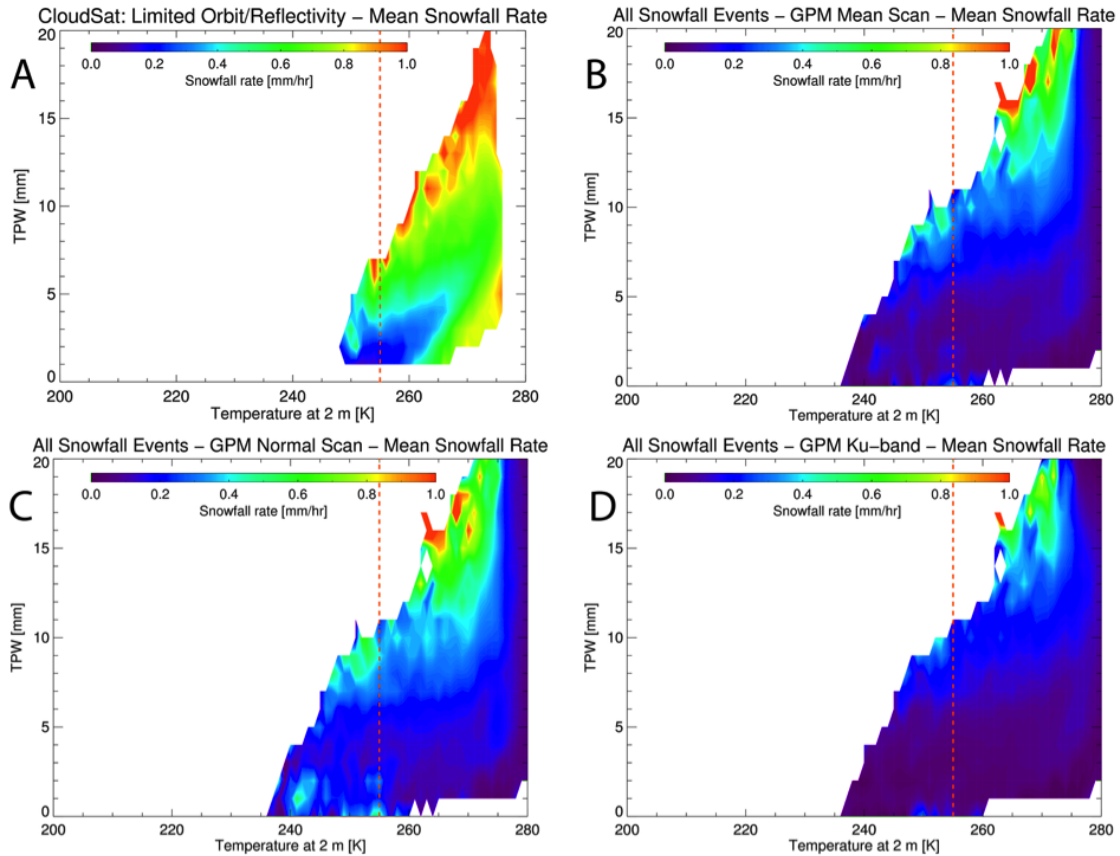


FIGURE 5.29: Comparison of the relative frequency of occurrence, or fraction, of snowfall as observed by CloudSat, the GPM Mean Scan (MS), the GPM Normal Scan (NS) and the GPM Ku-band. CloudSat's reflectivity is limited to an approximately equivalent minimum detectable reflectivity and its orbit is limited to be within 65° latitude.

database creates a very small number of instances where CloudSat would be used for the GPROF precipitation retrievals during Day 1. Therefore, if GPM overpasses a snowfall event that is over ocean but above 255 K (and, say, below 273 K), then the Day 1 GPROF database used to assign a precipitation rate is a modified TRMM database that utilizes truncated vertical profiles above the freezing level to mimic frozen surface precipitation at higher latitudes. Using a database populated by precipitation retrievals



..

FIGURE 5.30: Comparison of the mean snowfall rate as observed by CloudSat, the GPM Mean Scan (MS), the GPM Normal Scan (NS) and the GPM Ku-band. CloudSat’s reflectivity is limited to an approximately equivalent minimum detectable reflectivity and its orbit is limited to be within 65° latitude.

gathered in the tropics (between 35° latitude) to assign snowfall rates can lead to inaccurate observations, as the microphysical properties associated with such observations may systematically differ and require different Z-S relationships to produce realistic snowfall rates.

Chapter 6

Conclusions

A complete global study of snowfall through the lens of multiple datasets is beneficial to determine future avenues for both models and observational platforms to study snowfall. Comparing multiple datasets will show any biases or differences that may affect the precipitation retrievals computed by the GPM GPROF radiometer algorithm, especially as it transitions from a collection of disparate radar/radiometer observational *a priori* retrieval databases to its fully parametric GPM-based format in 2016. This study leverages a combination of model (ERA-Interim) and components of the GPROF Day 1 observational datasets (CloudSat) to study global snowfall from a handful of unique perspectives. First, modeled snowfall accumulation output of a reanalysis dataset, ERA-Interim, was analyzed over a 35-year period to identify climatological global snowfall trends and to provide valuable climatological context for the relatively limited CloudSat observational period

used in this study. Next, the CloudSat snowfall dataset was compared against ERA-Interim to find any systematic differences between the two datasets. CloudSat snowfall observations, in conjunction with coincident AMSR-E and MHS brightness temperature observations, are used in the Day 1 version of the GPROF algorithm for assigning snowfall rates at very cold surface temperatures. The next section analyzed the CloudSat snowfall observations from the perspective of meteorological conditions (T2m and TPW), as the GPROF algorithm uses these as parameters to optimize retrievals. Lastly, the CloudSat database is compared to the preliminary GPM-derived snowfall dataset, which is also analyzed from a similar T2m/TPW meteorological perspective.

Initially, the ERA-Interim snowfall dataset was analyzed from the perspective of global snowfall distributions and accumulations. The availability of snowfall data that is both completely global as well as temporally long affords an analysis of snowfall trends and regional biases that occur year-to-year. A 35-year mean of ERA-Interim's snowfall output shows that snowfall occurs on every continent, though is less frequent at lower latitudes. The lower latitudinal extent of snowfall in the Northern hemisphere resembles that of a common mid-latitude storm track, whereas in the Southern hemisphere, it is much more linear. The Southern Ocean, mountainous regions, and areas such as Southeast Greenland and the Western Antarctic Coast (including the Antarctic Peninsula) experience relatively higher snowfall accumulations, on average, than the rest of the world. More recent years (2007-2010, years coincident with the CloudSat data in this study) show higher snowfall accumulations in these same regions relative to the rest of the globe, especially in 2008 and 2010. ERA-Interim indicated that global snowfall was far below the climatological

average during 2007 with many regions receiving far lower snowfall amounts. Global snowfall accumulations during 2009 were about average, yet obvious regional anomalies were also apparent in the ERA-Interim dataset. Lastly, finding the 35-year mean of zonal snowfall totals showed that within CloudSat's $|82|^\circ$ and GPM's $|65|^\circ$ latitudinal constraints, the satellites would miss 10.1% and 54.4% of global snowfall, respectively, irrespective of other possible instrument detectability issues.

Next, the just-analyzed ERA-Interim snowfall dataset was compared against the CloudSat 2C-SNOW-PROFILE dataset for the years 2007-2010. Global distributions of snowfall displayed CloudSat's higher snowfall estimates in regions where both CloudSat and ERA-Interim agree have relatively higher snowfall accumulations (e.g., southeast Greenland and the Southern Ocean – two broad regions that typically receive significant snowfall). Zonal mean snowfall accumulations during these years shows larger discrepancies between the two datasets' Southern hemisphere snowfall estimates than the Northern hemisphere, as well as the fact that both datasets display more snowfall occurring in the Southern hemisphere. A statistical analysis of all snowfall shows that CloudSat is biased high compared to ERA-Interim; however, when splitting data into different snowfall modes based on a CloudSat product, ERA-Interim is biased higher for shallow snowfall during most individual years (but considering all 4 years together, CloudSat is still biased high). CloudSat samples the globe on a 16 day repeat cycle and is limited to $|82|^\circ$ latitude and thus can't account for the entire globe's snowfall (both spatially and temporally), and further studies must investigate how to better compare these two datasets. Because this is the first global analysis of these two snowfall datasets together, further investigation

will identify systematic difference causes between them (see Future Work for further discussion on this topic).

Then, a CloudSat-only analysis of snowfall data was performed through the lens of the GPROF algorithm. Because the GPROF uses T2m and TPW in order to optimize the *a priori* database search in the retrieval scheme, joint histograms were created to show the global snowfall population contained in the CloudSat database from both frequency of occurrence and T2m/TPW bin-averaged snowfall rate perspectives, with special attention paid to snowfall occurrences at or below a T2m of 255 K. These histograms were partitioned to identify trends based on snowfall mode (shallow convective and nimbostratus) and geographical constraints (land versus ocean, Northern versus Southern hemisphere), thus creating a unique and valuable global snowfall analysis that can be used to evaluate other observational and modeling datasets (see Future Work for more details). A CloudSat database with coincident $T2m \leq 255$ K, as is the requirement for the GPROF algorithm, is made up of 22.5% of the 2006-2010 CloudSat snowfall dataset.

Lastly, the results presented a preliminary analysis and comparison of the Version 3 DPR-derived snowfall dataset to CloudSat's snowfall dataset. Despite CloudSat having a temporally longer dataset, all 3 of GPM's DPR-derived snowfall datasets contain approximately half the amount of CloudSat's due to GPM's scanning radar. GPM's snowfall data may contain mixed precipitation as well, due to more occurrences of snowfall at warmer temperatures. An initial comparison of CloudSat's snowfall data with GPM shows two distinctly different global snowfall populations as a function of T2m/TPW and reflects

the difference in respective radar sensitivities as well as the latitudinal boundaries of the satellites. The CloudSat database was limited to only include snowfall in the same latitude boundaries as GPM as well as what was measured at or above a reflectivity approximately equivalent to GPM's minimum detectable reflectivity. CloudSat is unable to capture lighter snowfall events as well as snowfall in colder environments (compared to GPM) when limited in this manner, thus revealing GPM's strength in its scanning radar.

This work leads to the following final conclusions and recommendations for the GPROF algorithm community. The CloudSat database may have been underutilized for the Day 1 retrievals of the GPROF algorithm. This is partly due to GPM's latitudinal constraints that lead to less observations over colder surfaces, and partly due to GPM's less sensitive radar that may not be identifying lighter snowfall rates on colder surfaces. One suggestion is explore possible avenue to continue using the CloudSat dataset in later GPROF versions to make use of the CloudSat/AMSR-E/MHS database for colder surfaces in the GPROF retrievals. Another suggestion is to make use of the CloudSat/AMSR-E/MHS database above 255 K, possibly up to 273 K, to utilize this rich snowfall dataset that captures a much larger spectrum of snowfall events due to CloudSat's impressive radar sensitivity. The CloudSat dataset also provides important combined radar/radiometer signatures of unique snowfall modes like shallow cumuliform snowfall that occur above the ad hoc 255 K temperature threshold. Many of these shallow cumuliform events are lighter and are probably not detectable by the GPM DPR, but GMI radiometer observations may still provide valuable information about these types of snowfall events. Finding ways to link the CloudSat snowfall rates with GMI observations to augment the GPROF high latitude

precipitation retrievals should be explored in future research. The CloudSat dataset, however, may be adversely affected by amplified attenuation at higher precipitation rates and thus should be used in conjunction with the GPM DPR observations that are less immune to severe attenuation for GPROF retrievals. The GPM and CloudSat datasets are both valuable snowfall datasets and should be used synergistically to best characterize global snowfall.

Chapter 7

Future Work

Results from global comparisons of ERA-Interim and CloudSat snowfall datasets reveal systematic differences between respective annual snowfall accumulations. Future work will concentrate on isolating the causes for these disparities. Possible causes for these differences include: (1) CloudSat sampling issues, (2) systematic biases due to CloudSat's snowfall product and its clutter flag, (3) ERA-Interim model physics, and/or (4) Rain/snow partitioning near freezing temperatures. Additionally, the CloudSat and ERA-interim datasets indicate distinctive regional anomalies between the datasets in the northern Atlantic Ocean and Southern Oceanic belt that imply disparities between the snowfall modes that CloudSat observes and ERA-Interim models. These regions have been identified by Kulie et al. (2016) as prominent shallow cumuliform snowfall zones. The current study attempts to isolate these regions by comparing snowfall accumulations from ERA-Interim and CloudSat in grid boxes where CloudSat indicates a majority of

shallow snowfall (both by frequency of occurrence and accumulation thresholds), but this comparison is imperfect since it does not isolate the ERA-Interim snowfall attributed to different snowfall modes. This research pathway, however, motivates future work to compare CloudSat's shallow cumuliform snowfall, as defined in this study, and the available ERA-Interim convective snowfall product. This exercise will help to determine how well the datasets agree both on snowfall mode as well as the annual accumulation totals. Other regionally or geographically focused studies can be undertaken (e.g., isolating mountainous areas, Arctic sea ice regions, and cold continental areas such as interior Russia that have not been extensively studied) to document further differences between the datasets.

A more thorough analysis of the GPM data will also be performed with the Version 3 data as well as the most updated version of the DPR-derived snowfall rates. The dataset will be partitioned in a similar manner as the CloudSat dataset partitioning presented in this study to identify more systematic biases in the GPM dataset. The less-sensitive and spatially lower resolution DPR cannot distinguish cloud types like the CloudSat CPR can, and therefore different snowfall modes may not be as easily distinguished. However, CloudSat is still collecting data and sometimes takes measurements that are near coincident with GPM overpasses. These measurements by the DPR can be compared directly to CloudSat for all snow events to assess typical radar sensitivity deficiencies contained in each respective dataset. Additionally, the DPR observations can be given the same snowfall mode identification as the near-coincident CloudSat snowfall mode to distinguish the biases that occur with each satellite based on snowfall mode. Furthermore, GMI brightness

temperature observations will be analyzed to determine if different snowfall modes cause systematic brightness temperature signatures (e.g., are there systematic high microwave frequency ice scattering signatures associated with different snowfall modes?).

As part of an NASA Earth System Science Fellowship (NESSF) proposal (submitted 2016), long-term future work includes merging the GPM and CloudSat snowfall datasets to create a larger dataset with more global coverage. This new snowfall dataset will be compared against reanalysis datasets (ERA-Interim and the NASA Modern-Era Retrospective Analysis for Research and Applications, or MERRA) and climate models (the 5th Phase of the Coupled Model Intercomparison Project, or CMIP5 ensemble, and the Community Earth System Model, or CESM ensemble). Comparisons between the observational and modeling datasets will be facilitated by using similar analysis metrics highlighted in this study (e.g., comparing respective snowfall populations as a function of environmental parameters). Snowfall will be used as an emergent constraint to determine which models most realistically portray global snowfall based on the merged CloudSat/GPM dataset attributes. Climate model snowfall output will be analyzed in future decades to determine what the future of snowfall looks like, both from an accumulation standpoint as well as from a regional standpoint. Special attention will be paid to models that most closely resemble the CloudSat/GPM dataset (spatially, quantitatively, and based on environmental parameters), as these model datasets will presumably possess the physical modeling schemes to produce realistic global snowfall and thus be considered the most accurate to investigate the future of global snowfall in a warming climate.

Bibliography

- Berrisford, P., D. P. Dee, P. Poli, R. Brugge, K. Fielding, M. Fuentes, P. W. Kållberg, S. Kobayashi, S. Uppala, and A. Simmons, 2011: The ERA-Interim archive Version 2.0. Tech. rep., ECMWF, Shinfield Park, Reading, UK.
- Cao, Q., Y. Hong, S. Chen, J. J. Gourley, J. Zhang, and P. E. Kirstetter, 2014: Snowfall detectability of NASA's CloudSat: The first cross-investigation of its 2C-SNOW-PROFILE product and National Multi-Sensor Mosaic QPE (NMQ) snowfall data. *Prog. Electromagn. Res.*, **148**, 55–61.
- Comiso, J. C., C. L. Parkinson, R. Gersten, and L. Stock, 2008: Accelerated decline in the Arctic Sea ice cover. *Geophys. Res. Lett.*, **35**, L01703.
- Dee, D. P., S. M. Uppala, A. J. Simmons, P. Berrisford, P. Poli, S. Kobayashi, U. Andrae, M. A. Balmaseda, G. Balsamo, P. Bauer, P. Bechtold, A. C. M. Beljaars, L. van de Berg, J. Bidlot, N. Bormann, C. Delsol, R. Dragani, M. Fuentes, A. J. Geer, L. Haimberger, S. B. Healy, H. Hersbach, E. V. Hólm, L. Isaksen, P. Kållberg, M. Köhler, M. Matricardi, A. P. McNally, B. M. Monge-Sanz, J.-J. Morcrette, B.-K. Park, C. Peubey, P. de Rosnay, C. Tavolato, J.-N. Thépaut, and F. Vitart, 2011: The ERA-Interim

- reanalysis: Configuration and performance of the data assimilation system. *Quart. J. Roy. Meteor. Soc.*, **137**, 553–597.
- Ellis, T. D., T. L’Ecuyer, J. M. Haynes, and G. L. Stephens, 2009: How often does it rain over the global oceans? The perspective from CloudSat. *Geophys. Res. Lett.*, **36**, L03815.
- GPROF ATBD, cited 2016: GPM GPROF (Level 2) Algorithm Theoretical Basis Document (ATBD). [Available online at <http://pmm.nasa.gov/resources/documents/gpm-gprof-level-2-algorithm-theoretical-basis-document-atbd>.]
- Hiley, M. J., M. S. Kulie, and R. Bennartz, 2011: Uncertainty analysis for CloudSat snowfall retrievals. *J. Appl. Meteor. Climatol.*, **50**, 399–418.
- Hinzman, L. D., N. D. Bettez, W. R. Bolton, F. S. Chapin, M. B. Dyurgerov, C. L. Fastie, B. Griffith, R. D. Hollister, A. Hope, H. P. Huntington, A. M. Jensen, G. J. Jia, T. Jorgenson, D. L. Kane, D. R. Klein, G. Kofinas, A. H. Lynch, A. H. Lloyd, A. D. McGuire, F. E. Nelson, W. C. Oechel, T. E. Osterkamp, C. H. Racine, V. E. Romanovsky, R. S. Stone, D. A. Stow, M. Sturm, C. E. Tweedie, G. L. Vourlitis, M. D. Walker, D. A. Walker, P. J. Webber, J. M. Welker, K. S. Winker, and K. Yoshikawa, 2005: Evidence and implications of recent climate change in northern Alaska and other Arctic regions. *Climatic Change*, **72**, 251–298.
- Hou, A. Y., R. K. Kakar, S. Neeck, A. A. Azarbarzin, C. D. Kummerow, M. Kojima, R. Oki, K. Nakamura, and T. Iguchi, 2014: The Global Precipitation Measurement Mission. *Bull. Amer. Meteor. Soc.*, **95**, 701–722.

- Kulie, M. S. and R. Bennartz, 2009: Utilizing space-borne radars to retrieve dry snowfall. *J. Appl. Meteor. Climatol.*, **48**, 2564–2580.
- Kulie, M. S., L. Milani, N. Wood, S. Tushaus, R. Bennartz, and T. S. L’Ecuyer, 2016: A shallow cumuliform snowfall census using spaceborne radar. *J. Hydrometeorol.*, **17**, 1261–1279.
- Kummerow, C. D., D. L. Randel, M. S. Kulie, N.-Y. Wang, R. Ferraro, S. J. Munchak, and V. Petkovic, 2015: The evolution of the Goddard Profiling Algorithm to a fully parametric scheme. *J. Atmos. Oceanic Technol.*, **32**, 2265–2280.
- Kummerow, C. D., S. Ringerud, J. Crook, D. Randel, and W. Berg, 2011: An observationally generated a-priori database for microwave rainfall retrievals. *J. Atmos. Oceanic Technol.*, **28**, 113–130.
- Lebsock, M. D. and T. S. L’Ecuyer, 2011: The retrieval of warm rain from CloudSat. *J. Geophys. Res.*, **116**, D20209.
- Lebsock, M. D., T. S. L’Ecuyer, and G. L. Stephens, 2011: Detecting the ratio of rain and cloud water in low-latitude shallow marine clouds. *J. Appl. Meteor. and Clim.*, **50**, 419–432.
- Liu, C. and E. J. Zipser, 2009: “Warm rain” in the Tropics: Seasonal and regional distributions based on 9 years of TRMM data. *J. Clim.*, **22**, 767–779.
- Liu, G., 2008: Deriving snow cloud characteristics from CloudSat observations. *J. Geophys. Res. Atmos.*, **113**, D00A09.

- Lorenz, C. and H. Kuntsmann, 2012: The hydrological cycle in three state-of-the-art reanalyses: Intercomparison and performance analysis. *J. Hydrometeor.*, **13**, 1397–1420.
- Luckman, A., T. Murray, R. de Lange, and E. Hanna, 2006: Rapid and synchronous ice-dynamic changes in East Greenland. *Climatic Change*, **33**, L03503.
- Maahn, M., C. Burgard, S. Crewell, I. V. Gorodetskaya, S. Kneifel, S. Lhermitte, K. V. Tricht, and N. P. M. van Lipzig, 2014: How does the spaceborne radar blind zone affect derived surface snowfall statistics in polar regions? *J. Geophys. Res. Atmos.*, **119**, 13604–13620.
- Norin, L., A. Devasthale, T. S. L’Ecuyer, N. B. Wood, and M. Smalley, 2015: Intercomparison of snowfall estimates derived from the CloudSat Cloud Profiling Radar and the ground-based weather radar network over Sweden. *Atmos. Meas. Tech.*, **8**, 5009–5021.
- Palermé, C., J. E. Kay, C. Genthon, T. L’Ecuyer, N. B. Wood, and C. Claud, 2014: How much snow falls on the Antarctic ice sheet? *The Cryosphere*, **8**, 1577–1587.
- Petty, G. W., 2008: *A First Course in Atmospheric Thermodynamics - First Edition*. Sundog Publishing, 337 pp.
- Rapp, A. D., M. Lebsock, and T. L’Ecuyer, 2013: Low cloud precipitation climatology in the southeastern Pacific marine stratocumulus region using CloudSat. *Environ. Res. Lett.*, **8**, 014027.

- Sassen, K. and Z. Wang, 2008: Classifying clouds around the globe with the CloudSat radar: 1-year of results. *Geophys. Res. Lett.*, **35**, L04805.
- Schumacher, C. and R. A. Houze, 2003: The TRMM precipitation radar's view of shallow, isolated rain. *J. Appl. Meteor.*, **42**, 1519–1524.
- Screen, J. A. and I. Simmonds, 2012: Declining summer snowfall in the Arctic: Causes, impacts and feedbacks. *Clim. Dynam.*, **38**, 2243–2256.
- Short, D. A. and K. Nakamura, 2000: TRMM radar observations of shallow precipitation over the tropical oceans. *J. Clim.*, **13**, 4107–4124.
- Simmons, A. J., K. M. Willett, P. D. Jones, P. W. Thorne, and D. P. Dee, 2010: Low-frequency variations in surface atmospheric humidity, temperature and precipitation: Inferences from reanalyses and monthly gridded observational data sets. *J. Geophys. Res.*, **115**, D01110.
- Smalley, M., T. L'Ecuyer, M. Lebsock, and J. Haynes, 2014: A comparison of precipitation occurrence from the NCEP Stage IV QPE product and the CloudSat Cloud Profiling Radar. *J. Hydrometeor.*, **15**, 444–458.
- Stephens, G. L., D. G. Vane, R. J. Boain, G. G. Mace, K. Sassen, Z. Wang, A. J. Illingworth, E. J. O'Connor, W. B. Rossow, S. L. Durden, S. D. Miller, R. T. Austin, A. Benedetti, C. Mitrescu, and the CloudSat Science Team, 2002: The CloudSat Mission and the A-Train: A new dimension of space-based observations of clouds and precipitation. *Bull. Amer. Meteor. Soc.*, **83**, 1771–1790.

- Stroeve, J. C., M. C. Serreze, M. M. Holland, J. E. Kay, J. Malanik, and A. P. Barrett, 2012: The Arctic's rapidly shrinking sea ice cover: a research synthesis. *Climatic Change*, **110**, 1005–1027.
- Tanelli, S., S. L. Durden, E. Im, K. S. Pak, D. G. Reinke, P. Partain, J. M. Haynes, and R. T. Marchand, 2008: CloudSat's cloud profiling radar after two years in orbit: Performance, calibration, and processing. *IEEE Trans. Geosci. Remote Sens.*, **46**, 3560–3573.
- Waliser, D. E., J. F. Li, T. S. L'Ecuyer, and W. T. Chen, 2011: The impact of precipitating ice and snow on the radiation balance in global climate models. *Geophys. Res. Lett.*, **38**, L06802.
- Wood, N. B., T. S. L'Ecuyer, A. J. Heymsfield, and G. L. Stephens, 2015: Microphysical constraints on millimeter-wavelength scattering properties of snow particles. *J. Appl. Meteor.*, **52**, 341–362.
- Wood, N. B., T. S. L'Ecuyer, A. J. Heymsfield, G. L. Stephens, D. R. Hudak, and P. Rodrigues, 2014: Estimating snow properties using collocated multisensory observations. *J. Geophys. Res. Atmos.*, **119**, 8941–8961.
- Wood, N. B., T. S. L'Ecuyer, D. Vane, G. L. Stephens, and P. Partain, 2013: Level 2C Snow Profile process description and interface control document. Tech. rep., Colorado State University.